JAEA-Research
2024-002
DOI:10.11484/jaea-research-2024-002

JAEA-Research

Analysis of the Relationship Between Operational Quantity Used for Area Monitoring and Protection Quantity for External Exposure

Akira ENDO

Sector of Nuclear Science Research

May 2024

Japan Atomic Energy Agency

日本原子力研究開発機構

国立研究開発法人日本原子力研究開発機構　研究開発推進部　科学技術情報課
〒 319-1112　茨城県那珂郡東海村大字村松 4 番地 49
E-mail: ird-support@jaea.go.jp

JAEA-Research 2024-002

Analysis of the Relationship Between Operational Quantity Used for Area Monitoring and Protection Quantity for External Exposure

Akira ENDO

Sector of Nuclear Science Research
Japan Atomic Energy Agency
Tokai-mura, Naka-gun, Ibaraki-ken

(Received January 16, 2024)

This report presents a comprehensive analysis of the relationship between three quantities used for area monitoring — ambient dose equivalent $H^*(10)$, maximum dose equivalent $H^*_{\max}$, and ambient dose H^* — and effective dose for external irradiation by photons, neutrons, electrons, positrons, protons, muons, pions, and helium ions. For the analysis, calculations were performed using PHITS (Particle and Heavy Ion Transport code System) and the ICRU sphere. The analysis result shows that $H^*(10)$ and $H^*_{\max}$ can induce large differences in the estimation of effective dose over a wide energy range for various particle types covered by ICRP Publication 116 while H^* can conservatively estimate effective dose within the acceptable range for area monitoring. In other words, $H^*(10)$ and $H^*_{\max}$ have limitations in estimating effective dose, and using H^* is recommended as a more appropriate quantity for the purpose. This conclusion supports the proposal of ICRU Report 95 to use H^* for estimating effective dose in various external exposure situations. The use of ambient dose H^* is particularly important in situations where various types of radiation are encountered, such as the use of radiation in the medical and academic fields and exposure in aviation and can meet the evolving requirements of radiation monitoring for the expansion of the field of radiological protection.

Keywords: External Radiation, Operational Quantity, Protection Quantity, ICRU Report 95, Area Monitoring, Ambient Dose Equivalent, Maximum Dose Equivalent, Ambient Dose, Effective Dose

外部被ばくに対するエリアモニタリングに使われる実用量と防護量の関係の分析

日本原子力研究開発機構　原子力科学研究部門

遠藤　章

(2024 年 1 月 16 日 受理)

本報告書は，光子，中性子，電子，陽電子，陽子，ミューオン，パイ中間子及びヘリウムイオンによる外部被ばくについて，エリアモニタリングに用いられる 3 つの量である周辺線量当量 $H^*(10)$，最大線量当量 H^*_{max} 及び周辺線量 H^* と実効線量との関係を包括的に分析した結果を示す。分析のための計算は，PHITS (Particle and Heavy Ion Transport code System) と ICRU 球を用いて行った。その結果，ICRP Publication 116 で対象としている幅広いエネルギー範囲における外部被ばくに対して，$H^*(10)$ と H^*_{max} は実効線量の評価に大きな差を生じる場合がある一方，H^* はエリアモニタリングに許容される範囲で実効線量を保守的に評価できることが分かった。すなわち，実効線量を評価するために，$H^*(10)$ と H^*_{max} には限界があり，より適切な量として H^* の使用が推奨される。この結論は，多様な被ばく状況における実効線量の評価に H^* を導入した ICRU Report 95 の提案を支持するものである。周辺線量 H^* の利用は，医療や学術研究における放射線利用や航空機搭乗時の被ばく等の様々な種類の放射線により被ばくする状況で特に重要であり，放射線防護の対象の拡大に伴う放射線モニタリングの新たなニーズに応えることができる。

原子力科学研究所：〒 319–1195　茨城県那珂郡東海村大字白方 2 番地 4

Contents

1 Introduction **1**

2 Materials and methods **2**
2.1 Definitions of quantities 2
2.2 Radiation transport code 3
2.3 Calculation model and method 4

3 Results and discussion **5**
3.1 Validation of calculation 5
3.1.1 Comparison of $h^*(10)$ 6
3.1.2 Comparison of h^*_{max} 8
3.2 Overview of $d^*(10)$, $h^*(10)$, and Q 9
3.3 Comparison of $H^*(10)$ and E_{max} 11
3.4 Comparison of H^*_{max} and E_{max} 13
3.5 Comparison of H^* and E 14
3.6 Discussion on appropriate quantity for use in area monitoring for assessment of effective dose from external radiation 16

4 Conclusion **17**

Acknowledgements **17**

References **18**

目　次

1　序　論 **1**

2　研究方法 **2**
2.1　量の定義 2
2.2　放射線輸送計算コード 3
2.3　計算モデル及び方法 4

3　結果と考察 **5**
3.1　計算の検証 5
3.1.1　$h^*(10)$ の比較 6
3.1.2　h^*_{max} の比較 8
3.2　$d^*(10), h^*(10)$ 及び Q の概要 9
3.3　$H^*(10)$ と E_{max} の比較 11
3.4　H^*_{max} と E_{max} の比較 13
3.5　H^* と E の比較 14
3.6　外部放射線に対する実効線量評価のためのエリアモニタリングに用いる適切な量の検討 16

4　結　論 **17**

謝　辞 **17**

参考文献 **18**

List of Tables

Table 1 Particles and energy ranges for calculation of dose coefficients. 21
Table 2 Photons: $d^*(10)$, $h^*(10)$, Q, h^*_{max}, and h^* values. 22
Table 3 Neutrons: $d^*(10)$, $h^*(10)$, Q, h^*_{max}, and h^* values. 24
Table 4 Electrons: $d^*(10)$, $h^*(10)$, Q, h^*_{max}, and h^* values. 26
Table 5 Positrons: $d^*(10)$, $h^*(10)$, Q, h^*_{max}, and h^* values. 27
Table 6 Protons: $d^*(10)$, $h^*(10)$, Q, h^*_{max}, and h^* values. 28
Table 7 Negative muons: $d^*(10)$, $h^*(10)$, Q, h^*_{max}, and h^* values. 29
Table 8 Positive muons: $d^*(10)$, $h^*(10)$, Q, h^*_{max}, and h^* values. 30
Table 9 Negative pions: $d^*(10)$, $h^*(10)$, Q, h^*_{max}, and h^* values. 31
Table 10 Positive pions: $d^*(10)$, $h^*(10)$, Q, h^*_{max}, and h^* values. 33
Table 11 Helium ions: $d^*(10)$, $h^*(10)$, Q, h^*_{max}, and h^* values. 35

List of Figures

Figure 1 Quality factor, Q, as a function of linear energy transfer, L. 36
Figure 2 Model used for calculation of $D^*(d)$ and $H^*(d)$. 36
Figure 3 Distributions of dose equivalent in the ICRU sphere irradiated by photons. 37
Figure 4 Comparison of $h^*(10)$ for photons. 38
Figure 5 Comparison of $h^*(10)$ for neutrons. 38
Figure 6 Comparison of $h^*(10)$ for electrons. 39
Figure 7 Comparison of $h^*(10)$ for positrons. 39
Figure 8 Comparison of $h^*(10)$ for protons. 40
Figure 9 Comparison of $h^*(10)$ for negative muons. 40
Figure 10 Comparison of $h^*(10)$ for positive muons. 41
Figure 11 Comparison of $h^*(10)$ for negative pions. 41
Figure 12 Comparison of $h^*(10)$ for positive pions. 42
Figure 13 Comparison of $d^*(10)$ and $h^*(10)$ for photons calculated by FLUKA and PHITS. 43
Figure 14 Comparison of h^*_{max} for photons. 44
Figure 15 Comparison of h^*_{max} for neutrons. 44
Figure 16 Comparison of h^*_{max} for electrons. 45
Figure 17 Comparison of h^*_{max} for positrons. 45
Figure 18 Comparison of h^*_{max} for protons. 46
Figure 19 Comparison of h^*_{max} for negative muons. 46
Figure 20 Comparison of h^*_{max} for positive muons. 47
Figure 21 Comparison of h^*_{max} for negative pions. 47
Figure 22 Comparison of h^*_{max} for positive pions. 48
Figure 23 Absorbed dose distribution in the frontal region of the ICRU sphere. 49
Figure 24 Effect of radius of the scoring region on h^*_{max}. 49
Figure 25 Photons: $d^*(10)$, $h^*(10)$, and Q. 50
Figure 26 Neutrons: $d^*(10)$, $h^*(10)$, and Q. 51

Figure 27 Electrons: $d^*(10)$, $h^*(10)$, and Q. 52
Figure 28 Positrons: $d^*(10)$, $h^*(10)$, and Q. 53
Figure 29 Protons: $d^*(10)$, $h^*(10)$, and Q. 54
Figure 30 Negative muons: $d^*(10)$, $h^*(10)$, and Q. 55
Figure 31 Positive muons: $d^*(10)$, $h^*(10)$, and Q. 56
Figure 32 Negative pions: $d^*(10)$, $h^*(10)$, and Q. 57
Figure 33 Positive pions: $d^*(10)$, $h^*(10)$, and Q. 58
Figure 34 Helium ions: $d^*(10)$, $h^*(10)$, and Q. 59
Figure 35 LET distributions of charged particles in the ICRU sphere irradiated by protons. . 60
Figure 36 Photons: $h^*(10)$, $e_{\max}$, and $h^*(10)/e_{\max}$. 61
Figure 37 Neutrons: $h^*(10)$, $e_{\max}$, and $h^*(10)/e_{\max}$. 62
Figure 38 Electrons: $h^*(10)$, $e_{\max}$, and $h^*(10)/e_{\max}$. 63
Figure 39 Positrons: $h^*(10)$, $e_{\max}$, and $h^*(10)/e_{\max}$. 64
Figure 40 Protons: $h^*(10)$, $e_{\max}$, and $h^*(10)/e_{\max}$. 65
Figure 41 Negative muons: $h^*(10)$, $e_{\max}$, and $h^*(10)/e_{\max}$. 66
Figure 42 Positive muons: $h^*(10)$, $e_{\max}$, and $h^*(10)/e_{\max}$. 67
Figure 43 Negative pions: $h^*(10)$, $e_{\max}$, and $h^*(10)/e_{\max}$. 68
Figure 44 Positive pions: $h^*(10)$, $e_{\max}$, and $h^*(10)/e_{\max}$. 69
Figure 45 Helium ions: $h^*(10)$, $e_{\max}$, and $h^*(10)/e_{\max}$. 70
Figure 46 Photons: $h^*_{\max}$, $e_{\max}$, and $h^*_{\max}/e_{\max}$. 71
Figure 47 Neutrons: $h^*_{\max}$, $e_{\max}$, and $h^*_{\max}/e_{\max}$. 72
Figure 48 Electrons: $h^*_{\max}$, $e_{\max}$, and $h^*_{\max}/e_{\max}$. 73
Figure 49 Positrons: $h^*_{\max}$, $e_{\max}$, and $h^*_{\max}/e_{\max}$. 74
Figure 50 Protons: $h^*_{\max}$, $e_{\max}$, and $h^*_{\max}/e_{\max}$. 75
Figure 51 Negative muons: $h^*_{\max}$, $e_{\max}$, and $h^*_{\max}/e_{\max}$. 76
Figure 52 Positive muons: $h^*_{\max}$, $e_{\max}$, and $h^*_{\max}/e_{\max}$. 77
Figure 53 Negative pions: $h^*_{\max}$, $e_{\max}$, and $h^*_{\max}/e_{\max}$. 78
Figure 54 Positive pions: $h^*_{\max}$, $e_{\max}$, and $h^*_{\max}/e_{\max}$. 79
Figure 55 Helium ions: $h^*_{\max}$, $e_{\max}$, and $h^*_{\max}/e_{\max}$. 80
Figure 56 Photons: e and h^*/e. 81
Figure 57 Neutrons: e and h^*/e. 82
Figure 58 Electrons: e and h^*/e. 83
Figure 59 Positrons: e and h^*/e. 84
Figure 60 Protons: e and h^*/e. 85
Figure 61 Negative muons: e and h^*/e. 86
Figure 62 Positive muons: e and h^*/e. 87
Figure 63 Negative pions: e and h^*/e. 88
Figure 64 Positive pions: e and h^*/e. 89
Figure 65 Helium ions: e and h^*/e. 90

1 Introduction

Protection against the health effects of ionizing radiation requires preventing tissue reactions (deterministic effects) and limiting cancer risks and hereditary effects (stochastic effects). The International Commission on Radiological Protection (ICRP) developed risk-related dosimetric quantities called "protection quantities" to meet these requirements[1–3]. The most recent definitions of protection quantities, given in the 2007 Recommendations of ICRP[3], include the mean absorbed dose in an organ or tissue, the equivalent dose in an organ or tissue, and the effective dose.

The body-related protection quantities are not measurable in practice; therefore, they cannot be used directly as quantities in radiation monitoring. The International Commission on Radiation Units and Measurements (ICRU) has developed a set of "operational quantities" to assess equivalent and effective doses via a series of reports[4–8]. The operational quantities are intended to provide a reasonable, generally conservative, estimate of protection quantity values associated with an exposure or a potential exposure of persons under various irradiation conditions[3].

The relationship between the protection quantities and the operational quantities is established using dose coefficients which relate the operational and protection quantities to physical quantities describing the radiation field. ICRU Reports 43[5] and 47[6], and ICRP Publication 74[9]/ICRU Report 57[10] reported sets of dose coefficients to these quantities from radiometric and dosimetric quantities.

The currently used operational quantities were defined in the 1980s and have been implemented in practice in many countries under radiation protection directives and regulations during the last 30 years. Nevertheless, the existing system of operational quantities has limitations and needs further improvement to consider changes in the application of protection and operational quantities[3,11–13]. The types and energy range of particles used in medical diagnostics and therapy and scientific research have been expanded. The ICRP Recommendations include natural radiation sources[2]; aircraft crews are one of the most exposed occupational groups, and the radiation field at flight altitudes includes a large component of high-energy particles from cosmic radiation.

To meet the evolving requirements for the expansion of the field of radiological protection, ICRP developed dose coefficients of the protection quantities that extend particle types and energy ranges to higher regions and published the dataset of dose coefficients in Publication 116[14] together with ICRU. The dataset of ICRP Publication 116 superseded those of ICRP Publication 74 and ICRU Report 57. However, ICRP Publication 116 highlighted that the operational quantities defined in ICRU Reports 39[4] and 51[7] are not always close estimates of the protection quantities in higher energy fields[14]. Thus, ICRU established the Report Committee 26 in 2010 to address these issues. The Report Committee 26 reviewed the shortcomings and limitations of the existing system of operational quantities, considering an extension of the range of particle types and energies of the dose coefficients in ICRP Publication 116. As a result of extensive discussion, the Report Committee 26 decided to introduce new operational quantities defined using the dose coefficient values of the protection quantities for external exposures. The definitions of the operational quantities and a set of dose coefficients were published in ICRU Report 95[15].

ICRU Report 95 provided a comparison of the dose coefficients for area monitoring defined in Reports 39 and 51 and those newly proposed in Report 95 to indicate the limitations of the existing system defined in Reports 39 and 51. The comparisons were limited for photons, neutrons, electrons, positrons, and protons, and they were provided in graphical form only.

To gain a deeper understanding of the background of motivation for introducing new operational quantities by ICRU, the present report analyzes the limitations of the existing system by comparing

several quantities used for area monitoring with effective dose. The analysis result validates the decision of the Report Committee 26 and shows the advantages of the new operational quantities.

2 Materials and methods

2.1 Definitions of quantities

This section provides definitions for three quantities used in area monitoring and effective dose, which are the subjects being compared in this report.

1) Ambient dose equivalent

The ambient dose equivalent, $H^*(d)$, at a point in a radiation field, is the dose equivalent that would be produced by the corresponding expanded and aligned field in the ICRU sphere at a depth, d, on the radius opposing the direction of the aligned field[7]. The unit of the ambient dose equivalent is J kg^{-1} and has the special name sievert (Sv). For strongly penetrating radiation, a depth of 10 mm is currently recommended. The ambient dose equivalent for this depth is then denoted by $H^*(10)$.

A quantity analogous to ambient dose equivalent can be defined in terms of absorbed dose, known as the ambient absorbed dose, $D^*(d)$. Its unit is J kg^{-1} and has the special name gray (Gy).

The dose equivalent, H, is the product of Q and D at a point in a tissue, where Q is the quality factor and D is the absorbed dose at that point; thus, $H = QD$. Consequently, in this report, a value of $H^*(10)$ is derived from Q at 10-mm depth and $D^*(10)$ of the ICRU sphere.

Q is defined in ICRP Publication 60[2] as a function of the unrestricted linear energy transfer (LET), L, in water at the point of interest, as follows.

$$Q(L) = 1 \qquad (L < 10 \text{ keV } \mu\text{m}^{-1}) \tag{1}$$

$$Q(L) = 0.32L - 2.2 \qquad (10 \leq L \leq 100 \text{ keV } \mu\text{m}^{-1}) \tag{2}$$

$$Q(L) = 300/\sqrt{L} \qquad (L > 100 \text{ keV } \mu\text{m}^{-1}) \tag{3}$$

Figure 1 illustrates the relationship between Q and L defined by **Equations (1)–(3)**.

2) Maximum dose equivalent

The maximum dose equivalent, $H^*_{\max}$, represents the maximum value of the dose equivalent that would be produced by the corresponding expanded and aligned field in the ICRU sphere on the radius opposing the direction of the aligned field. The unit of the maximum dose equivalent is J kg^{-1} and has the special name sievert (Sv).

Note that the definition of the maximum dose equivalent, $H^*_{\max}$, used in this report is different from the maximum dose equivalent in an irradiated body (MADE)[16] and the dose equivalent index[17,18]. Furthermore, as stated in Appendix B of ICRU Report 43[5], the maximum dose equivalent in a 30 cm diameter sphere exposed to a unidirectional beam may not occur exactly on the central axis. However, in this study, the focus is on examining the maximum dose equivalent value along the central axis within the ICRU sphere to facilitate comparison with previous research[19].

3) Ambient dose

The ambient dose, H^*, at a point in a radiation field, is the product of the particle fluence at that point, Φ, and dose coefficient, h^*, which relates the particle fluence to the maximum value of effective dose, $E_{\max}$, for various irradiation conditions[15]; therefore, $H^* = \Phi h^*$. The unit of the ambient dose is J kg^{-1} and has the special name sievert (Sv).

For a specific particle type i with kinetic energy E_{p}, the dose coefficient

$$h_i^*(E_{\mathrm{p}}) = E_{\max,i}(E_{\mathrm{p}})/\Phi_i(E_{\mathrm{p}}) \qquad \mathrm{Sv\ cm^2} \tag{4}$$

$$= e_{\max,i}(E_{\mathrm{p}}) \tag{5}$$

is calculated for the exposure of the ICRP/ICRU adult reference phantoms[20] for broad uniform parallel beams of the incident radiation field. The irradiation geometries are antero–posterior (AP), postero–anterior (PA), left lateral (LLAT), right lateral (RLAT), rotational (ROT), isotropic (ISO), superior hemisphere semi-isotropic (SS-ISO), and inferior hemisphere semi-isotropic (IS-ISO) fields for photons, neutrons, and protons; AP, PA, ISO, SS-ISO, and IS-ISO fields for electrons, positrons, muons, and pions; and AP, PA, and ISO for helium ions. The effective dose coefficients for these irradiation geometries are presented in ICRP Publication 116[14].

4) Effective dose

The effective dose, E, is the tissue-weighted sum of the equivalent doses in all specified organs and tissues of the body and is given by the expression

$$E = \sum_{\mathrm{T}} w_{\mathrm{T}} \sum_{\mathrm{R}} w_{\mathrm{R}} D_{\mathrm{T,R}} = \sum_{\mathrm{T}} w_{\mathrm{T}} H_{\mathrm{T}} \tag{6}$$

where H_{T} is the equivalent dose in an organ or tissue T, $D_{\mathrm{T,R}}$ is the mean absorbed dose in an organ or tissue T from radiation of type R, and w_{T} is the tissue weighting factor[3]. This sum is made over organs and tissues considered to be sensitive to the induction of stochastic effects. The unit of the effective dose is J kg^{-1} and has the special name sievert (Sv).

2.2 Radiation transport code

The calculation of $D^*(d)$ and $H^*(d)$ was performed using PHITS (Particle and Heavy Ion Transport code System)[21]. PHITS is a versatile Monte Carlo code that enables the simulation of the transport and interaction of hadrons, leptons, and heavy ions in arbitrary three-dimensional geometries. It uses several nuclear reaction models and data libraries. PHITS version 3.32 was used for the calculation. The models and parameters used in the calculation are described in detail below.

The dynamic stage of hadron-induced nuclear reactions was simulated using the intranuclear cascade models JAM[22]/INCL4.6[23], while nuclei-induced reactions were simulated using an improved version of the quantum molecular dynamics model, JQMD[24]. To simulate nucleus–nucleus reactions exceeding 3 GeV n^{-1}, a hybrid method integrating JAM and JQMD, called JAMQMD, was applied. The generalized evaporation and fission model GEM[25] was used to simulate the static stage of these reactions.

The ATIMA algorithm[26] using the continuous slowing down approximation was used to calculate the energy loss of charged particles, excluding electrons and positrons. The transport of neutrons with energies ≤ 20 MeV was simulated using evaluated neutron data libraries; specifically, JENDL-4.0[27] was used in this calculation. For the scattering of low-energy neutrons, the effect of chemical bonding of hydrogen was considered using S(α, β) data for hydrogen in water.

The transport of photons, electrons, and positrons was modeled using an algorithm of the EGS5 code[28] integrated with PHITS. JAM and JQMD were used to simulate photonuclear reactions[29]. Furthermore, the models for muon-induced nuclear reactions were integrated, including virtual photonuclear reactions and the negative muon capture reaction following muonic atom formation[30].

$H^*(d)$ was determined using the PHITS t-deposit tally. The t-deposit tally calculates the dose equivalent H based on the quality factor Q, which is a function of the LET of charged particles recommended in ICRP Publication 60[31].

Additional validation calculations were performed for photons with the FLUKA code, specifically using FLUKA2011[32]. Within FLUKA, while users have the flexibility to specify models and parameters for calculations, predefined parameter sets optimized for simulations are also available. The parameter set designated as "PRECISIOn" was used for the calculations presented in this report. In particular, "PRECISIOn" is tailored for precise simulations and allows the activation of processes important for particle transport and interaction over a wide energy range.

2.3 Calculation model and method

Figure 2 illustrates the geometry used to calculate $D^*(d)$ and $H^*(d)$, following a previous study by Ferrari and Pelliccioni[33]. The ICRU sphere was irradiated with a monoenergetic parallel particle beam uniformly expanded over its front surface. The ICRU sphere is a tissue-equivalent sphere with a density of 1 g cm^{-3}, diameter of 30 cm, and a mass composition of 76.2 % oxygen, 11.1 % carbon, 10.1 % hydrogen, and 2.6 % nitrogen[34]. The space between the particle source and ICRU sphere was assumed to be vacuum.

To obtain the depth dose distributions along the central axis of the sphere, the deposited energy was evaluated using a series of cylindrical structures aligned along the central axis of the sphere, as shown in **Figure 2**. Different grids were used depending on the depth: 0.2 cm-long longitudinal grids were used up to 1.7 cm, 0.3 cm for a depth of 1.7–2.0 cm, and 1.0 cm for beyond 2.0 cm, with a cylinder radius of 0.5 cm.

The $D^*(d)$ values were derived from the energy deposited per unit mass within the cylindrical regions. $H^*(10)$ was calculated from the value of Q as a function of LET in water, as determined by the t-deposit tally in PHITS. Specifically, $D^*(10)$ and $H^*(10)$ were determined for the cylindrical region with a depth of 0.9–1.1 cm and a radius of 0.5 cm. This region is called the 10-mm depth region in this report. H^*_{max} was obtained from the maximum value of $H^*(d)$.

The values of $D^*(10)$, $H^*(10)$, and H^*_{max} are normalized to the incident particle fluence, Φ, and are presented in units of Gy cm^2 and Sv cm^2 as

$$d^*(10) = D^*(10)/\Phi \qquad \text{Gy cm}^2 \tag{7}$$

$$h^*(10) = H^*(10)/\Phi \qquad \text{Sv cm}^2 \tag{8}$$

$$h^*_{\mathrm{max}} = H^*_{\mathrm{max}}/\Phi \qquad \text{Sv cm}^2 \tag{9}$$

Table 1 summarizes particle types and energy ranges considered for the calculations of $d^*(10)$, $h^*(10)$, and h^*_{max} in this report. These were determined with reference to the conditions employed for calculating the dose coefficients for the protection quantities given in ICRP Publication 116[14]. Note that the lower energy limits for electrons, positrons, protons, and helium ions are higher than those reported in ICRP Publication 116. These particles with the energies below the lower energy limits have extremely short ranges in the ICRU sphere. Furthermore, considering secondary particles produced by the low-energy particles' interactions in the ICRU sphere, an enormous amount of computational time is required to give a statistically significant energy to the 10-mm depth region in the ICRU sphere. Therefore, these low-energy particles were excluded from the dose coefficient calculation. Note that the exclusion of these extremely low-energy particles is expected to have no significant effect on area monitoring because their contribution to doses is small.

The total number of incident particles was sufficiently large to maintain the standard deviation of $h^*(10)$ typically below 3 %.

3 Results and discussion

Tables 2–11 present the numerical values of the dose coefficients from particle fluence to ambient absorbed dose, $d^*(10)$, ambient dose equivalent, $h^*(10)$, and maximum dose equivalent, h^*_{max}, calculated using PHITS for photons, neutrons, electrons, positrons, protons, muons, pions, and helium ions. The definitions of $d^*(10)$, $h^*(10)$, and h^*_{max} are given in **Equations (7)–(9)**. In addition, the tables show the corresponding quality factor, Q, at the 10-mm depth region evaluated from $d^*(10)$ and $h^*(10)$. Furthermore, the dose coefficients for the ambient dose, h^*, central to the discussion in this report, are taken from ICRU Report 95[15] and are provided in these tables.

Figure 3 illustrates a sample set of dose equivalent distributions on a cross-section traversing the central axis of the ICRU sphere via photon incidence at three different energies. At 0.1 MeV, the maximum dose equivalent occurs in a superficial region of the sphere. Notably, with increasing photon energy, this maximum value moves to deeper regions within the sphere. This suggests that $H^*(10)$, representing the dose equivalent at a depth of 10 mm in the ICRU sphere, may not be an appropriate quantity for assessing effective dose to the human body from high-energy photon irradiation.

The characteristics of the energy dependence of $d^*(10)$, $h^*(10)$, and Q for each particle are described in **Section 3.2**.

3.1 Validation of calculation

The calculations performed with PHITS were validated by comparing the values of $h^*(10)$ and h^*_{max} presented in **Tables 2–10** with data published by Ferrari and Pelliccioni[19,33,35–39]. Ferrari and Pelliccioni computed $h^*(10)$ and h^*_{max} for photons, neutrons, electrons, positrons, protons, muons, and pions over a wide energy range using the FLUKA code[33,35–39]. The compiled dataset was subsequently published in 2000[19]. Despite the limited incident particle energy points, the data serve as valuable reference points for validating the calculations presented in this report. Note that the comparison does not include the helium ion data presented in **Table 11** as it was not part of the Ferrari and Pelliccioni study and is therefore missing from the analysis.

In addition, the $h^*(10)$ values for photons, neutrons, and electrons were compared with those presented in ICRP Publication 74[9] and ICRU Report 57[10]. This comparison demonstrates the impact of different calculation methods on the dose coefficient values. In particular, ICRP Publication 74 and ICRU Report 57 used a calculation method known as the kerma approximation. This approximation assumes that all secondary particles, especially charged particles, are in equilibrium with the primary particle at the point of interest. However, the calculations used in this report and by Ferrari and Pelliccioni did not use the kerma approximation and tracked secondary particles.

Sections 3.1.1 and **3.1.2** provide comparisons of $h^*(10)$ and h^*_{max}, respectively.

3.1.1 Comparison of $h^*(10)$

Figures 4–12 show comparisons of $h^*(10)$ values. Overall, the values calculated by PHITS and FLUKA for electrons (**Figure 6**), positrons (**Figure 7**), and protons (**Figure 8**) correlate satisfactorily. However, noticeable differences are observed for photons (**Figure 4**), neutrons (**Figure 5**), negative and positive muons (**Figures 9** and **10**), and negative and positive pions (**Figures 11** and **12**). These discrepancies are investigated below to determine possible underlying causes.

1) Photons (Figure 4)

The $h^*(10)$ values calculated using PHITS and FLUKA for photons show good agreement up to 10 MeV. However, in the PHITS calculation, remarkable broad peaks are observed from 20 MeV to 100 MeV and from 200 MeV to 3 GeV, which are absent in the FLUKA result. These peaks in the PHITS result are due to quality factors greater than one caused by charged particles produced by photon-induced nuclear reactions. Further analysis of these phenomena is given in **Section 3.2**.

Notably, two peaks in the $h^*(10)$ plot are not observed in the calculation of Ferrari and Pelliccioni. While their papers lack specific information regarding the treatment of photon-induced nuclear reactions[19,33,35], the discrepancies between PHITS and FLUKA calculations are attributed to different approaches employed for simulating the photon interaction. To clarify this discrepancy, the author has performed calculations for $d^*(10)$ and $h^*(10)$ using the FLUKA code, version FLUKA2011[32], and the results are shown in **Figure 13**. In terms of the energy dependence of $d^*(10)$ and $h^*(10)$, which activated photon-induced nuclear reactions, PHITS and FLUKA calculations in this study show good agreement. In particular, the two peaks in the $h^*(10)$ plot, which are missing in the calculations reported by Ferrari and Pelliccioni, confirm the validity of the PHITS calculations, considering all processes of photon transport and interaction.

Figure 4 also shows the $h^*(10)$ values obtained from ICRP Publication 74 and ICRU Report 57. Below 3 MeV, these values are very close to those calculated using PHITS and FLUKA. However, the values reported in ICRP Publication 74/ICRU Report 57 increase substantially beyond 3 MeV. This discrepancy is due to the kerma approximation used in ICRP Publication 74/ICRU Report 57, which deposits the energy of the secondary particles locally, while PHITS and FLUKA follow secondary particle transports. This simplification in ICRP Publication 74/ICRU Report 57 leads overestimation of $h^*(10)$ above 3 MeV.

2) Neutrons (Figure 5)

Figure 5 compares the $h^*(10)$ values for neutrons with those reported in ICRP Publication 74 and ICRU Report 57, which provide $h^*(10)$ values for up to 201 MeV. Below 200 MeV, the $h^*(10)$ values from PHITS calculation are in close agreement with the values obtained from the FLUKA calculation and reported in ICRP Publication 74/ICRU Report 57. However, above 200 MeV discrepancies arise between values obtained in the PHITS and FLUKA calculations.

The divergence above 200 MeV can be attributed to differences of types and energies of secondary particles produced by nuclear reactions. PHITS uses the INCL4.6 model in combination with GEM for energies between 20 MeV and 3.5 GeV, while it uses the JAM model with GEM for energies above 3.5 GeV. Meanwhile, FLUKA uses three models to describe hadronic inelastic interactions depending on projectile energy ranges above 20 MeV[38]. A specific model comprising an explicit intranuclear cascade stage and a pre-equilibrium stage based on a geometry-dependent excition approach is used for nucleons with energies in the range of approximately 20 MeV–2 GeV. Primary interactions between 2 and 5 GeV are described using resonance production and decay, while above 5 GeV interactions are simulated by multichain fragmentation in the framework of the Dual Parton Model. Based on the nuclear reaction models employed, the differences in the $h^*(10)$ values are likely due to differences in energy deposition at 10-mm depth within the ICRU sphere and/or differences in the energy spectra of the secondary charged particles contributing Q values.

3) Negative and positive muons (Figures 9 and 10)

The PHITS and FLUKA results generally correlate for negative and positive muons over the entire energy range. The energy dependence of the $h^*(10)$ values calculated using PHITS shows a peak at 15 MeV of incident muons, corresponding to the range of a 15-MeV muon, which spans approximately 10 mm in ICRU soft tissue[40]. The 15-MeV muon reaches the 10-mm depth region of the ICRU sphere and deposits its energy, resulting in the peak in the energy dependence of $h^*(10)$. Because Pelliccioni did not perform calculations between 10 and 50 MeV[39], this peak does not appear in the FLUKA results.

4) Negative and positive pions (Figures 11 and 12)

Figures 11 and **12** highlight the comparison of $h^*(10)$ values for negative and positive pions, respectively, showing differences between PHITS and FLUKA results above 1 GeV. These differences could be due to variations in the $d^*(10)$ values. For example, considering negative pions at 100 GeV, the PHITS results of this study show $h^*(10)$ and Q values of 1.45×10^{-9} Sv cm^2 and 1.93, respectively, as shown in **Table 9**. In contrast, the corresponding values for FLUKA provided by Pelliccioni[39] are 7.13×10^{-10} Sv cm^2 and 1.7, respectively. The significant difference in $h^*(10)$ compared to the discrepancy in Q suggests a probable divergence in the $d^*(10)$ values, which could be due to the calculation of the stopping power of the pions. Unfortunately, a more in-depth analysis is hampered because Pelliccioni's paper does not present the $d^*(10)$ values, making a comprehensive comparison impossible.

The energy dependence of the $h^*(10)$ values calculated using PHITS shows a peak at 15 MeV for negative and positive pions, corresponding to the range of 15-MeV pions, which is about 10 mm within the ICRU sphere. Because Pelliccioni did not perform calculations between 10 and 50 MeV[39], this peak does not exist in the FLUKA results, as in the case of muons.

3.1.2 Comparison of h^*_{max}

Figures 14–22 present comparisons of the h^*_{max} values. Overall, the h^*_{max} values derived from PHITS and FLUKA show substantial agreement for neutrons (**Figure 15**), electrons (**Figure 16**), positrons (**Figure 17**), protons (**Figure 18**), positive muons (**Figure 20**), and positive pions (**Figure 22**). However, noticeable discrepancies exist for photons (**Figure 14**), negative muons (**Figure 19**), and negative pions (**Figure 21**). These discrepancies are further investigated below to identify possible underlying causes.

1) Photons (Figure 14)

Figure 14 illustrates a noticeable difference in h^*_{max} for photons with incident energies between 10 and 20 keV. For low-energy photon incidence, h^*_{max} tends to concentrate in the frontal region facing the incident photon direction, considerably affecting the absorbed dose sensitivity due to scoring region geometry.

Figure 23 shows the scoring region geometries used in the PHITS and FLUKA calculations, and absorbed dose distribution in the frontal region facing the incident direction of 10-keV photons. In this study using PHITS, a cylindrical scoring region with a radius of 0.5 cm was used for calculating absorbed doses. By contrast, a larger radius of 1.0 cm was used in the FLUKA calculations[33]. Specifically, in the spherical geometry, a scoring region closer to the cylinder side reduces the distance from the surface of sphere. Thus, photons are more likely to reach the scoring region within the 1.0-cm radius than the 0.5-cm radius. The higher h^*_{max} values observed in the FLUKA results are attributed to this geometric difference.

To confirm this result, **Figure 24** compares h^*_{max} calculated using the 0.5-cm radius scoring region by FLUKA in this study, along with the results from FLUKA reported by Ferrari and Pelliccioni, and PHITS. For a 0.5-cm radius scoring region, the PHITS and FLUKA calculations show excellent agreement. Therefore, the discrepancy in h^*_{max} below 40 keV in **Figure 14** is due to the choice of the scoring region radius.

2) Negative muons (Figure 19)

A remarkable difference is observed in h^*_{max} for negative muons at 1 MeV between PHITS and FLUKA. At this incident energy, h^*_{max} is found in the frontal region (0.1–0.3 cm depth) facing the direction of the incident muons. This discrepancy could be due to differences in the modeling of the negative muon behavior within the two codes. A negative muon is captured by an atom in matter just before it stops, resulting in the formation of a muonic atom. The captured muon cascades down to the 1s orbit, emitting characteristic X-rays, and then decays in the 1s orbit or is captured by the nucleus.

While PHITS and FLUKA consider muon capture reactions, PHITS uses models that follow negative muon capture in more detail[30]. Conversely, FLUKA's description of the muon capture reaction is not described in the paper[39]. Therefore, a more detailed analysis for the difference in h^*_{max} at 1 MeV between PHITS and FLUKA is hampered by the lack of specific information.

3) Negative pions (Figure 21)

Noticeable discrepancy in h^*_{max} is observed for negative pions at 1 MeV between PHITS and FLUKA. This discrepancy is due to differences in the modeling of the negative pion behavior within the two codes. When a negative pion reaches its stopping point, it is typically captured by a nucleus, producing various

secondary charged particles. PHITS and FLUKA include this process, where charged particle types and their energy distribution influence the determination of Q values. The differences in Q values could be due to the observed differences in h^*_{max} at 1 MeV between the two codes. However, the lack of detailed descriptions for the specifics of each model or their validity makes further detailed discussion difficult.

Furthermore, discrepancies in the h^*_{max} values appear from approximately 10 GeV and become more pronounced with increasing energy. This escalation is thought to be due to differences in stopping power calculation methods, as discussed in **Section 3.1.1**.

Sections 3.1.1 and **3.1.2** comprehensively compared the $h^*(10)$ and h^*_{max} values calculated using PHITS and FLUKA, showing good overall agreement. Cases of observed differences were clearly related to differences in the transport and nuclear reaction models employed within PHITS and FLUKA. Hence, it is important to acknowledge that the selection of these models may involve a degree of subjectivity.

Overall, the results lead to the conclusion that PHITS performs the calculations appropriately, given the context of the observed agreement and identified sources of discrepancies due to model variations.

3.2 Overview of $d^*(10)$, $h^*(10)$, and Q

Tables 2–11 present the numerical values for $d^*(10)$, $h^*(10)$, and Q for various particles — photons, neutrons, electrons, positrons, protons, muons, pions, and helium ions. **Figures 25–34** present two graphs each: the upper graph illustrates the energy dependence of $d^*(10)$ and $h^*(10)$ and lower graph shows Q. A brief review of the main characteristics of the energy dependence of the $d^*(10)$, $h^*(10)$, and Q values is given here.

1) Photons (Figure 25)

The values of $d^*(10)$ and $h^*(10)$ for photons are almost same from 10 keV to 15 MeV. Within this energy range, photons interact primarily through the photoelectric effect, Compton scattering, and pair (and triplet) production. Energy deposition occurs in matter is due to the energy transferred to and then lost by electrons and positrons along their paths. Electrons and positrons can produce secondary photons as bremsstrahlung and characteristic X-rays emitted after ionization and via particle annihilation of positrons. Because the Q values determined from the LET of electrons and positrons generated from photons in this energy range become one, $d^*(10)$ and $h^*(10)$ have the same values.

However, $h^*(10)$ shows two distinct peaks in the energy ranges 20 MeV–100 MeV and 200 MeV–3 GeV. These peaks correspond to the Q values greater than one, which result from charged particles produced by photon-induced nuclear reactions.

2) Neutrons (Figure 26)

Neutrons interact with nuclei through various interactions, including scattering (elastic and inelastic scatterings), absorption (capture, fission), and transfer reactions (neutron emission, charged particle ejection). The cross-sections for these interactions vary with incident neutron energy and target nucleus. The complexity of the neutron interactions affects $d^*(10)$ values and LET distributions for the produced charged particles. Consequently, this diversity in interactions and subsequent particle production leads to variability in the values of Q and $h^*(10)$ associated with the neutron energy, as shown in **Figure 26**.

3) Electrons and positrons (Figures 27 and 28)

For electrons and positrons, a noticeable increase in the $d^*(10)$ and $h^*(10)$ values occurs at approximately 2 MeV because electron and positron ranges in the ICRU sphere become about 10 mm. Above this energy, the energy dependence of the $d^*(10)$ and $h^*(10)$ values is small for electrons and positrons.

A distinct difference between electrons and positrons appears below 2 MeV. Positrons produce photons via annihilation with electrons, considerably increasing the energy deposition. Hence, $d^*(10)$ values for positrons substantially exceed than those of electrons due to the photon contribution to energy deposition. Despite these differences, the value of Q remains close to one because the primary contributors to energy deposition are predominantly electrons and positrons in this energy range.

4) Protons (Figure 29)

The values of $d^*(10)$ and $h^*(10)$ for protons increase rapidly around 30 MeV because the range of protons in the ICRU sphere becomes at approximately 10 mm. Beyond 300 MeV, the energy dependence of the $d^*(10)$ and $h^*(10)$ values is small.

The Q value increases gradually with increasing energy, except for a transient and sharp increase at 30 MeV. This phenomenon at 30 MeV is due to the LET distribution of protons within the ICRU sphere. **Figure 35** shows the LET distributions in the 10-mm depth region for incidence with 30- and 40-MeV protons. As defined in **Figure 1**, the Q values remain at one until L = 10 keV μm^{-1} and then increase to 30 as L increases. For incidence of 30-MeV protons, the LET distribution of protons ranges from 3 to 80 keV μm^{-1}, with a peak observed at 15 keV μm^{-1}, where the Q value exceeds one, as indicated in **Figure 1**. Conversely, for incidence of 40-MeV protons, the peak is observed between 2 and 3 keV μm^{-1} in the LET distribution of protons, where the Q value remains at one. The LET distribution shows that higher LET protons also contribute to the energy deposition, but in a smaller proportion. A 30-MeV proton shows elevated LET values for protons at 10-mm depth within the ICRU sphere, corresponding to the position where it almost stops. As a result, this provokes a notable increase in the Q value, as shown in **Figure 29**.

5) Negative and positive muons (Figures 30 and 31)

The energy dependence of the $d^*(10)$ and $h^*(10)$ values shows similarity with negative and positive muons, with a peak at 15 MeV for incident muons. The range of the 15-MeV muon is approximately 10 mm in the ICRU soft tissue[40], and the 15-MeV muon deposits energy in the 10-mm depth region of the ICRU sphere, resulting in a peak in the energy dependence of $h^*(10)$. Regardless of muon energy, the Q values remain consistently close to one, except for the low-energy negative muons where negative muon capture occurs.

6) Negative and positive pions (Figures 32 and 33)

The energy dependence of $d^*(10)$ and $h^*(10)$ shows a peak at 15 MeV for negative and positive pions. This peak corresponds to the range of 15-MeV pions, which is approximately 10 mm within the ICRU sphere. Above this energy, the energy dependence of $d^*(10)$ and $h^*(10)$ is similar for negative and positive pions.

Meanwhile, notable differences are observed in the energy dependence of the $h^*(10)$ and Q values below 15 MeV between negative and positive pions. These differences are due to the peculiar behavior of negative pions. Upon reaching a rest state, negative pions are often captured by a nucleus, producing charged particles that increase the Q and $h^*(10)$ values.

7) Helium ions (Figure 34)

The values of $d^*(10)$ and $h^*(10)$ for helium ions show a rapid increase at energies above 30 MeV n^{-1}, coinciding with a range of about 10 mm within the ICRU sphere. Beyond this energy, the energy dependence of $d^*(10)$ and $h^*(10)$ becomes relatively small.

The value of Q reaches a maximum at about 10 MeV n^{-1} and remains at about 1.5–2 for higher energy ranges. This increase in Q, peaking at 10 MeV n^{-1}, is attributed to the LET distribution of helium ions, contributing substantially to energy deposition.

3.3 Comparison of $H^*(10)$ and E_{max}

A comparison is made between $H^*(10)$, defined in ICRU Reports 39[4] and 51[7] for area monitoring and used worldwide, and E_{max}, which represents the maximum value of effective dose for different directions of incident particle on the anthropomorphic phantoms, as published in ICRP Publication 116[14]. The operational quantities are intended to provide a reasonable, generally conservative, estimate of the protection quantity values associated with an exposure or a potential exposure of persons under various irradiation conditions[3]. The comparison in this section aims to analyze whether $H^*(10)$, the operational quantity, meets the requirements for estimating E_{max}, the protection quantity for external exposures.

The comparison is performed using the dose coefficients $h^*(10)$ and e_{max}, normalized to the particle fluence defined in **Equations (8)** and **(5)**, respectively. The $h^*(10)$ values were obtained from **Tables 2–11**, while the e_{max} values were evaluated from the dataset of ICRP Publication 116. Note that, as defined in **Equation (5)**, the e_{max} values are numerically equal to the h^* values tabulated in **Tables 2–11**. **Figures 36–45** graphically show the energy dependence of $h^*(10)$ and e_{max} (upper graph) and their ratio, $h^*(10)/e_{max}$ (lower graph).

In the graph of $h^*(10)/e_{max}$, a horizontal line is drawn at the point where the vertical axis equals one. $h^*(10)$ exceeds e_{max} for data points plotted above this line, indicating that the operational quantity overestimates the protection quantity, consistent with the objectives of the operational quantity. However, extremely large values of $h^*(10)/e_{max}$ suggest an undesirable level of overestimation. Conversely, $h^*(10)$ is less than e_{max} for data points below the line. In such cases, the operational quantity underestimates the protection quantity, which is undesirable from a radiation monitoring perspective.

Detailed comparisons of $h^*(10)$ and e_{max} for each particle are shown below.

1) Photons (Figure 36)

The values of $h^*(10)/e_{max}$ for photons are ≥ 1 in the energy range from 10 keV to 3 MeV. In particular, at 15–50 keV, $h^*(10)/e_{max}$ is remarkably high, reaching a maximum of 5.3 at 15 keV. However, once the energy exceeds 3 MeV, the ratios fall below one and decrease with increasing energy, dropping below 0.1 beyond 500 MeV. This suggests that $H^*(10)$ is unsuitable for evaluating E_{max} for energies above 3 MeV.

2) Neutrons (Figure 37)

The values of $h^*(10)/e_{max}$ for neutrons undergo complex variations depending on the neutron energy. In the energy range from 1×10^{-9} to 2 MeV, the ratio is almost always greater than one, indicating that $H^*(10)$ conservatively estimates E_{max}. However, in the high-energy region beyond 50 MeV, the ratios fall below one, indicating that $H^*(10)$ underestimates E_{max}.

3) Electrons and positrons (Figures 38 and 39)

For electrons in the energy range from 100 keV to 1.5 MeV, the $e_{\max}$ values are considerably higher than those of $h^*(10)$, resulting in $h^*(10)/e_{\max}$ values becoming substantially lower than one. The increased values of $e_{\max}$ for low-energy electrons are primarily due to the skin dose. This results from the direct exposure of the skin region in the computational phantoms to the incident electrons[14], in contrast to the depth of 10 mm in the ICRU sphere below 2 MeV. The values of $h^*(10)$ increase sharply around 2 MeV, because electrons reach the 10-mm depth in the ICRU sphere. Above 10 MeV, $h^*(10)$ remains nearly constant regardless of the incident electron energy, while $e_{\max}$ increases as electrons reach organs located deep inside the body. Hence, $h^*(10)/e_{\max}$ for electrons is less than one from 100 keV to 2 MeV, exceeds one from 3 to 30 MeV, and falls below one again beyond 40 MeV. Thus, $H^*(10)$ conservatively evaluates $E_{\max}$ only in the energy range from 3 MeV to 30 MeV.

For positrons, because photons produced by positron annihilation with electrons contribute to energy deposition, the $h^*(10)$ values exceed those of electrons below 2 MeV. The values of $h^*(10)/e_{\max}$ remain slightly larger than one in the 100–600 keV range, in contrast to those of electrons. Above approximately 2 MeV, $h^*(10)$ trend for positrons is similar to that of electrons.

4) Protons (Figure 40)

In the energy range from 10 to 30 MeV, the $e_{\max}$ values are much higher than those of $h^*(10)$, resulting in $h^*(10)/e_{\max}$ values becoming remarkably lower than one. From 40 to 60 MeV, $h^*(10)/e_{\max}$ exceeds one, falling below one again above 80 MeV. Similar to electrons, the use of $H^*(10)$ for protons is limited in the 40–60 MeV range for the conservative estimation of $E_{\max}$.

5) Negative and positive muons (Figures 41 and 42)

The energy dependence of $h^*(10)$ shows a peak at around 15 MeV for negative and positive muons, corresponding to the 10-mm range in the ICRU sphere. At other energies, energy dependence for negative and positive muons is small. The values of $h^*(10)/e_{\max}$ fall below one in the 40–150 MeV range and are close to or greater than one at other energies for negative and positive muons.

6) Negative and positive pions (Figures 43 and 44)

Negative and positive pions show a peak at approximately 15 MeV in $h^*(10)$, corresponding to the 10-mm range in the ICRU sphere. Above 15 MeV, the energy dependence of $h^*(10)$ is similar for negative and positive pions.

However, below 15 MeV, negative pions show higher $h^*(10)$ values than positive pions due to the behavior of negative pions described in **Section 3.1.2**. **Figures 43** and **44** reveal that $H^*(10)$ underestimates $E_{\max}$ in several energy regions for negative and positive pions.

7) Helium ions (Figure 45)

The $h^*(10)$ values increase sharply between 30 and 50 MeV n^{-1}, corresponding to the 10-mm range of helium ions in the ICRU sphere. At the lower energies, $h^*(10)$ is considerably smaller than $e_{\max}$. Even above 50 MeV n^{-1}, $h^*(10)$ remains an order of magnitude smaller than $e_{\max}$, indicating that $H^*(10)$ is not suitable for evaluating $E_{\max}$ for helium ions.

The main points of the comparison between $H^*(10)$ and E_{max} for all particles discussed in this section are as follows. The energy dependence of $h^*(10)$ and e_{max} is determined by the interaction properties of each particle in matter. Hence, the $h^*(10)/e_{max}$ values demonstrate a complex and different energy dependence for each particle. While $H^*(10)$ conservatively estimates E_{max} to a reasonable extent in certain energy regions, it greatly overestimates or underestimates E_{max} in many other energy regions. Based on the requirement that the operational quantities provide a reasonable estimate, generally conservative, of the protection quantity values under most irradiance conditions, it can be concluded that $H^*(10)$ has limitations for assessing E_{max} for all irradiance types and energy ranges provided in ICRP Publication 116.

3.4 Comparison of H^*_{max} and E_{max}

In **Section 3.3**, limitations were identified regarding $H^*(10)$ for evaluating E_{max}. This section explores whether H^*_{max} can serve as an alternative operational quantity for evaluating E_{max} by analyzing the energy dependence of their dose coefficients h^*_{max} and e_{max} and their ratio h^*_{max}/e_{max} for each particle.

The h^*_{max} values were obtained from **Tables 2–11**, while the e_{max} values were evaluated from the dataset of ICRP Publication 116[14]. **Figures 46–55** illustrate the energy dependence of h^*_{max} and e_{max} (upper graph) and h^*_{max}/e_{max} (lower graph). A horizontal line in the h^*_{max}/e_{max} graph represents the point where the vertical axis equals one. h^*_{max} exceeds e_{max} for data points above this line, representing an overestimation of the protection quantity by the operational quantity. Conversely, data points below the line indicate an underestimation, which is undesirable for radiation monitoring.

1) Photons (Figure 46)

The h^*_{max}/e_{max} plot shows that H^*_{max} conservatively estimates E_{max} over all energy ranges. However, a significant overestimation occurs for energies below 50 keV, especially at 10 keV by a factor of 46.

2) Neutrons (Figure 47)

Although the values of h^*_{max}/e_{max} mostly exceed one, they fall below one for a limited energy range. H^*_{max} increasingly overestimates E_{max} as the neutron energy decreases towards 1×10^{-9} MeV.

3) Electrons and positrons (Figures 48 and 49)

For electrons, the h^*_{max} values are considerably smaller than those of e_{max} below 30 keV, but they are substantially higher by up to two orders of magnitude from 40 keV to 10 MeV.

For positrons, the h^*_{max}/e_{max} graph demonstrates that H^*_{max} generally overestimates E_{max} and a substantial overestimation occurs in the 500 keV–3 MeV energy range.

4) Protons (Figure 50)

The h^*_{max}/e_{max} values fall slightly below one for a limited energy range; however, their values mostly exceed one excessively below 50 MeV.

5) Negative and positive muons (Figures 51 and 52)

Negative and positive muons have $h^*_{\mathrm{max}}/e_{\mathrm{max}}$ values below one for a limited range; however, their values are generally above one, with excessive highs between 4 and 15 MeV.

6) Negative and positive pions (Figures 53 and 54)

The $h^*_{\mathrm{max}}/e_{\mathrm{max}}$ values exceed one for negative and positive pions over a wide energy range, and the values are especially high below 100 MeV for negative pions.

7) Helium ions (Figure 55)

For helium ions, the $h^*_{\mathrm{max}}/e_{\mathrm{max}}$ values are mostly below one except for the 10–50 MeV n^{-1} energy range, indicating that H^*_{max} underestimates E_{max}. The degree of underestimation varies with the incident energy of helium ions.

The main points of the comparison between H^*_{max} and E_{max} for all particles discussed in this section are as follows. The use of H^*_{max}, which is the maximum dose equivalent along the central axis of the ICRU sphere, reduces the underestimation of E_{max} over a wide energy range compared to $H^*(10)$. However, H^*_{max} generally tends to overestimate E_{max}. Moreover, for certain energy ranges and particles, H^*_{max} shows extreme overestimation of E_{max}, especially in the low-energy region of incident particles, reaching two or three orders of magnitude, leading to excessive radiation protection measures. Therefore, H^*_{max} is not suitable for evaluating E_{max} for all particles presented in ICRP Publication 116.

3.5 Comparison of H^* and E

ICRU Report 95[15] introduced the concept of ambient dose, H^*, as an operational quantity for area monitoring to address the limitations associated with $H^*(10)$. H^* is defined as the maximum effective dose, E_{max}, calculated for various directions of particle incidence in radiation protection contexts; hence $H^* = E_{\mathrm{max}}$. This concept is considerably different from ICRU Reports 39[4] and 51[7], where the numerical values of the operational quantity are based on the dose equivalent at a fixed depth in the ICRU 4-element sphere. H^* is directly related to the effective dose values and will therefore provide a better estimate of the protection quantity. H^* usage simplifies systems of protection and operational quantities and helps users to understand the radiological protection quantities.

Here, a comparison is made between H^* and E for two representative irradiation geometries, antero–posterior (AP) and isotropic (ISO), using their dose coefficients, h^*, e_{AP}, and e_{ISO}, respectively. AP irradiation represents a state where a worker is facing a radiation source, while ISO irradiation represents a situation where a worker is exposed in a highly scattered radiation field and/or facing various directions. Each of **Figures 56–65** presents two graphs: the upper graph shows the dose coefficients for effective dose, e, obtained from ICRP Publication 116[14] for different irradiation geometries, including their maximum values, e_{max}, and lower graph shows the ratios, h^*/e_{AP} and h^*/e_{ISO}. Additionally, as defined in **Equation (5)**, the e_{max} values are numerically equal to the h^* values provided in **Tables 2–11**.

In the graphs of h^*/e, a horizontal line at the value of one indicates that h^* is equal to e_{AP} and e_{ISO}. Data points above this line correspond to h^* higher than e_{AP} and e_{ISO}, implying that the protection quantity E is overestimated by the operational quantity H^*. Conversely, data points below one imply that

H^* underestimates E, although it is theoretically impossible for h^*/e_{AP} and h^*/e_{ISO} to fall below one as h^* is defined based on $e_{\max}$.

1) Photons (Figure 56)

h^*/e_{AP} and h^*/e_{ISO} intersect at approximately 10 MeV. Below 10 MeV, the effective dose for AP irradiation is maximized among all geometries, leading to the coincidence of h^* and e_{AP}. Conversely, the h^* values exceed those of e_{ISO}. As the energy exceeds 10 MeV, photons penetrate deeply into the human body, causing the effective dose for ISO irradiation to exceed that for AP irradiation. Consequently, h^*/e_{ISO} approaches one, while the ratios of h^*/e_{AP} exceed one.

Over the entire energy range, the operational quantity H^* consistently overestimates effective dose E, with the magnitude of the overestimation reaching a maximum of 3.4 times for h^*/e_{AP} at 10 GeV.

2) Neutrons (Figure 57)

The e values for neutrons (upper graph) are dependent on the incident direction and energy, ranging from 1×10^{-9} to 100 MeV. However, beyond 100 MeV, these values show a reduced dependence on the incident direction and energy of neutrons.

The lower graph shows that h^*/e_{AP} and h^*/e_{ISO} intersect at about 100 MeV. Similar to photons, the effective dose for AP irradiation is maximized among all geometries up to about 100 MeV. Beyond this energy, the effective dose for ISO irradiation exceeds that for AP irradiation.

Over the entire energy range, H^* consistently overestimates E. This overestimation reaches a maximum of 2.4 times for h^*/e_{AP} at 1×10^{-9} MeV.

3) Electrons and positrons (Figures 58 and 59)

For electrons and positrons, the e values for AP irradiation are maximized in the energy range from 10 keV to 100 MeV, making the h^*/e_{AP} values are equal to one. Above 100 MeV, the e_{ISO} values become higher than those of e_{AP}.

While the h^*/e values vary with the incident energy of electrons and positrons, their peak values reach 3.1 for h^*/e_{ISO} at 2 MeV for electrons and 3.0 for h^*/e_{ISO} at 2 MeV for positrons.

4) Protons (Figure 60)

The e values for protons are dependent on the incident direction and energy between 1 and 200 MeV. However, the values show less dependence on the incident direction and energy of protons beyond 200 MeV. The range of 200-MeV protons in the human body is approximately 26 cm and passes through the trunk, resulting in reduced directional dependence.

While the values of h^*/e_{AP} and h^*/e_{ISO} vary with the energy of the incident protons, the maximum value reaches 3.1 for h^*/e_{ISO} at 20 MeV.

5) Negative and positive muons (Figures 61 and 62)

The energy dependence of e for negative and positive muons is quite similar, as shown in **Figures 61** and **62**, respectively. Up to 60 MeV, the e values depend on the incident direction and energy of muons. However, beyond this energy, the values of e become less dependent on the incident direction and energy of muons, as they penetrate through the trunk.

For negative and positive muons, the peak value reaches 2.6 for h^*/e_{ISO} at 10 MeV and the h^*/e_{AP} and h^*/e_{ISO} values are nearly one above 100 MeV.

6) Negative and positive pions (Figures 63 and 64)

The e values for negative and positive pions depend on the incident direction and energy of pions. The maximum value of h^*/e reaches 3.0 for h^*/e_{ISO} at 8 MeV for negative pions, while that of positive pions reaches 2.8 for h^*/e_{ISO} at 10 MeV.

7) Helium ions (Figure 65)

The e values for helium ions are dependent on the incident direction of the helium ion between 15 and 150 MeV n^{-1}. However, as the energy reaches 200 MeV n^{-1}, the range of helium ions extends across the trunk, leading to a reduced directional dependence of the e values.

The observed peak of h^*/e for helium ions reaches 3.2 for h^*/e_{ISO} at 20 MeV n^{-1}.

The main points of the comparison between H^* and E for all particles discussed in this section are as follows. Because H^* is defined as the maximum effective dose, E_{max}, calculated for various directions of particle incidence, it does not underestimate E. H^* reasonably estimates E for the AP and ISO incident conditions, which are typical workplace irradiation geometries. Although occasional overestimation of E by H^* may occur, such instances are limited to a factor of 3 or less. This would be acceptable than situations where $H^*(10)$ or H^*_{max} often overestimates E by two or three orders of magnitude.

3.6 Discussion on appropriate quantity for use in area monitoring for assessment of effective dose from external radiation

Sections 3.3–3.5 compared the relationship between three quantities used for area monitoring — ambient dose equivalent $H^*(10)$, maximum dose equivalent H^*_{max}, and ambient dose H^* — and effective dose E for external irradiation from various particles, including photons, neutrons, electrons, positrons, protons, muons, pions, and helium ions.

The ambient dose equivalent $H^*(10)$ is defined as the dose equivalent at a fixed depth of 10 mm in the ICRU sphere irradiated in the expanded and aligned field. The effective dose E is defined as the weighted sum of absorbed doses for all specified organs and tissues in the human body irradiated from different directions. Comparison of the dose coefficients for $H^*(10)$ and E, $h^*(10)$ and e, respectively, shows that the $h^*(10)$ and e values have different energy dependencies for each particle. Hence, $H^*(10)$ underestimates or overestimates E under many conditions of the type and energy of incident particles.

Compared with $H^*(10)$, the maximum dose equivalent H^*_{max}, defined as the maximum value of the dose equivalent along the central axis of the ICRU sphere, reduces the underestimation of E. However, H^*_{max} tends to extremely overestimate E, especially for the incidence of low-energy particles.

The comparative analysis across all particles highlights the consistent and conservative nature of H^* in the evaluation of E for various incident directions and particle energies provided in ICRP Publication 116[14]. While H^* overestimates E occasionally, such instances are limited to a factor of 3 or less. Unlike $H^*(10)$ and H^*_{max}, which exhibit significant underestimation or overestimation of E by two or three orders of magnitude, overestimation by H^* is more controlled. The potential for extreme overestimation in $H^*(10)$ and H^*_{max} can lead to unwarranted and excessive radiation protection measures. Therefore, H^* is aligned with the criteria of the operational quantity, aiming to provide a reasonable, generally conservative, estimate of the protection quantity values for various exposure scenarios[3].

Consequently, H^* emerges as a suitable candidate for evaluating E over all radiation types and energy ranges presented in ICRP Publication 116. This confirms the decision of the ICRU Report Committee 26 to adopt H^* for area monitoring.

4 Conclusion

The present study analyzed the relationship between three quantities used for area monitoring — ambient dose equivalent $H^*(10)$, maximum dose equivalent H^*_{max}, and ambient dose H^* — and effective dose E for external irradiation from various particles, including photons, neutrons, electrons, positrons, protons, muons, pions, and helium ions. The analysis reveals limitations of $H^*(10)$ and H^*_{max}, and highlights the superiority of H^* for estimating E over various particle types and energy ranges covered in ICRP Publication 116. The results support the use of H^* for area monitoring due to its tendency to provide a controlled margin of overestimation in estimating E compared to $H^*(10)$ and H^*_{max}. Radiation monitoring using $H^*(10)$ and H^*_{max} can result in substantial underestimation or overestimation of E, while H^* provides a more consistent estimate that is more in line with protection quantities. The conclusion of this study supports the decision of the Report Committee 26 of ICRU to recommend H^* for the estimation of E for various exposure scenarios. This recommendation provides reasonable estimates of E in radiation monitoring, particularly in situations where various types of radiation are encountered, such as the use of radiation in the medical and academic fields and exposure in aviation. The proposed adoption of H^* increases the reliability of practical radiation monitoring and ensures more effective and appropriate radiation protection measures.

Acknowledgements

The author is grateful to the members, consultants, and sponsors of the ICRU Report Committee 26 for their support and fruitful discussions. The calculations described in this report were performed on the HPE SGI8600 supercomputer at the Center for Computational Science & e-Systems, Japan Atomic Energy Agency.

References

1) ICRP. Recommendations of the International Commission on Radiological Protection. International Commission on Radiological Protection, ICRP Publication 26, Ann. ICRP 1(3), 1977, 53p.

2) ICRP. 1990 Recommendations of the International Commission on Radiological Protection. International Commission on Radiological Protection, ICRP Publication 60, Ann. ICRP 21(1–3), 1991, 201p.

3) ICRP. The 2007 Recommendations of the International Commission on Radiological Protection. International Commission on Radiological Protection, ICRP Publication 103, Ann. ICRP 37(2–4), 2007, 332p.

4) ICRU. Determination of Dose Equivalents Resulting from External Radiation Sources. International Commission on Radiation Units and Measurements, ICRU Report 39, J. ICRU os-20(2), 1985, 10p.

5) ICRU. Determination of Dose Equivalents from External Radiation Sources – Part 2. International Commission on Radiation Units and Measurements, ICRU Report 43, J. ICRU os-22(2), 1988, 51p.

6) ICRU. Measurements of Dose Equivalents from External Photon and Electron Radiations. International Commission on Radiation Units and Measurements, ICRU Report 47, J. ICRU os-24(2), 1992, 40p.

7) ICRU. Quantities and Units in Radiation Protection Dosimetry. International Commission on Radiation Units and Measurements, ICRU Report 51, J. ICRU os-26(2), 1993, 19p.

8) ICRU. Determination of Operational Dose Equivalent Quantities for Neutrons. International Commission on Radiation Units and Measurements, ICRU Report 66, J. ICRU 1(3), 2001, 94p.

9) ICRP. Conversion Coefficients for Use in Radiological Protection Against External Radiation. International Commission on Radiological Protection, ICRP Publication 74, Ann. ICRP 26(3–4), 1996, 205p.

10) ICRU. Conversion Coefficients for Use in Radiological Protection Against External Radiation. International Commission on Radiation Units and Measurements, ICRU Report 57, J. ICRU os-29(2), 1998, 137p.

11) Bartlett, D.T., Dietze, G. ICRU Operational Quantities. Radiation Protection Dosimetry, 139(4), 2010, pp. 475–476.

12) ICRU. Reference Data for the Validation of Doses from Cosmic-Radiation Exposure of Aircraft Crew. International Commission on Radiation Units and Measurements, ICRU Report 84, J. ICRU 10(2), 2010, 35p.

13) Endo, A. “Operational Quantities and New Approach by ICRU”. Proceedings of the Third International Symposium on the System of Radiological Protection. Seoul, Korea, 20-22 October 2015, International Commission on Radiological Protection. Ann. ICRP 45, Supplement 1, 2016, pp. 178–187.

14) ICRP. Conversion Coefficients for Radiological Protection Quantities for External Radiation Exposures. International Commission on Radiological Protection, ICRP Publication 116, Ann. ICRP 40(2–5), 2010, 257p.

15) ICRU. Operational Quantities for External Radiation Exposure. International Commission on Radiation Units and Measurements, ICRU Report 95, J. ICRU 20(1), 2020, 130p.

16) ICRU. Radiation Protection Instrumentation and Its Application. International Commission on Radiation Units and Measurements, ICRU Report 20, J. ICRU os-11(1), 1971, 60p.

17) ICRU. Radiation Quantities and Units. International Commission on Radiation Units and Measurements, ICRU Report 19, J. ICRU os-10(2), 1971, 20p.

18) ICRU. Conceptual Basis for the Determination of Dose Equivalent. International Commission on Radiation Units and Measurements, ICRU Report 25, J. ICRU os-13(2), 1976, 21p.

19) Pelliccioni, M. Overview of Fluence-to-Effective Dose and Fluence-to-Ambient Dose Equivalent Conversion Coefficients for High Energy Radiation Calculated Using the FLUKA Code. Radiation Protection Dosimetry, 88(4), 2000, pp. 279–297.

20) ICRP. Adult Reference Computational Phantoms. International Commission on Radiological Protection, ICRP Publication 110. Ann. ICRP 39(2), 2009, 164p.

21) Sato, T., Iwamoto, Y., Hashimoto, S., Ogawa, T., Furuta, T., Abe, S., Kai, T., Matsuya, Y., Matsuda, N., Hirata, Y., Sekikawa, T., Yao, L., Tsai, P.E., Ratliff, H.N., Iwase, H., Sakaki, Y., Sugihara, K., Shigyo, N., Sihver, L., Niita, K. Recent Improvements of the Particle and Heavy Ion Transport Code System – PHITS Version 3.33. J. Nucl. Sci. Technol., 61(1), 2024, pp. 127–135.

22) Nara, Y., Otuka, H., Ohnishi, A., Niita, K., Chiba, S. Relativistic Nuclear Collisions at 10A GeV Energies from p+Be to Au+Au with the Hadronic Cascade Model. Phys. Rev., C61(2), 2000, 024901.

23) Boudard, A., Cugnon, J., David, J. C., Leray, S., Mancusi, D. New Potentialities of the Liège Intranuclear Cascade Model for Reactions Induced by Nucleons and Light Charged Particles. Phys. Rev., C87(1), 2013, 014606.

24) Ogawa, T., Sato, T., Hashimoto, S., Satoh, D., Tsuda, S., Niita, K. Energy-dependent Fragmentation Cross Sections of Relativistic C-12. Phys. Rev., C92(2), 2015, 024614.

25) Furihata, S. Statistical Analysis of Light Fragment Production from Medium Energy Proton-induced Reactions. Nucl. Instrum. Meth., B171(3), 2000, pp. 251–258.

26) Geissel, H., Scheidenberger, C., Malzacher, P., Kunzendorf, J., Weick, H. “ATIMA”. http://web-docs.gsi.de/~weick/atima/ (accessed 2023-11-28).

27) Shibata, K., Iwamoto, O., Nakagawa, T., Iwamoto, N., Ichihara, A., Kunieda, S., Chiba, S., Furutaka, K., Otuka, N., Ohsawa, T., Murata, T., Matsunobu, H., Zukeran, A., Kamada, S., Katakura, J. JENDL-4.0: A New Library for Nuclear Science and Engineering. J. Nucl. Sci. Technol., 48(1), 2011, pp. 1–30.

28) Hirayama, H., Namito, Y., Bielajew, A.F., Wilderman, S.J., Nelson, W.R. The EGS5 Code System. Stanford Linear Accelerator Center, SLAC-R-730, 2005, 441p; High Energy Accelerator Research Organization, KEK Report 2005-8, 2005, 441p.

29) Noda, S., Hashimoto, S., Sato, T., Fukahori, T., Chiba, S., Niita, K. Improvement of Photonuclear Reaction Model Below 140 MeV in the PHITS Code. J. Nucl. Sci. Technol., 52(1), 2015, pp. 57–62.

30) Abe, S., Sato, T. Implementation of Muon Interaction Models in PHITS. J. Nucl. Sci. Technol., 54(1), 2016, pp. 101–110.

31) Iwamoto, Y., Niita, K., Sakamoto, Y., Sato, T., Matsuda, N. "Validation of the Event Generator Mode in the PHITS Code and Its Application". Proceedings of International Conference on Nuclear Data for Science and Technology (ND2007), Vol. 2. Nice, France, 22-27 April 2007, Commissariat à l'énergie atomique. EDP sciences, 2008, pp. 945–948.

32) Ferrari, A., Sala, P.R., Fassò, A., Ranft, J. FLUKA: A Multi-particle Transport Code. European Organization for Nuclear Research, CERN-2005-010, 2005, 439p.

33) Ferrari, A., Pelliccioni, M. On the Conversion Coefficients from Fluence to Ambient Dose Equivalent. Radiation Protection Dosimetry, 51(4), 1994, pp. 251–255.

34) ICRU. Radiation Quantities and Units. International Commission on Radiation Units and Measurements, ICRU Report 33, J. ICRU os-17(2), 1980, 25p.

35) Ferrari, A., Pelliccioni, M. "Fluence-to-Dose Equivalent Conversion Coefficients for Electrons and Photons of Energy up to 10 GeV". Proceedings of the 8th International Conference on Radiation Shielding. Arlington, Texas, USA, 24-28 April 1994, American Nuclear Society. 1994, pp. 893–899.

36) Ferrari, A., Pelliccioni, M. Dose Equivalents for Monoenergetic Electrons Incident on the ICRU Sphere. Radiation Protection Dosimetry, 55(3), 1994, pp. 207–210.

37) Ferrari, A., Pelliccioni, M. Dose Equivalents for Monoenergetic Positrons Incident on the ICRU Sphere. Radiation Protection Dosimetry, 55(4), 1994, pp. 309–312.

38) Ferrari, A., Pelliccioni, M. Fluence to Dose Equivalent Conversion Data and Effective Quality Factors for High Energy Neutrons. Radiation Protection Dosimetry, 76(4), 1998, pp. 215–224.

39) Pelliccioni, M. Fluence to Dose Equivalent Conversion Data and Radiation Weighting Factors for High Energy Radiation. Radiation Protection Dosimetry, 77(4), 1998, pp. 159–170.

40) Groom, D.E., Mokhov, N.V., Striganov, S.I. Muon Stopping-power and Range Tables: 10 MeV–100 TeV. Atomic Data and Nuclear Data Tables, 78(2), 2001, pp. 183–356.

Table 1 Particles and energy ranges for calculation of dose coefficients.

Particle type	Lower energy (MeV)	Upper energy (MeV)
Photon	1.0E-02	1.0E+04
Neutron	1.0E-09	1.0E+04
Electron	1.0E-01	1.0E+04
Positron	1.0E-01	1.0E+04
Proton	1.0E+01	1.0E+04
Negative muon	1.0E+00	1.0E+04
Positive muon	1.0E+00	1.0E+04
Negative pion	1.0E+00	2.0E+05
Positive pion	1.0E+00	2.0E+05
Helium ion‡	2.0E+00	1.0E+05

‡ The unit of energy for helium ion is MeV n^{-1} (MeV per nucleon).

Table 2 Photons: $d^*(10)$, $h^*(10)$, Q, h^*_{max}, and h^* values.

E_p / MeV	$d^*(10)$ / Gy cm^2	$h^*(10)$ / Sv cm^2	Q ‡	h^*_{max} / Sv cm^2	h^* / Sv cm^2 §
1.0E-02	6.90E-14	6.90E-14	1.00	3.12E-12	6.85E-14
1.5E-02	8.25E-13	8.25E-13	1.00	2.51E-12	1.56E-13
2.0E-02	1.01E-12	1.01E-12	1.00	1.67E-12	2.25E-13
3.0E-02	8.22E-13	8.22E-13	1.00	9.23E-13	3.12E-13
4.0E-02	6.30E-13	6.30E-13	1.00	6.72E-13	3.50E-13
5.0E-02	5.15E-13	5.15E-13	1.00	5.59E-13	3.69E-13
6.0E-02	5.14E-13	5.14E-13	1.00	5.27E-13	3.89E-13
7.0E-02	5.30E-13	5.30E-13	1.00	5.34E-13	4.11E-13
8.0E-02	5.49E-13	5.49E-13	1.00	5.53E-13	4.43E-13
1.0E-01	6.22E-13	6.22E-13	1.00	6.29E-13	5.18E-13
1.5E-01	8.98E-13	8.98E-13	1.00	9.07E-13	7.47E-13
2.0E-01	1.21E-12	1.21E-12	1.00	1.23E-12	1.00E-12
3.0E-01	1.76E-12	1.76E-12	1.00	1.88E-12	1.51E-12
4.0E-01	2.39E-12	2.39E-12	1.00	2.46E-12	2.00E-12
5.0E-01	2.90E-12	2.90E-12	1.00	3.03E-12	2.47E-12
6.0E-01	3.31E-12	3.31E-12	1.00	3.53E-12	2.91E-12
8.0E-01	4.23E-12	4.23E-12	1.00	4.70E-12	3.73E-12
1.0E+00	5.26E-12	5.26E-12	1.00	5.44E-12	4.49E-12
1.5E+00	7.12E-12	7.12E-12	1.00	7.12E-12	6.12E-12
2.0E+00	8.50E-12	8.50E-12	1.00	8.60E-12	7.48E-12
3.0E+00	1.03E-11	1.03E-11	1.00	1.09E-11	9.75E-12
4.0E+00	1.09E-11	1.09E-11	1.00	1.34E-11	1.17E-11
5.0E+00	1.04E-11	1.04E-11	1.00	1.49E-11	1.34E-11
6.0E+00	1.02E-11	1.02E-11	1.00	1.71E-11	1.50E-11
8.0E+00	9.48E-12	9.48E-12	1.00	2.12E-11	1.86E-11
1.0E+01	8.74E-12	8.74E-12	1.00	2.44E-11	2.21E-11
1.5E+01	8.44E-12	8.44E-12	1.00	3.34E-11	3.04E-11
2.0E+01	8.48E-12	9.20E-12	1.09	4.15E-11	3.82E-11
3.0E+01	8.88E-12	1.36E-11	1.53	6.13E-11	5.13E-11
4.0E+01	9.10E-12	1.49E-11	1.63	7.71E-11	6.18E-11
5.0E+01	9.23E-12	1.13E-11	1.22	8.94E-11	7.23E-11
6.0E+01	9.43E-12	9.73E-12	1.03	1.04E-10	8.21E-11
8.0E+01	9.98E-12	1.11E-11	1.11	1.28E-10	9.81E-11
1.0E+02	9.93E-12	1.03E-11	1.04	1.50E-10	1.10E-10
1.5E+02	1.00E-11	1.01E-11	1.01	1.95E-10	1.30E-10
2.0E+02	1.05E-11	1.07E-11	1.02	2.23E-10	1.44E-10
3.0E+02	1.28E-11	1.90E-11	1.49	2.65E-10	1.61E-10
4.0E+02	1.35E-11	2.15E-11	1.59	2.93E-10	1.73E-10
5.0E+02	1.29E-11	1.73E-11	1.34	3.11E-10	1.81E-10
6.0E+02	1.29E-11	1.76E-11	1.37	3.26E-10	1.87E-10
8.0E+02	1.29E-11	1.62E-11	1.26	3.48E-10	1.96E-10

‡ Q value at 10-mm depth

§ h^* cited from ICRU Report 95[15)]

Table 2 (Continued).

E_p / MeV	$d^*(10)$ / Gy cm^2	$h^*(10)$ / Sv cm^2	Q ‡	h^*_{max} / Sv cm^2	h^* / Sv cm^2 §
1.0E+03	1.30E-11	1.64E-11	1.27	3.66E-10	2.06E-10
1.5E+03	1.30E-11	1.62E-11	1.24	3.97E-10	2.13E-10
2.0E+03	1.31E-11	1.59E-11	1.22	4.18E-10	2.36E-10
3.0E+03	1.32E-11	1.61E-11	1.22	4.48E-10	2.53E-10
4.0E+03	1.32E-11	1.57E-11	1.19	4.70E-10	2.67E-10
5.0E+03	1.32E-11	1.53E-11	1.16	4.87E-10	2.77E-10
6.0E+03	1.32E-11	1.54E-11	1.17	5.01E-10	2.85E-10
8.0E+03	1.32E-11	1.49E-11	1.13	5.22E-10	2.99E-10
1.0E+04	1.33E-11	1.54E-11	1.16	5.39E-10	3.07E-10

‡ Q value at 10-mm depth
§ h^* cited from ICRU Report 95[15)]

Table 3 Neutrons: $d^*(10)$, $h^*(10)$, Q, h^*_{max}, and h^* values.

E_p / MeV	$d^*(10)$ / Gy cm^2	$h^*(10)$ / Sv cm^2	Q ‡	h^*_{max} / Sv cm^2	h^* / Sv cm^2 §
1.0E-09	1.67E-12	6.42E-12	3.84	1.73E-11	3.09E-12
1.0E-08	2.13E-12	9.08E-12	4.26	1.50E-11	3.55E-12
2.5E-08	2.39E-12	1.09E-11	4.57	1.24E-11	4.00E-12
1.0E-07	2.91E-12	1.28E-11	4.42	1.28E-11	5.20E-12
2.0E-07	3.01E-12	1.31E-11	4.37	1.37E-11	5.87E-12
5.0E-07	3.07E-12	1.26E-11	4.12	1.41E-11	6.59E-12
1.0E-06	3.21E-12	1.35E-11	4.21	1.49E-11	7.03E-12
2.0E-06	3.20E-12	1.24E-11	3.89	1.47E-11	7.39E-12
5.0E-06	3.13E-12	1.14E-11	3.64	1.45E-11	7.71E-12
1.0E-05	3.01E-12	1.07E-11	3.57	1.45E-11	7.82E-12
2.0E-05	2.86E-12	1.01E-11	3.52	1.44E-11	7.84E-12
5.0E-05	2.77E-12	9.71E-12	3.51	1.41E-11	7.82E-12
1.0E-04	2.66E-12	9.31E-12	3.51	1.35E-11	7.79E-12
2.0E-04	2.64E-12	9.07E-12	3.44	1.34E-11	7.73E-12
5.0E-04	2.46E-12	7.83E-12	3.18	1.30E-11	7.54E-12
1.0E-03	2.47E-12	7.89E-12	3.20	1.26E-11	7.54E-12
2.0E-03	2.42E-12	8.02E-12	3.31	1.25E-11	7.61E-12
5.0E-03	2.45E-12	7.73E-12	3.16	1.20E-11	7.97E-12
1.0E-02	2.69E-12	9.59E-12	3.56	1.22E-11	9.11E-12
2.0E-02	3.10E-12	1.45E-11	4.68	1.77E-11	1.22E-11
3.0E-02	3.70E-12	2.06E-11	5.58	2.84E-11	1.57E-11
5.0E-02	4.59E-12	3.56E-11	7.75	5.08E-11	2.30E-11
7.0E-02	5.41E-12	5.16E-11	9.54	7.39E-11	3.06E-11
1.0E-01	6.72E-12	7.68E-11	11.42	1.05E-10	4.19E-11
1.5E-01	8.62E-12	1.19E-10	13.84	1.58E-10	6.06E-11
2.0E-01	1.06E-11	1.58E-10	14.93	2.01E-10	7.88E-11
3.0E-01	1.33E-11	2.23E-10	16.83	2.69E-10	1.14E-10
5.0E-01	1.80E-11	3.04E-10	16.89	3.28E-10	1.77E-10
7.0E-01	2.20E-11	3.55E-10	16.16	3.76E-10	2.32E-10
9.0E-01	2.57E-11	4.05E-10	15.76	4.22E-10	2.79E-10
1.0E+00	2.82E-11	4.46E-10	15.81	5.11E-10	3.01E-10
1.2E+00	2.80E-11	4.13E-10	14.76	4.47E-10	3.30E-10
1.5E+00	3.03E-11	4.18E-10	13.79	4.49E-10	3.65E-10
2.0E+00	3.58E-11	4.37E-10	12.22	4.44E-10	4.07E-10
3.0E+00	4.21E-11	4.30E-10	10.21	4.38E-10	4.58E-10
4.0E+00	4.94E-11	4.51E-10	9.11	4.72E-10	4.83E-10
5.0E+00	4.84E-11	3.86E-10	7.98	4.14E-10	4.94E-10
6.0E+00	4.78E-11	3.43E-10	7.18	3.97E-10	4.98E-10
7.0E+00	5.14E-11	3.44E-10	6.69	3.86E-10	4.99E-10
8.0E+00	5.48E-11	3.61E-10	6.59	3.89E-10	4.99E-10
9.0E+00	5.91E-11	4.30E-10	7.28	4.44E-10	5.00E-10

‡ Q value at 10-mm depth

§ h^* cited from ICRU Report 95[15)]

Table 3 (Continued).

E_p / MeV	$d^*(10)$ / Gy cm^2	$h^*(10)$ / Sv cm^2	Q ‡	h^*_{max} / Sv cm^2	h^* / Sv cm^2 §
1.0E+01	6.55E-11	4.94E-10	7.55	5.12E-10	5.00E-10
1.2E+01	6.83E-11	4.84E-10	7.09	4.99E-10	4.99E-10
1.4E+01	7.28E-11	5.49E-10	7.55	5.49E-10	4.95E-10
1.5E+01	7.28E-11	5.39E-10	7.41	5.63E-10	4.93E-10
2.1E+01	6.90E-11	4.78E-10	6.93	5.14E-10	4.74E-10
3.0E+01	7.26E-11	4.65E-10	6.41	4.92E-10	4.53E-10
5.0E+01	6.46E-11	3.69E-10	5.72	4.28E-10	4.33E-10
7.5E+01	5.50E-11	3.25E-10	5.91	3.91E-10	4.39E-10
1.0E+02	5.10E-11	3.21E-10	6.29	3.95E-10	4.44E-10
1.3E+02	4.88E-11	3.15E-10	6.44	4.09E-10	4.46E-10
1.5E+02	4.84E-11	3.20E-10	6.61	4.17E-10	4.46E-10
1.8E+02	4.93E-11	3.29E-10	6.67	4.33E-10	4.47E-10
2.0E+02	5.01E-11	3.41E-10	6.80	4.41E-10	4.48E-10
3.0E+02	5.54E-11	3.73E-10	6.73	4.89E-10	4.73E-10
4.0E+02	6.17E-11	4.24E-10	6.87	5.52E-10	5.15E-10
5.0E+02	7.19E-11	4.65E-10	6.46	6.32E-10	5.33E-10
6.0E+02	7.99E-11	5.01E-10	6.27	6.91E-10	5.69E-10
7.0E+02	8.70E-11	5.38E-10	6.18	7.46E-10	6.25E-10
8.0E+02	9.23E-11	5.51E-10	5.96	7.73E-10	6.38E-10
9.0E+02	9.44E-11	5.53E-10	5.86	7.89E-10	6.45E-10
1.0E+03	9.85E-11	5.56E-10	5.65	8.13E-10	6.63E-10
2.0E+03	1.08E-10	5.81E-10	5.36	8.99E-10	7.69E-10
5.0E+03	1.33E-10	6.77E-10	5.08	1.30E-09	1.04E-09
1.0E+04	1.44E-10	7.00E-10	4.86	1.71E-09	1.39E-09

‡ Q value at 10-mm depth

§ h^* cited from ICRU Report 95[15)]

Table 4 Electrons: $d^*(10)$, $h^*(10)$, Q, h^*_{max}, and h^* values.

E_p / MeV	$d^*(10)$ / Gy cm^2	$h^*(10)$ / Sv cm^2	Q ‡	h^*_{max} / Sv cm^2	h^* / Sv cm^2 §
1.0E-01	7.28E-16	7.27E-16	1.00	3.05E-15	2.75E-13
1.5E-01	1.41E-15	1.41E-15	1.00	5.57E-15	4.18E-13
2.0E-01	2.17E-15	2.17E-15	1.00	8.24E-15	5.69E-13
3.0E-01	4.38E-15	4.38E-15	1.00	1.58E-14	8.89E-13
4.0E-01	6.97E-15	6.97E-15	1.00	1.82E-11	1.24E-12
5.0E-01	1.04E-14	1.04E-14	1.00	1.00E-10	1.63E-12
6.0E-01	1.49E-14	1.49E-14	1.00	2.02E-10	2.05E-12
8.0E-01	2.50E-14	2.50E-14	1.00	4.00E-10	4.04E-12
1.0E+00	3.78E-14	3.78E-14	1.00	5.07E-10	7.10E-12
1.5E+00	8.38E-14	8.38E-14	1.00	4.90E-10	1.50E-11
2.0E+00	7.35E-12	7.35E-12	1.00	4.98E-10	2.24E-11
3.0E+00	3.26E-10	3.26E-10	1.00	4.66E-10	3.61E-11
4.0E+00	4.47E-10	4.47E-10	1.00	4.47E-10	4.82E-11
5.0E+00	4.27E-10	4.27E-10	1.00	4.36E-10	5.93E-11
6.0E+00	3.85E-10	3.85E-10	1.00	4.30E-10	7.06E-11
8.0E+00	3.53E-10	3.53E-10	1.00	4.14E-10	9.79E-11
1.0E+01	3.27E-10	3.27E-10	1.00	3.80E-10	1.25E-10
1.5E+01	3.19E-10	3.19E-10	1.00	3.69E-10	1.88E-10
2.0E+01	3.16E-10	3.16E-10	1.00	3.52E-10	2.36E-10
3.0E+01	3.11E-10	3.11E-10	1.00	3.46E-10	3.02E-10
4.0E+01	3.11E-10	3.11E-10	1.00	3.48E-10	3.29E-10
5.0E+01	3.11E-10	3.11E-10	1.00	3.51E-10	3.37E-10
6.0E+01	3.13E-10	3.13E-10	1.00	3.53E-10	3.44E-10
8.0E+01	3.12E-10	3.12E-10	1.00	3.59E-10	3.58E-10
1.0E+02	3.09E-10	3.09E-10	1.00	3.63E-10	3.66E-10
1.5E+02	3.14E-10	3.14E-10	1.00	3.99E-10	3.79E-10
2.0E+02	3.07E-10	3.07E-10	1.00	4.36E-10	3.88E-10
3.0E+02	3.14E-10	3.18E-10	1.01	4.86E-10	4.11E-10
4.0E+02	3.12E-10	3.12E-10	1.00	5.30E-10	4.35E-10
5.0E+02	3.11E-10	3.11E-10	1.00	5.75E-10	4.49E-10
6.0E+02	3.16E-10	3.16E-10	1.00	6.00E-10	4.64E-10
8.0E+02	3.10E-10	3.10E-10	1.00	6.38E-10	4.88E-10
1.0E+03	3.12E-10	3.12E-10	1.00	6.76E-10	5.08E-10
1.5E+03	3.11E-10	3.11E-10	1.00	7.70E-10	5.25E-10
2.0E+03	3.11E-10	3.11E-10	1.00	8.11E-10	5.68E-10
3.0E+03	3.11E-10	3.11E-10	1.00	8.78E-10	6.08E-10
4.0E+03	3.16E-10	3.16E-10	1.00	9.52E-10	6.38E-10
5.0E+03	3.06E-10	3.06E-10	1.00	9.72E-10	6.61E-10
6.0E+03	3.11E-10	3.11E-10	1.00	1.08E-09	6.83E-10
8.0E+03	3.11E-10	3.11E-10	1.00	1.09E-09	7.16E-10
1.0E+04	3.21E-10	3.21E-10	1.00	1.17E-09	7.42E-10

‡ Q value at 10-mm depth

§ h^* cited from ICRU Report 95[15)]

Table 5 Positrons: $d^*(10)$, $h^*(10)$, Q, h^*_{max}, and h^* values.

E_p / MeV	$d^*(10)$ / Gy cm^2	$h^*(10)$ / Sv cm^2	Q ‡	h^*_{max} / Sv cm^2	h^* / Sv cm^2 §
1.0E-01	5.76E-12	5.76E-12	1.00	9.66E-12	3.53E-12
1.5E-01	5.68E-12	5.68E-12	1.00	1.00E-11	3.67E-12
2.0E-01	5.81E-12	5.80E-12	1.00	9.60E-12	3.84E-12
3.0E-01	5.69E-12	5.69E-12	1.00	1.06E-11	4.16E-12
4.0E-01	5.92E-12	5.92E-12	1.00	2.93E-11	4.52E-12
5.0E-01	6.40E-12	6.40E-12	1.00	1.15E-10	4.90E-12
6.0E-01	6.18E-12	6.18E-12	1.00	2.18E-10	5.36E-12
8.0E-01	6.33E-12	6.33E-12	1.00	4.12E-10	7.41E-12
1.0E+00	6.46E-12	6.46E-12	1.00	5.11E-10	1.05E-11
1.5E+00	7.31E-12	7.31E-12	1.00	4.82E-10	1.83E-11
2.0E+00	1.73E-11	1.73E-11	1.00	4.85E-10	2.57E-11
3.0E+00	3.42E-10	3.42E-10	1.00	4.54E-10	3.91E-11
4.0E+00	4.22E-10	4.22E-10	1.00	4.22E-10	5.10E-11
5.0E+00	3.97E-10	3.97E-10	1.00	4.30E-10	6.17E-11
6.0E+00	3.57E-10	3.57E-10	1.00	4.03E-10	7.29E-11
8.0E+00	3.32E-10	3.32E-10	1.00	3.73E-10	9.90E-11
1.0E+01	3.19E-10	3.19E-10	1.00	3.64E-10	1.26E-10
1.5E+01	3.11E-10	3.11E-10	1.00	3.39E-10	1.84E-10
2.0E+01	3.14E-10	3.14E-10	1.00	3.34E-10	2.29E-10
3.0E+01	3.07E-10	3.07E-10	1.00	3.30E-10	2.94E-10
4.0E+01	3.12E-10	3.12E-10	1.00	3.24E-10	3.20E-10
5.0E+01	3.07E-10	3.07E-10	1.00	3.32E-10	3.27E-10
6.0E+01	3.10E-10	3.10E-10	1.00	3.40E-10	3.34E-10
8.0E+01	3.15E-10	3.15E-10	1.00	3.45E-10	3.49E-10
1.0E+02	3.13E-10	3.13E-10	1.00	3.52E-10	3.57E-10
1.5E+02	3.10E-10	3.10E-10	1.00	4.21E-10	3.71E-10
2.0E+02	3.13E-10	3.13E-10	1.00	4.43E-10	3.83E-10
3.0E+02	3.11E-10	3.11E-10	1.00	4.87E-10	4.12E-10
4.0E+02	3.18E-10	3.18E-10	1.00	5.29E-10	4.35E-10
5.0E+02	3.18E-10	3.18E-10	1.00	5.45E-10	4.49E-10
6.0E+02	3.20E-10	3.20E-10	1.00	5.77E-10	4.62E-10
8.0E+02	3.18E-10	3.18E-10	1.00	6.49E-10	4.85E-10
1.0E+03	3.12E-10	3.12E-10	1.00	6.75E-10	5.05E-10
1.5E+03	3.14E-10	3.14E-10	1.00	7.52E-10	5.22E-10
2.0E+03	3.11E-10	3.11E-10	1.00	8.09E-10	5.66E-10
3.0E+03	3.15E-10	3.15E-10	1.00	8.75E-10	6.04E-10
4.0E+03	3.17E-10	3.17E-10	1.00	9.58E-10	6.33E-10
5.0E+03	3.20E-10	3.24E-10	1.01	9.92E-10	6.59E-10
6.0E+03	3.15E-10	3.15E-10	1.00	1.02E-09	6.83E-10
8.0E+03	3.12E-10	3.12E-10	1.00	1.10E-09	7.16E-10
1.0E+04	3.12E-10	3.12E-10	1.00	1.09E-09	7.46E-10

‡ Q value at 10-mm depth

§ h^* cited from ICRU Report 95[15)]

Table 6 Protons: $d^*(10)$, $h^*(10)$, Q, h^*_{max}, and h^* values.

E_p / MeV	$d^*(10)$ / Gy cm^2	$h^*(10)$ / Sv cm^2	Q ‡	h^*_{max} / Sv cm^2	h^* / Sv cm^2 §
1.0E+01	7.78E-15	7.95E-15	1.02	1.57E-08	5.49E-11
1.5E+01	3.57E-14	3.97E-14	1.11	2.16E-08	1.89E-10
2.0E+01	7.82E-14	9.34E-14	1.19	2.07E-08	4.28E-10
3.0E+01	2.24E-13	5.33E-13	2.38	2.24E-08	7.50E-10
4.0E+01	3.91E-09	4.42E-09	1.13	2.19E-08	1.02E-09
5.0E+01	2.63E-09	3.08E-09	1.17	4.71E-09	1.18E-09
6.0E+01	2.09E-09	2.42E-09	1.16	4.28E-09	1.48E-09
8.0E+01	1.55E-09	1.81E-09	1.16	3.70E-09	2.16E-09
1.0E+02	1.28E-09	1.52E-09	1.18	5.30E-09	2.51E-09
1.5E+02	9.42E-10	1.18E-09	1.25	3.85E-09	2.82E-09
2.0E+02	7.84E-10	1.07E-09	1.36	3.11E-09	2.18E-09
3.0E+02	6.29E-10	9.32E-10	1.48	1.03E-09	1.45E-09
4.0E+02	5.55E-10	8.88E-10	1.60	1.01E-09	1.30E-09
5.0E+02	5.21E-10	9.14E-10	1.76	1.01E-09	1.24E-09
6.0E+02	4.96E-10	9.08E-10	1.83	1.04E-09	1.23E-09
8.0E+02	4.72E-10	8.97E-10	1.90	1.09E-09	1.23E-09
1.0E+03	4.59E-10	8.94E-10	1.95	1.11E-09	1.23E-09
1.5E+03	4.44E-10	9.07E-10	2.04	1.16E-09	1.25E-09
2.0E+03	4.37E-10	8.73E-10	2.00	1.17E-09	1.28E-09
3.0E+03	4.45E-10	9.18E-10	2.06	1.21E-09	1.35E-09
4.0E+03	4.69E-10	1.03E-09	2.21	1.50E-09	1.48E-09
5.0E+03	4.80E-10	1.03E-09	2.15	1.60E-09	1.46E-09
6.0E+03	4.87E-10	1.07E-09	2.20	1.69E-09	1.71E-09
8.0E+03	4.99E-10	1.05E-09	2.11	1.90E-09	1.88E-09
1.0E+04	5.09E-10	1.07E-09	2.09	2.03E-09	1.93E-09

‡ Q value at 10-mm depth
§ h^* cited from ICRU Report 95[15)]

Table 7 Negative muons: $d^*(10)$, $h^*(10)$, Q, h^*_{max}, and h^* values.

E_p / MeV	$d^*(10)$ / Gy cm^2	$h^*(10)$ / Sv cm^2	Q ‡	h^*_{max} / Sv cm^2	h^* / Sv cm^2 §
1.0E+00	3.83E-10	4.12E-10	1.08	6.28E-10	1.80E-10
1.5E+00	3.83E-10	4.09E-10	1.07	6.38E-10	1.80E-10
2.0E+00	3.86E-10	4.14E-10	1.07	6.54E-10	1.84E-10
3.0E+00	3.95E-10	4.33E-10	1.10	7.35E-10	1.88E-10
4.0E+00	4.01E-10	4.41E-10	1.10	4.98E-09	1.93E-10
5.0E+00	4.14E-10	4.41E-10	1.07	6.16E-09	2.05E-10
6.0E+00	4.29E-10	4.57E-10	1.07	7.18E-09	2.42E-10
8.0E+00	4.60E-10	4.88E-10	1.06	6.97E-09	2.93E-10
1.0E+01	5.39E-10	5.76E-10	1.07	5.49E-09	3.32E-10
1.5E+01	1.90E-09	1.92E-09	1.01	6.13E-09	4.14E-10
2.0E+01	1.22E-09	1.24E-09	1.02	2.00E-09	4.65E-10
3.0E+01	7.73E-10	7.76E-10	1.00	2.04E-09	6.57E-10
4.0E+01	5.99E-10	6.03E-10	1.01	1.72E-09	7.35E-10
5.0E+01	5.02E-10	5.02E-10	1.00	1.35E-09	7.55E-10
6.0E+01	4.39E-10	4.39E-10	1.00	1.01E-09	7.75E-10
8.0E+01	3.77E-10	3.78E-10	1.00	9.59E-10	5.05E-10
1.0E+02	3.54E-10	3.54E-10	1.00	3.54E-10	4.35E-10
1.5E+02	3.28E-10	3.28E-10	1.00	3.29E-10	3.55E-10
2.0E+02	3.19E-10	3.19E-10	1.00	3.20E-10	3.33E-10
3.0E+02	3.15E-10	3.15E-10	1.00	3.16E-10	3.22E-10
4.0E+02	3.14E-10	3.14E-10	1.00	3.15E-10	3.22E-10
5.0E+02	3.15E-10	3.15E-10	1.00	3.18E-10	3.24E-10
6.0E+02	3.17E-10	3.17E-10	1.00	3.22E-10	3.28E-10
8.0E+02	3.20E-10	3.20E-10	1.00	3.29E-10	3.33E-10
1.0E+03	3.24E-10	3.24E-10	1.00	3.35E-10	3.42E-10
1.5E+03	3.33E-10	3.33E-10	1.00	3.49E-10	3.38E-10
2.0E+03	3.40E-10	3.40E-10	1.00	3.58E-10	3.41E-10
3.0E+03	3.50E-10	3.50E-10	1.00	3.75E-10	3.44E-10
4.0E+03	3.57E-10	3.57E-10	1.00	3.86E-10	3.47E-10
5.0E+03	3.63E-10	3.63E-10	1.00	3.90E-10	3.48E-10
6.0E+03	3.77E-10	3.77E-10	1.00	4.35E-10	3.47E-10
8.0E+03	3.74E-10	3.74E-10	1.00	4.16E-10	3.49E-10
1.0E+04	3.79E-10	3.79E-10	1.00	4.08E-10	3.49E-10

‡ Q value at 10-mm depth
§ h^* cited from ICRU Report 95[15)]

Table 8 Positive muons: $d^*(10)$, $h^*(10)$, Q, h^*_{max}, and h^* values.

E_p / MeV	$d^*(10)$ / Gy cm^2	$h^*(10)$ / Sv cm^2	Q ‡	h^*_{max} / Sv cm^2	h^* / Sv cm^2 §
1.0E+00	3.81E-10	3.81E-10	1.00	6.18E-10	1.94E-10
1.5E+00	3.93E-10	3.93E-10	1.00	6.34E-10	1.96E-10
2.0E+00	3.98E-10	3.98E-10	1.00	6.52E-10	1.98E-10
3.0E+00	4.02E-10	4.02E-10	1.00	6.99E-10	2.02E-10
4.0E+00	4.26E-10	4.26E-10	1.00	3.67E-09	2.07E-10
5.0E+00	4.35E-10	4.35E-10	1.00	4.83E-09	2.16E-10
6.0E+00	4.34E-10	4.34E-10	1.00	5.76E-09	2.51E-10
8.0E+00	4.67E-10	4.67E-10	1.00	5.58E-09	3.00E-10
1.0E+01	5.55E-10	5.55E-10	1.00	4.78E-09	3.40E-10
1.5E+01	1.99E-09	1.99E-09	1.00	4.93E-09	4.25E-10
2.0E+01	1.25E-09	1.25E-09	1.00	1.81E-09	4.81E-10
3.0E+01	7.88E-10	7.88E-10	1.00	1.98E-09	6.74E-10
4.0E+01	5.99E-10	5.99E-10	1.00	1.52E-09	7.51E-10
5.0E+01	5.06E-10	5.06E-10	1.00	1.29E-09	7.68E-10
6.0E+01	4.40E-10	4.40E-10	1.00	9.23E-10	7.87E-10
8.0E+01	3.78E-10	3.78E-10	1.00	8.39E-10	5.10E-10
1.0E+02	3.54E-10	3.54E-10	1.00	3.54E-10	4.37E-10
1.5E+02	3.28E-10	3.28E-10	1.00	3.28E-10	3.54E-10
2.0E+02	3.19E-10	3.19E-10	1.00	3.20E-10	3.33E-10
3.0E+02	3.15E-10	3.15E-10	1.00	3.16E-10	3.20E-10
4.0E+02	3.14E-10	3.14E-10	1.00	3.15E-10	3.21E-10
5.0E+02	3.15E-10	3.15E-10	1.00	3.18E-10	3.23E-10
6.0E+02	3.17E-10	3.17E-10	1.00	3.22E-10	3.25E-10
8.0E+02	3.20E-10	3.20E-10	1.00	3.29E-10	3.30E-10
1.0E+03	3.24E-10	3.24E-10	1.00	3.35E-10	3.34E-10
1.5E+03	3.33E-10	3.33E-10	1.00	3.49E-10	3.39E-10
2.0E+03	3.40E-10	3.40E-10	1.00	3.58E-10	3.41E-10
3.0E+03	3.50E-10	3.50E-10	1.00	3.75E-10	3.44E-10
4.0E+03	3.57E-10	3.57E-10	1.00	3.86E-10	3.47E-10
5.0E+03	3.63E-10	3.63E-10	1.00	3.90E-10	3.48E-10
6.0E+03	3.77E-10	3.77E-10	1.00	4.35E-10	3.47E-10
8.0E+03	3.74E-10	3.74E-10	1.00	4.16E-10	3.49E-10
1.0E+04	3.79E-10	3.79E-10	1.00	4.08E-10	3.49E-10

‡ Q value at 10-mm depth
§ h^* cited from ICRU Report 95[15)]

Table 9 Negative pions: $d^*(10)$, $h^*(10)$, Q, h^*_{max}, and h^* values.

E_p / MeV	$d^*(10)$ / Gy cm^2	$h^*(10)$ / Sv cm^2	Q ‡	h^*_{max} / Sv cm^2	h^* / Sv cm^2 §
1.0E+00	1.82E-10	1.15E-09	6.31	9.21E-09	4.06E-10
1.5E+00	1.85E-10	1.15E-09	6.25	1.03E-08	4.22E-10
2.0E+00	1.85E-10	1.17E-09	6.32	1.22E-08	4.33E-10
3.0E+00	1.90E-10	1.12E-09	5.91	2.39E-08	4.58E-10
4.0E+00	2.03E-10	1.21E-09	5.97	2.25E-07	4.91E-10
5.0E+00	2.12E-10	1.23E-09	5.80	3.08E-07	5.28E-10
6.0E+00	2.30E-10	1.32E-09	5.76	3.10E-07	6.73E-10
8.0E+00	3.01E-10	1.54E-09	5.12	3.09E-07	9.65E-10
1.0E+01	5.04E-10	2.22E-09	4.41	3.04E-07	1.09E-09
1.5E+01	5.67E-09	1.53E-08	2.70	2.96E-07	1.25E-09
2.0E+01	1.43E-09	2.75E-09	1.92	1.93E-07	1.28E-09
3.0E+01	9.15E-10	1.79E-09	1.95	5.43E-08	1.77E-09
4.0E+01	7.33E-10	1.41E-09	1.92	4.32E-08	1.92E-09
5.0E+01	6.51E-10	1.31E-09	2.02	3.20E-08	1.93E-09
6.0E+01	5.89E-10	1.24E-09	2.10	2.35E-08	1.99E-09
8.0E+01	5.36E-10	1.22E-09	2.28	1.30E-08	1.31E-09
1.0E+02	5.20E-10	1.31E-09	2.51	1.38E-08	1.03E-09
1.5E+02	5.06E-10	1.37E-09	2.71	1.47E-09	9.27E-10
2.0E+02	4.82E-10	1.31E-09	2.72	1.36E-09	9.02E-10
3.0E+02	4.43E-10	1.07E-09	2.41	1.14E-09	8.48E-10
4.0E+02	4.27E-10	9.74E-10	2.28	1.02E-09	8.50E-10
5.0E+02	4.24E-10	9.18E-10	2.16	9.63E-10	8.80E-10
6.0E+02	4.30E-10	9.07E-10	2.11	9.70E-10	9.17E-10
8.0E+02	4.43E-10	9.20E-10	2.08	1.01E-09	9.76E-10
1.0E+03	4.55E-10	9.60E-10	2.11	1.06E-09	1.02E-09
1.5E+03	4.64E-10	9.03E-10	1.95	1.12E-09	1.08E-09
2.0E+03	4.82E-10	9.59E-10	1.99	1.12E-09	1.12E-09
3.0E+03	4.94E-10	9.40E-10	1.90	1.17E-09	1.13E-09
4.0E+03	5.87E-10	1.23E-09	2.10	1.65E-09	1.17E-09
5.0E+03	6.05E-10	1.24E-09	2.05	1.78E-09	1.23E-09
6.0E+03	6.04E-10	1.17E-09	1.93	1.91E-09	1.26E-09
8.0E+03	6.24E-10	1.21E-09	1.95	2.11E-09	1.39E-09

‡ Q value at 10-mm depth

§ h^* cited from ICRU Report 95[15)]

Table 9 (Continued).

E_p / MeV	$d^*(10)$ / Gy cm^2	$h^*(10)$ / Sv cm^2	Q ‡	h^*_{max} / Sv cm^2	h^* / Sv cm^2 §
1.0E+04	6.39E-10	1.22E-09	1.91	2.31E-09	1.46E-09
1.5E+04	6.59E-10	1.20E-09	1.81	2.71E-09	1.60E-09
2.0E+04	6.75E-10	1.31E-09	1.93	3.09E-09	1.70E-09
3.0E+04	6.91E-10	1.27E-09	1.83	3.68E-09	1.86E-09
4.0E+04	7.08E-10	1.32E-09	1.86	4.00E-09	1.99E-09
5.0E+04	7.13E-10	1.34E-09	1.88	4.50E-09	2.11E-09
6.0E+04	7.23E-10	1.38E-09	1.91	4.73E-09	2.21E-09
8.0E+04	7.42E-10	1.45E-09	1.96	5.35E-09	2.42E-09
1.0E+05	7.52E-10	1.45E-09	1.93	5.79E-09	2.60E-09
1.5E+05	7.78E-10	1.47E-09	1.89	6.73E-09	2.98E-09
2.0E+05	8.06E-10	1.66E-09	2.06	7.55E-09	3.14E-09

‡ Q value at 10-mm depth
§ h^* cited from ICRU Report 95[15)]

Table 10 Positive pions: $d^*(10)$, $h^*(10)$, Q, h^*_{max}, and h^* values.

E_p / MeV	$d^*(10)$ / Gy cm^2	$h^*(10)$ / Sv cm^2	Q ‡	h^*_{max} / Sv cm^2	h^* / Sv cm^2 §
1.0E+00	2.21E-10	2.21E-10	1.00	9.20E-10	3.14E-10
1.5E+00	2.34E-10	2.34E-10	1.00	1.06E-09	3.24E-10
2.0E+00	2.52E-10	2.52E-10	1.00	1.25E-09	3.40E-10
3.0E+00	2.88E-10	2.88E-10	1.00	1.87E-09	3.79E-10
4.0E+00	3.40E-10	3.40E-10	1.00	6.00E-09	4.29E-10
5.0E+00	4.01E-10	4.02E-10	1.00	8.61E-09	4.89E-10
6.0E+00	4.20E-10	4.22E-10	1.00	9.93E-09	5.40E-10
8.0E+00	4.58E-10	4.60E-10	1.01	9.11E-09	7.17E-10
1.0E+01	5.11E-10	5.13E-10	1.00	8.59E-09	8.19E-10
1.5E+01	3.83E-09	4.55E-09	1.19	8.19E-09	1.00E-09
2.0E+01	1.64E-09	2.16E-09	1.32	7.32E-09	1.10E-09
3.0E+01	1.03E-09	1.57E-09	1.52	3.59E-09	1.52E-09
4.0E+01	7.97E-10	1.27E-09	1.60	2.27E-09	1.75E-09
5.0E+01	6.77E-10	1.13E-09	1.67	1.59E-09	1.83E-09
6.0E+01	6.16E-10	1.09E-09	1.77	1.43E-09	1.82E-09
8.0E+01	5.70E-10	1.15E-09	2.01	1.15E-09	1.38E-09
1.0E+02	5.72E-10	1.22E-09	2.13	1.25E-09	1.13E-09
1.5E+02	6.10E-10	1.41E-09	2.31	1.49E-09	1.22E-09
2.0E+02	5.96E-10	1.40E-09	2.36	1.52E-09	1.25E-09
3.0E+02	5.06E-10	1.13E-09	2.24	1.20E-09	1.10E-09
4.0E+02	4.58E-10	9.38E-10	2.05	1.05E-09	9.98E-10
5.0E+02	4.46E-10	8.58E-10	1.92	9.83E-10	9.70E-10
6.0E+02	4.47E-10	8.81E-10	1.97	9.87E-10	9.80E-10
8.0E+02	4.68E-10	9.67E-10	2.07	1.05E-09	1.04E-09
1.0E+03	4.77E-10	9.58E-10	2.01	1.08E-09	1.09E-09
1.5E+03	4.98E-10	9.76E-10	1.96	1.14E-09	1.16E-09
2.0E+03	5.08E-10	9.72E-10	1.91	1.18E-09	1.19E-09
3.0E+03	5.16E-10	9.78E-10	1.89	1.23E-09	1.18E-09
4.0E+03	5.96E-10	1.13E-09	1.89	1.68E-09	1.21E-09
5.0E+03	6.07E-10	1.20E-09	1.97	1.85E-09	1.27E-09
6.0E+03	6.19E-10	1.17E-09	1.89	1.95E-09	1.29E-09
8.0E+03	6.34E-10	1.20E-09	1.89	2.12E-09	1.39E-09

‡ Q value at 10-mm depth

§ h^* cited from ICRU Report 95[15)]

Table 10 (Continued).

E_p / MeV	$d^*(10)$ / Gy cm^2	$h^*(10)$ / Sv cm^2	Q ‡	h^*_{max} / Sv cm^2	h^* / Sv cm^2 §
1.0E+04	6.49E-10	1.26E-09	1.94	2.31E-09	1.46E-09
1.5E+04	6.65E-10	1.27E-09	1.91	2.74E-09	1.60E-09
2.0E+04	6.78E-10	1.26E-09	1.86	3.04E-09	1.69E-09
3.0E+04	6.98E-10	1.34E-09	1.92	3.62E-09	1.86E-09
4.0E+04	7.14E-10	1.35E-09	1.90	4.03E-09	1.97E-09
5.0E+04	7.20E-10	1.31E-09	1.82	4.40E-09	2.09E-09
6.0E+04	7.28E-10	1.32E-09	1.82	4.74E-09	2.20E-09
8.0E+04	7.43E-10	1.39E-09	1.87	5.41E-09	2.38E-09
1.0E+05	7.42E-10	1.27E-09	1.71	5.80E-09	2.53E-09
1.5E+05	7.76E-10	1.50E-09	1.94	6.72E-09	2.90E-09
2.0E+05	7.92E-10	1.52E-09	1.92	7.55E-09	3.24E-09

‡ Q value at 10-mm depth
§ h^* cited from ICRU Report 95[15)]

Table 11 Helium ions: $d^*(10)$, $h^*(10)$, Q, h^*_{max}, and h^* values.

E_p / MeV n^{-1}	$d^*(10)$ / Gy cm^2	$h^*(10)$ / Sv cm^2	Q ‡	h^*_{max} / Sv cm^2	h^* / Sv cm^2 §
2.0E+00	4.68E-16	5.24E-16	1.12	7.35E-16	4.38E-10
3.0E+00	2.44E-15	3.00E-15	1.23	4.01E-15	6.57E-10
5.0E+00	1.48E-14	2.87E-14	1.94	1.44E-13	1.09E-09
1.0E+01	1.09E-13	6.00E-13	5.50	2.34E-07	2.19E-09
1.4E+01	9.40E-13	3.54E-12	3.77	3.55E-07	4.61E-09
2.0E+01	9.23E-12	2.14E-11	2.31	3.55E-07	1.72E-08
3.0E+01	5.62E-11	1.15E-10	2.05	3.76E-07	3.01E-08
5.0E+01	1.04E-08	1.19E-08	1.15	7.35E-08	4.75E-08
7.5E+01	6.56E-09	7.61E-09	1.16	7.67E-08	8.05E-08
1.0E+02	5.05E-09	6.24E-09	1.24	7.05E-08	1.01E-07
1.5E+02	3.68E-09	4.42E-09	1.20	5.40E-08	1.10E-07
2.0E+02	3.04E-09	3.92E-09	1.29	2.10E-08	7.29E-08
3.0E+02	2.43E-09	3.36E-09	1.38	3.50E-09	5.33E-08
5.0E+02	1.99E-09	3.29E-09	1.65	3.31E-09	4.49E-08
7.0E+02	1.83E-09	3.23E-09	1.77	3.65E-09	4.60E-08
1.0E+03	1.72E-09	2.94E-09	1.71	3.87E-09	4.47E-08
2.0E+03	1.66E-09	2.92E-09	1.76	4.20E-09	4.80E-08
3.0E+03	1.67E-09	3.11E-09	1.86	4.34E-09	5.01E-08
5.0E+03	1.80E-09	3.32E-09	1.84	5.58E-09	5.17E-08
1.0E+04	1.97E-09	3.61E-09	1.83	7.51E-09	6.26E-08
2.0E+04	2.22E-09	3.80E-09	1.72	1.06E-08	7.10E-08
5.0E+04	2.64E-09	4.34E-09	1.64	1.60E-08	9.67E-08
1.0E+05	2.89E-09	4.92E-09	1.70	2.23E-08	1.24E-07

‡ Q value at 10-mm depth

§ h^* cited from ICRU Report 95[15)]

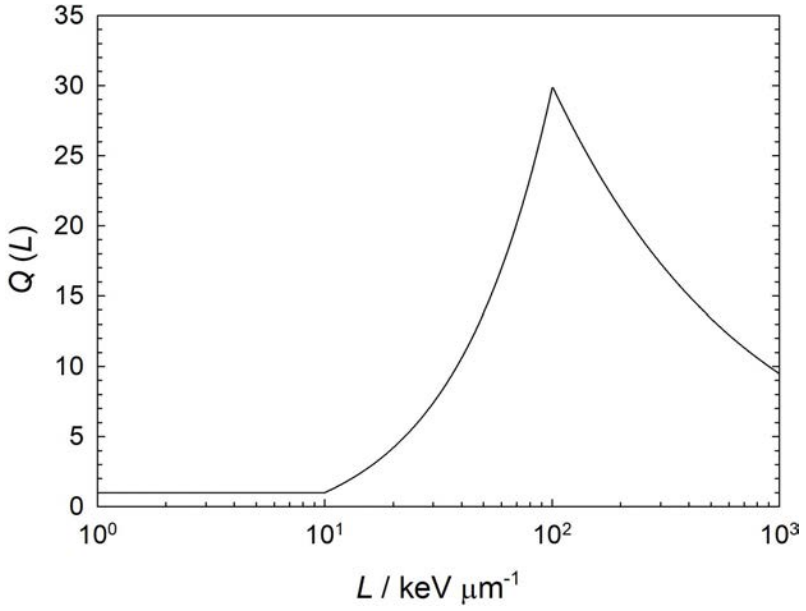

Figure 1 Quality factor, Q, as a function of linear energy transfer, L.

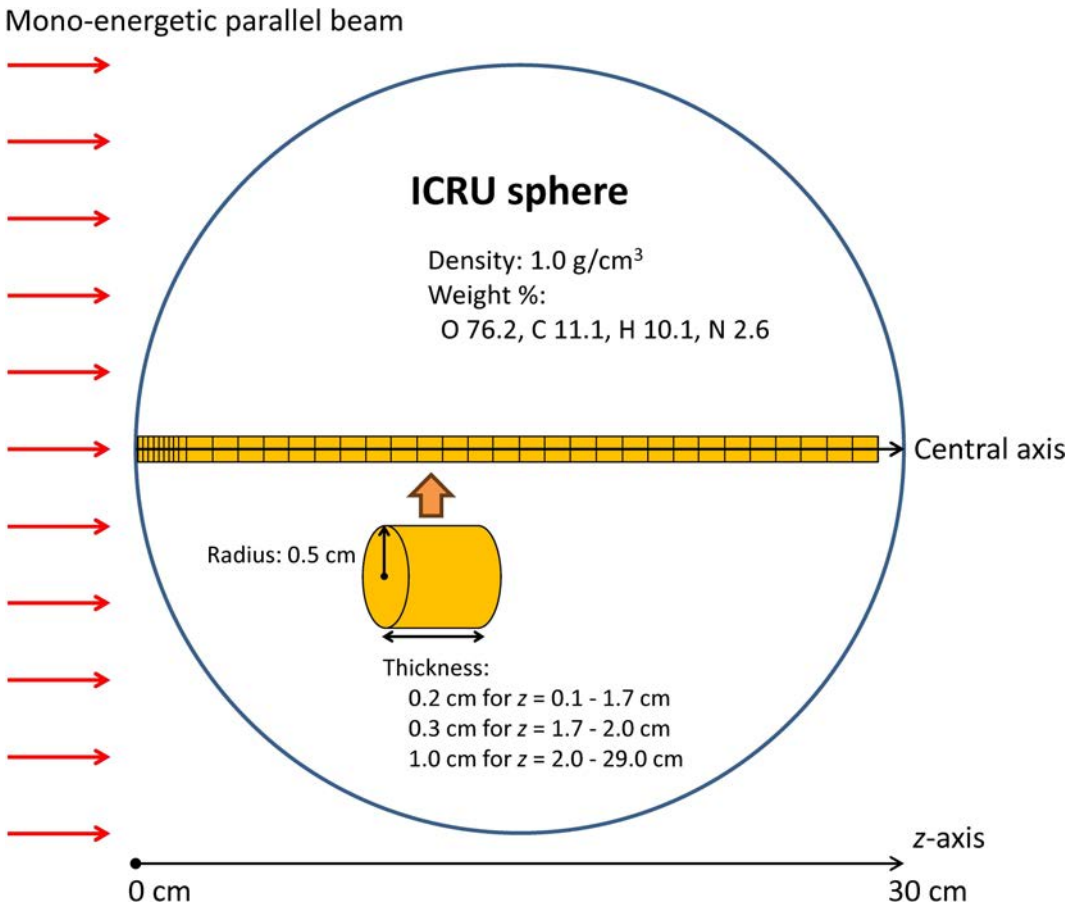

Figure 2 Model used for calculation of $D^*(d)$ and $H^*(d)$.

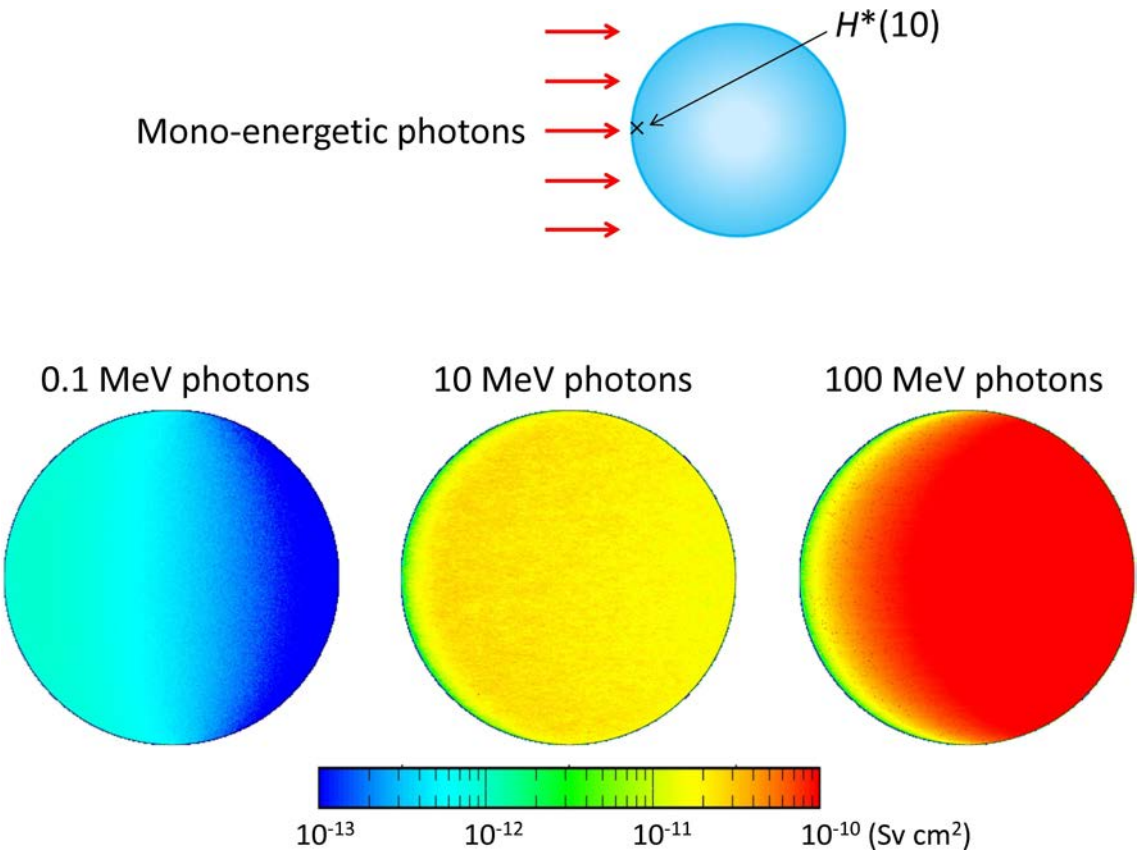

Figure 3 Distributions of dose equivalent in the ICRU sphere irradiated by photons.

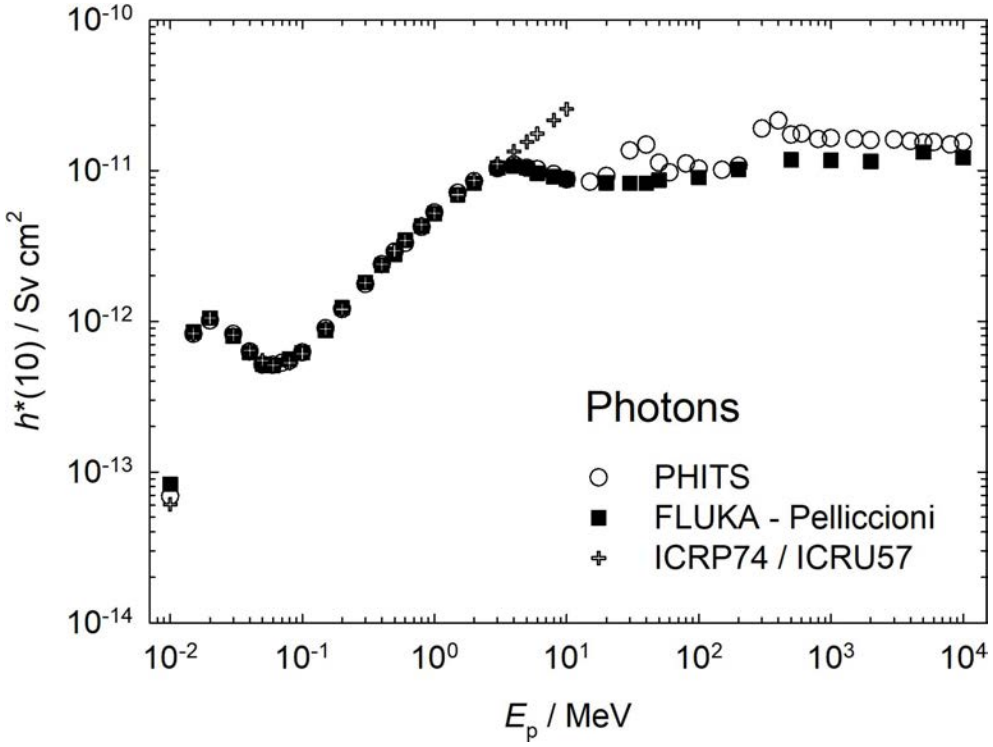

Figure 4 Comparison of $h^*(10)$ for photons.

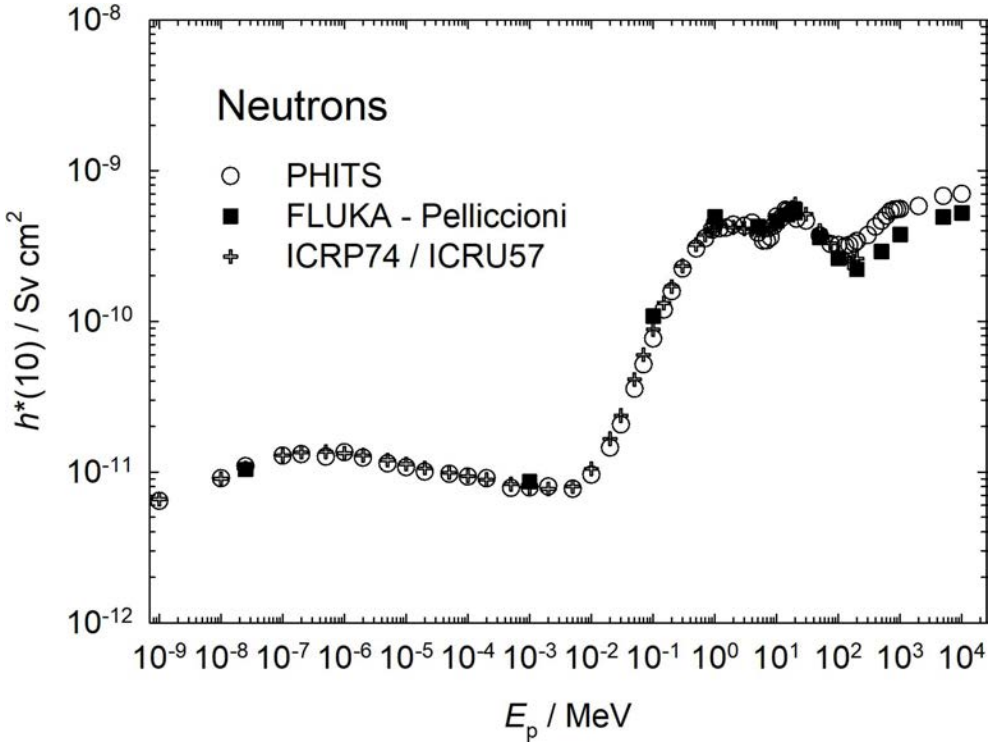

Figure 5 Comparison of $h^*(10)$ for neutrons.

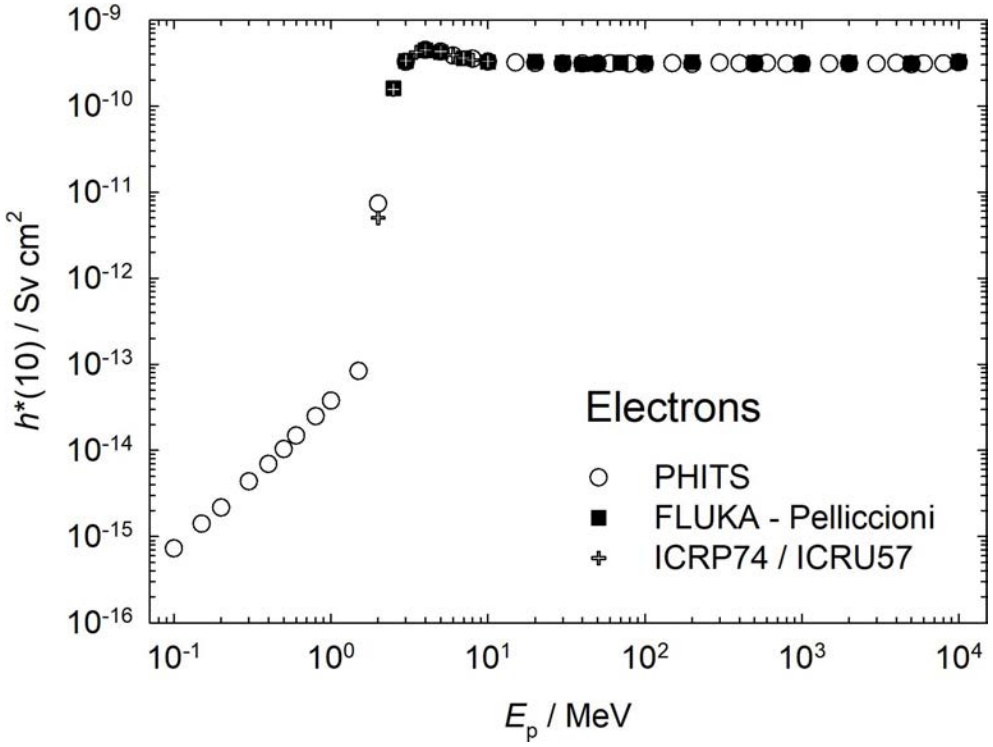

Figure 6 Comparison of $h^*(10)$ for electrons.

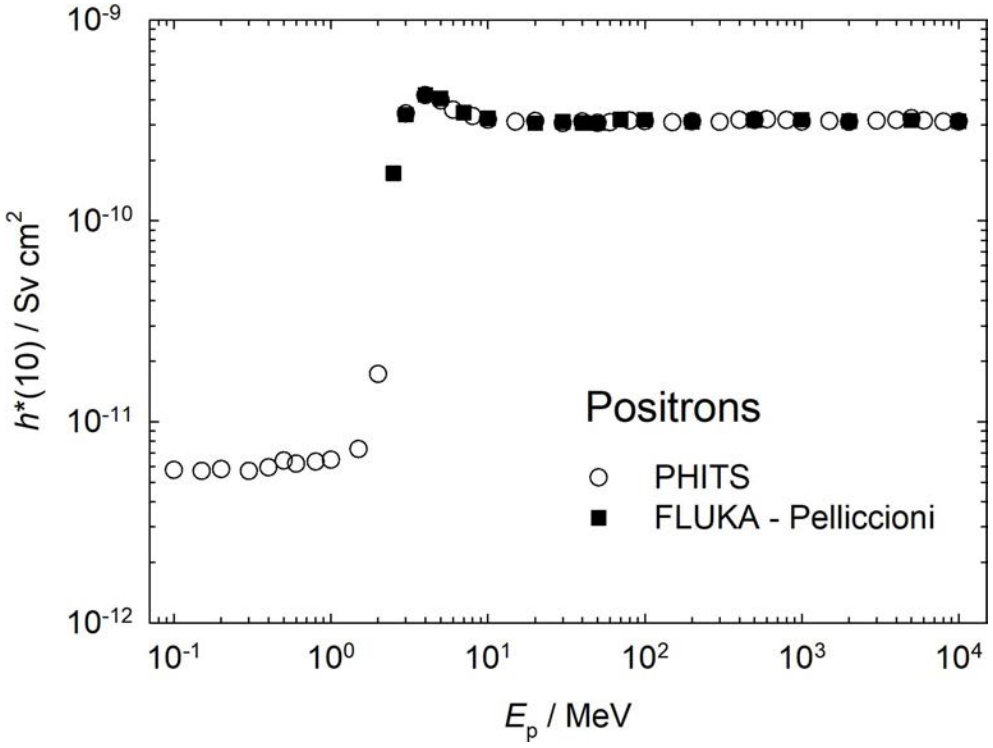

Figure 7 Comparison of $h^*(10)$ for positrons.

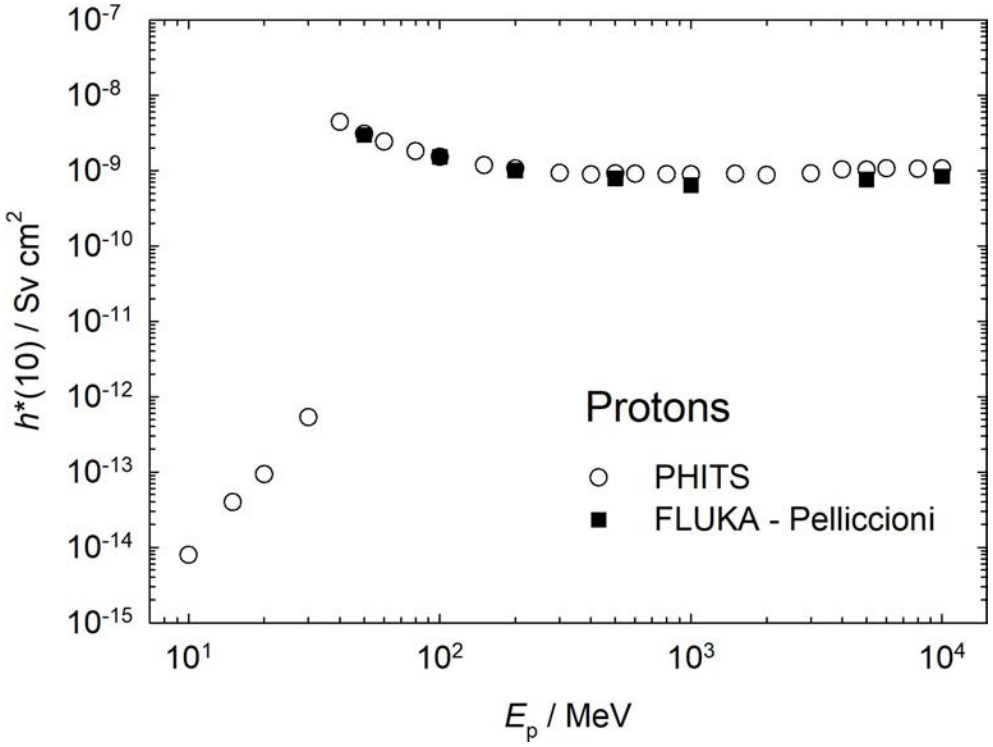

Figure 8 Comparison of $h^*(10)$ for protons.

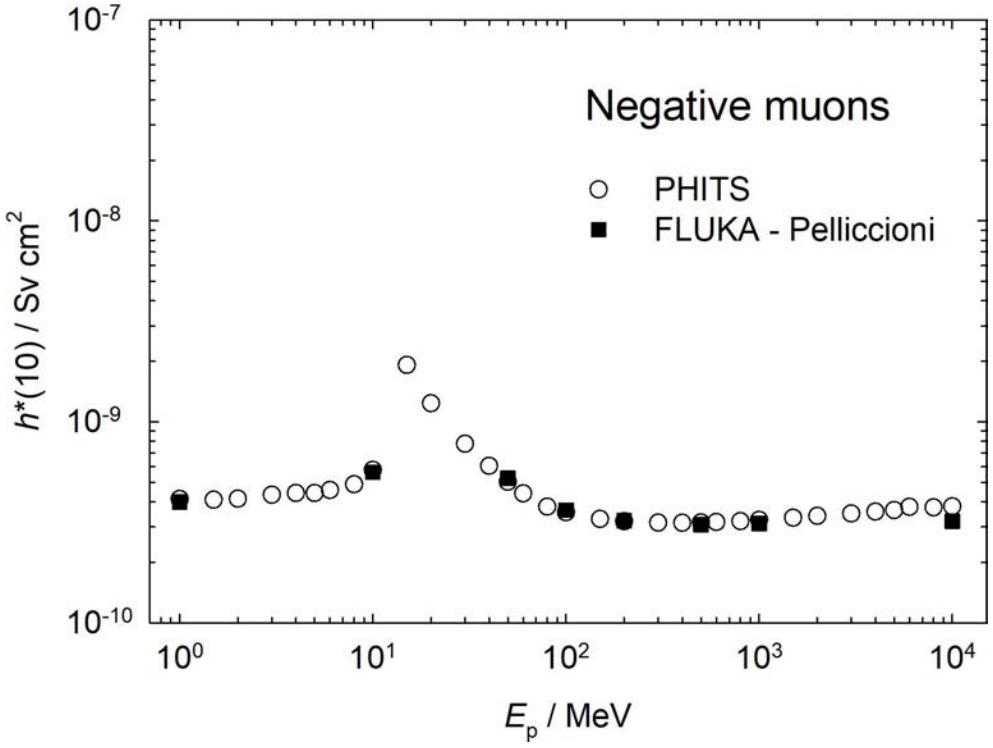

Figure 9 Comparison of $h^*(10)$ for negative muons.

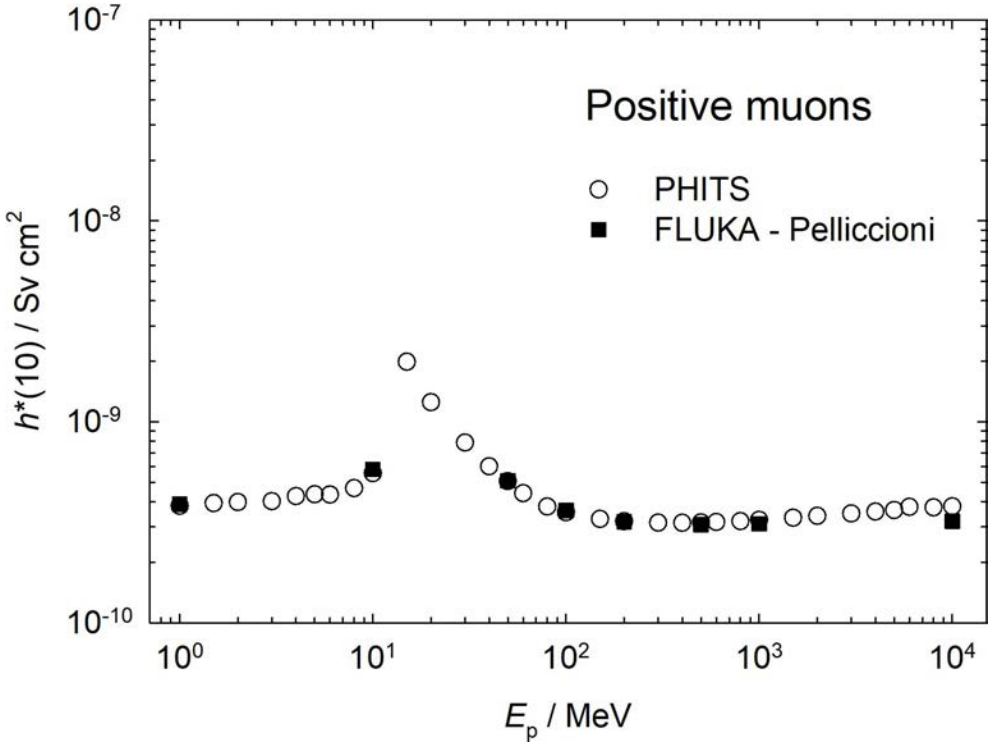

Figure 10 Comparison of $h^*(10)$ for positive muons.

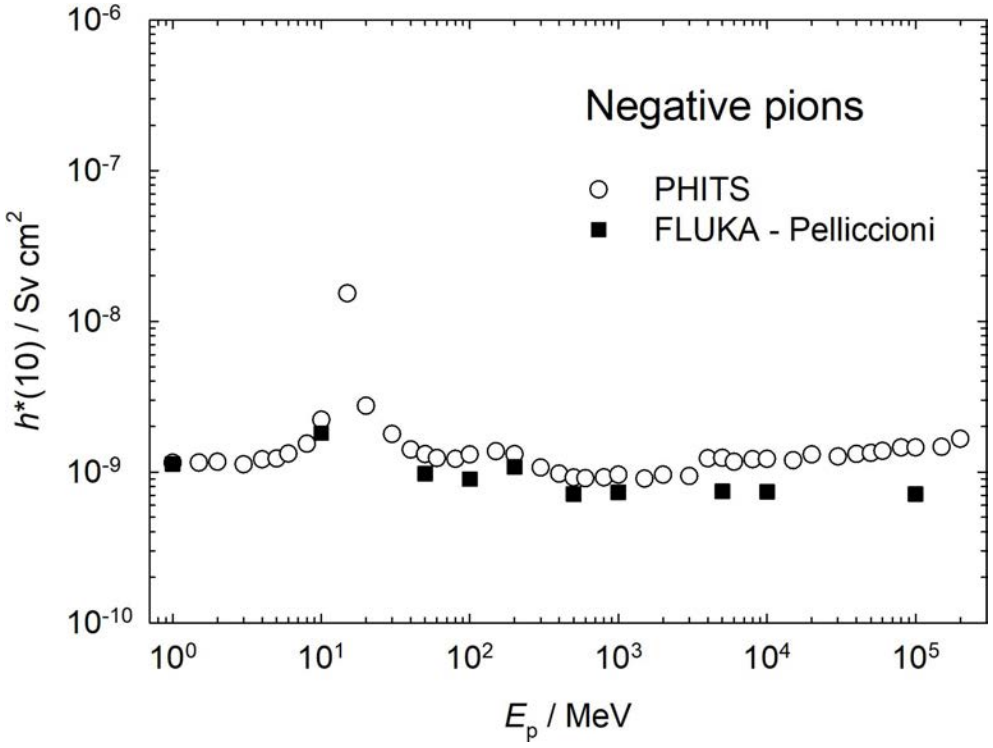

Figure 11 Comparison of $h^*(10)$ for negative pions.

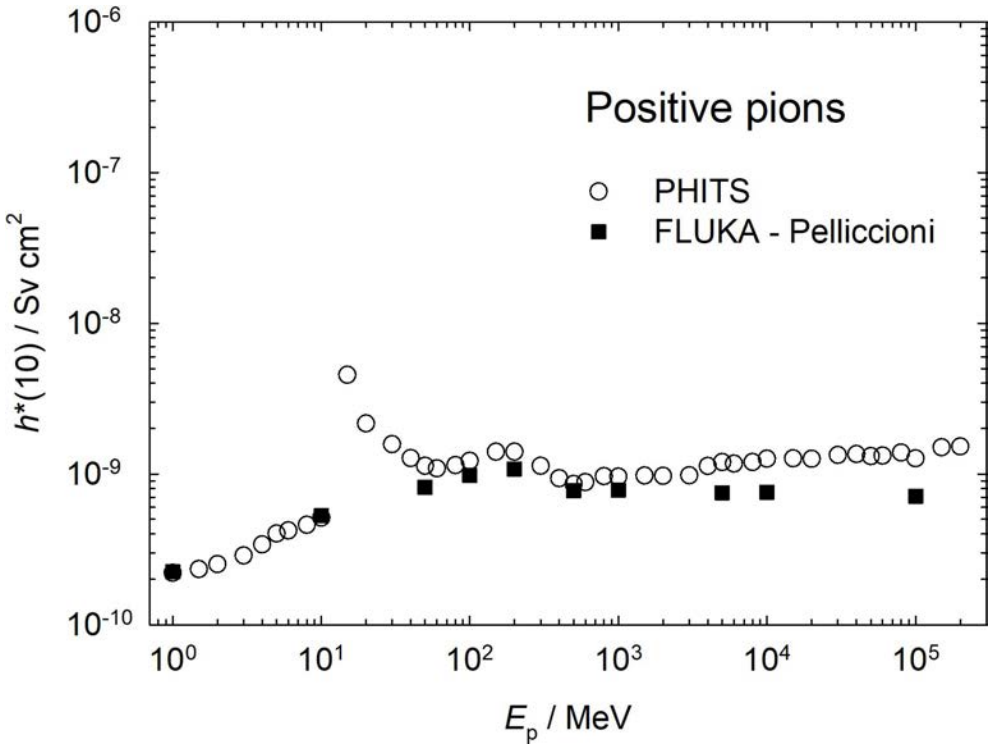

Figure 12 Comparison of $h^*(10)$ for positive pions.

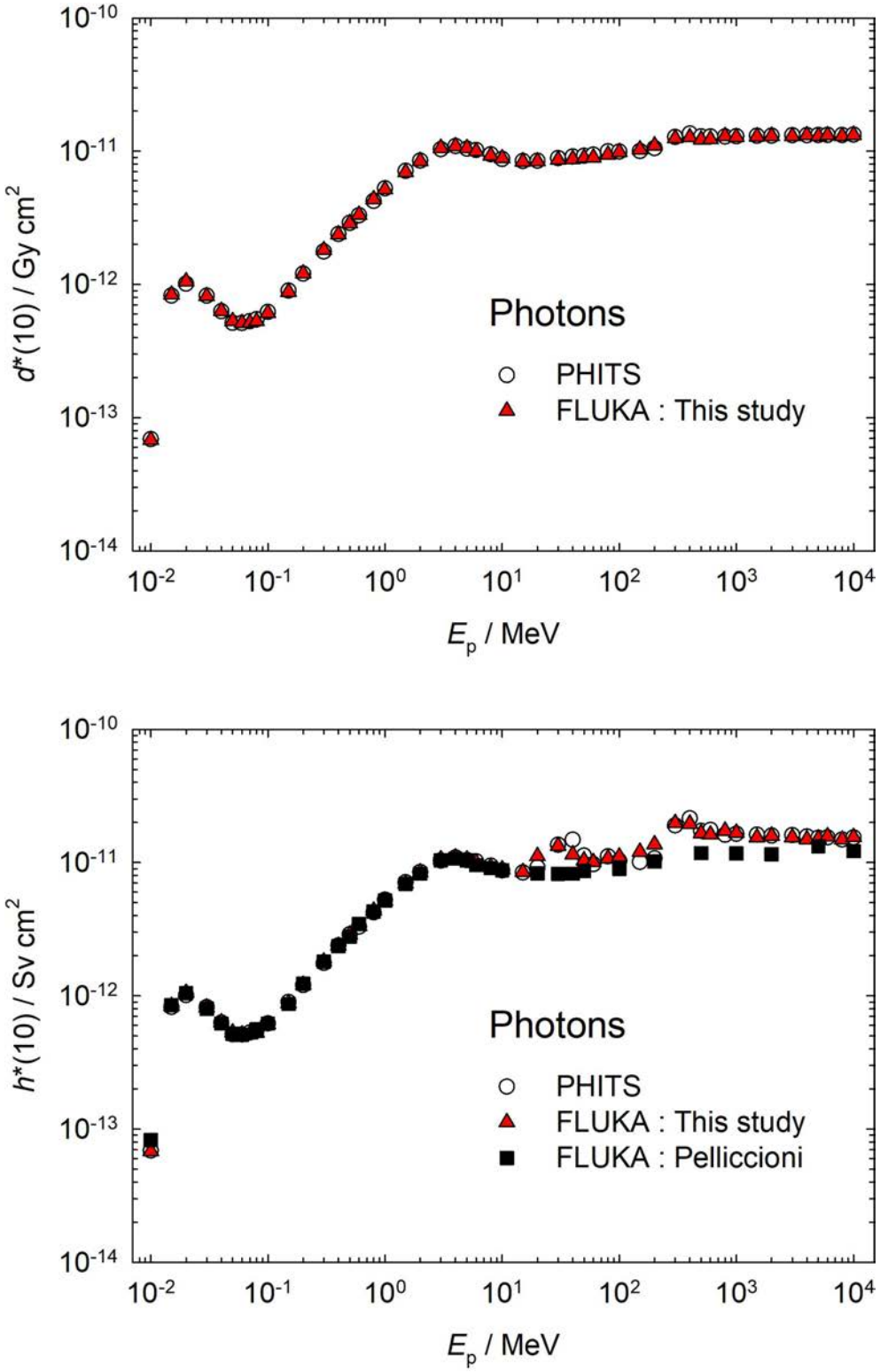

Figure 13 Comparison of $d^*(10)$ and $h^*(10)$ for photons calculated by FLUKA and PHITS.

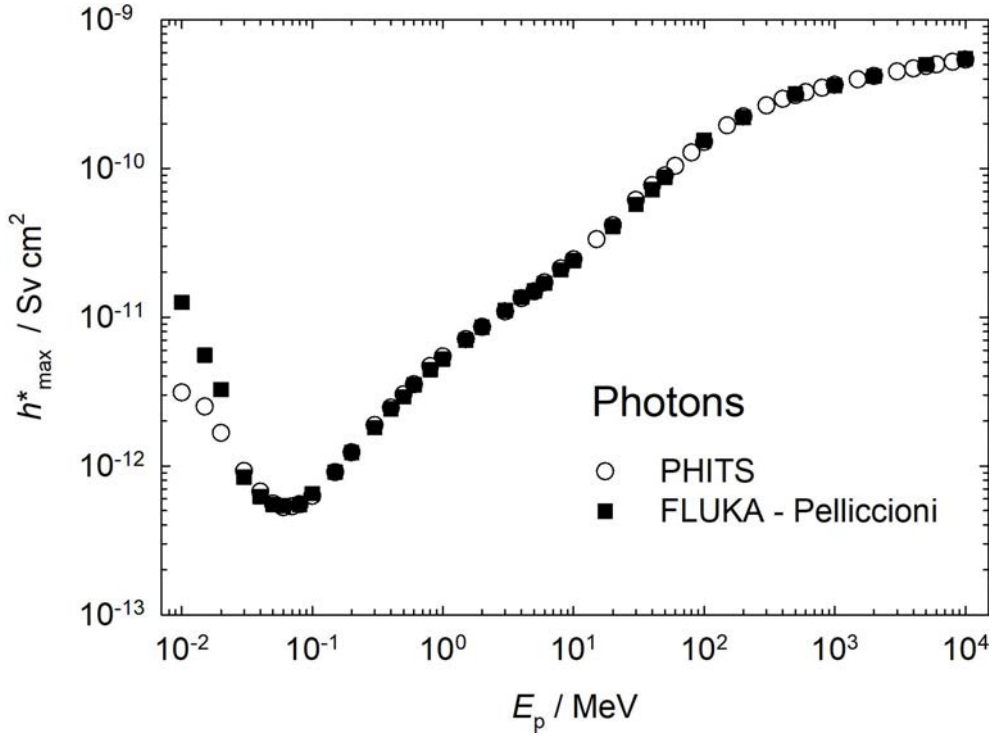

Figure 14 Comparison of h^*_{max} for photons.

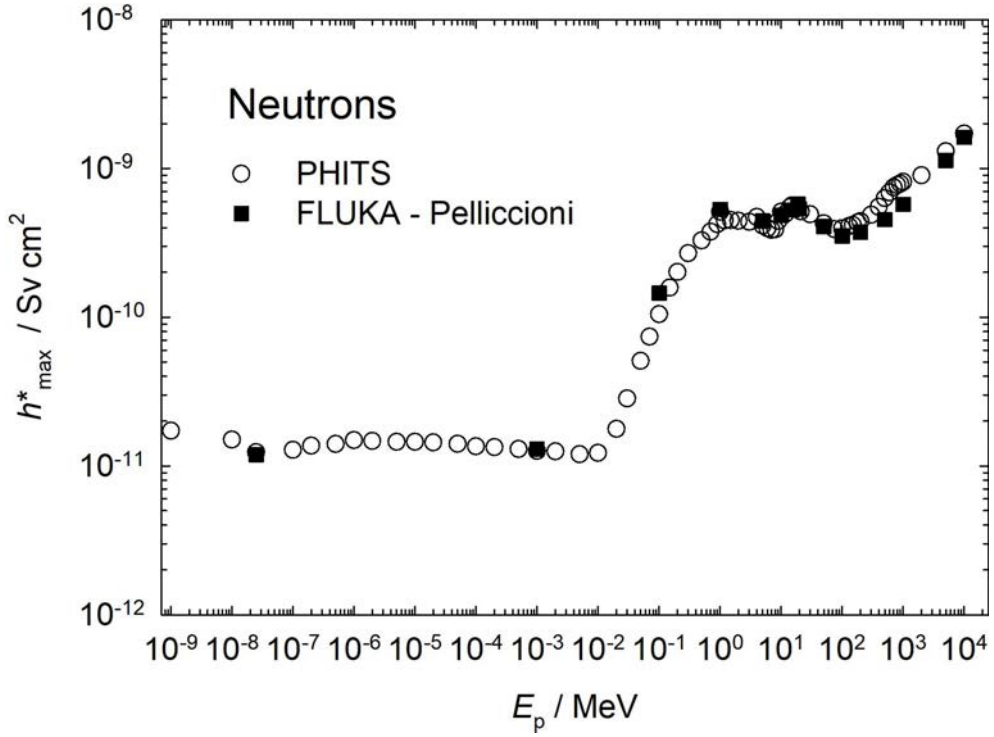

Figure 15 Comparison of h^*_{max} for neutrons.

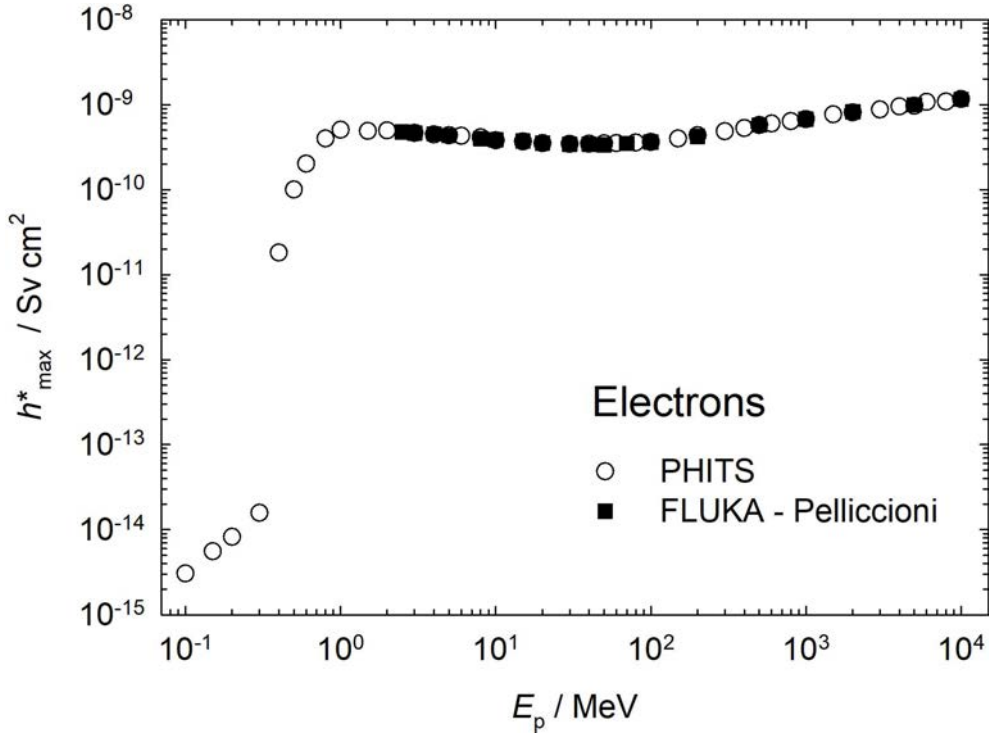

Figure 16 Comparison of h^*_{max} for electrons.

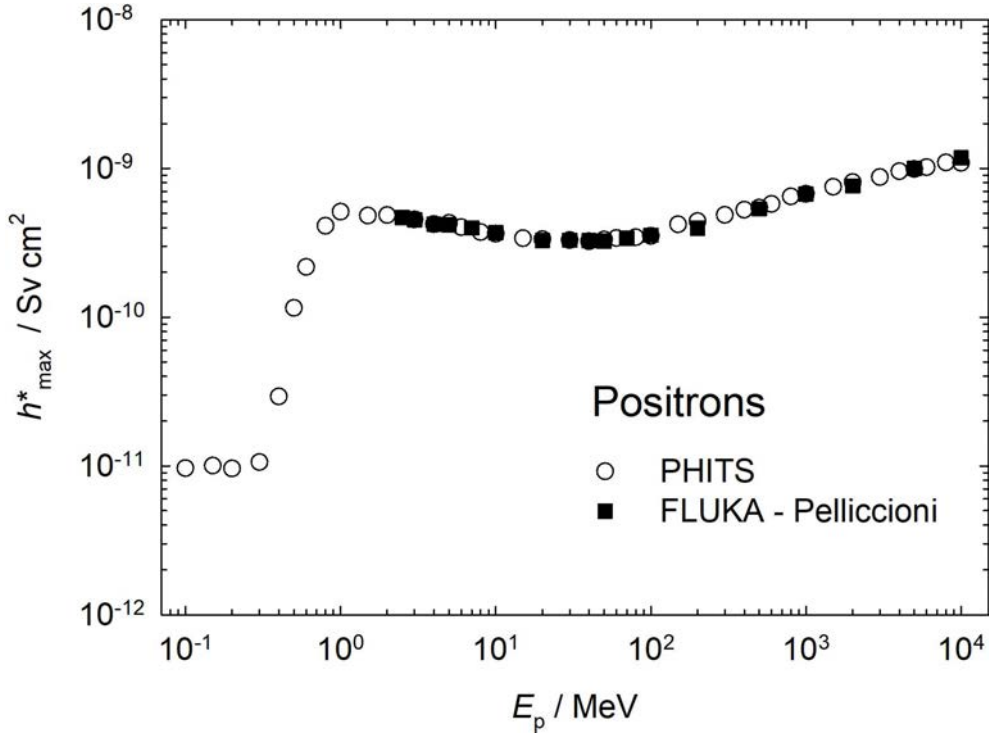

Figure 17 Comparison of h^*_{max} for positrons.

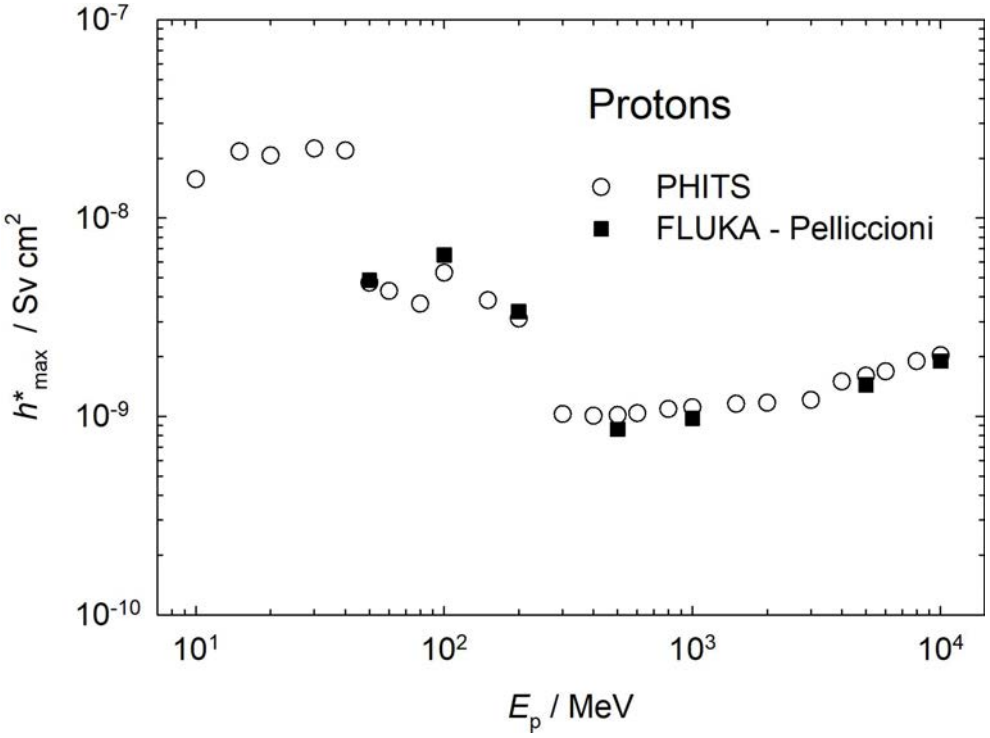

Figure 18 Comparison of h^*_{max} for protons.

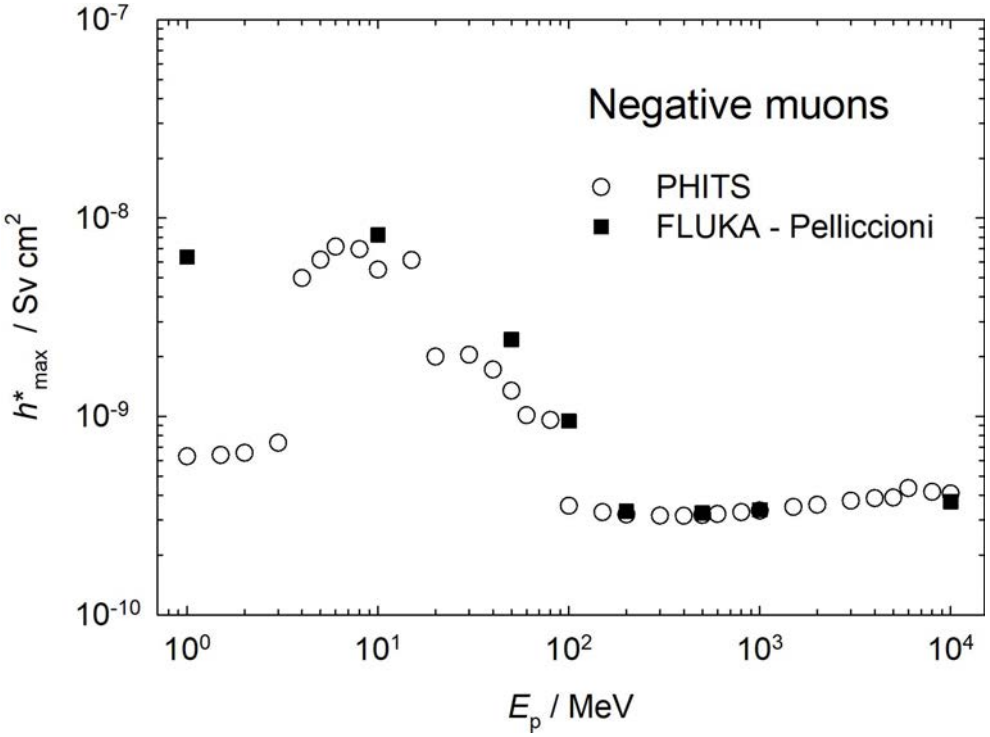

Figure 19 Comparison of h^*_{max} for negative muons.

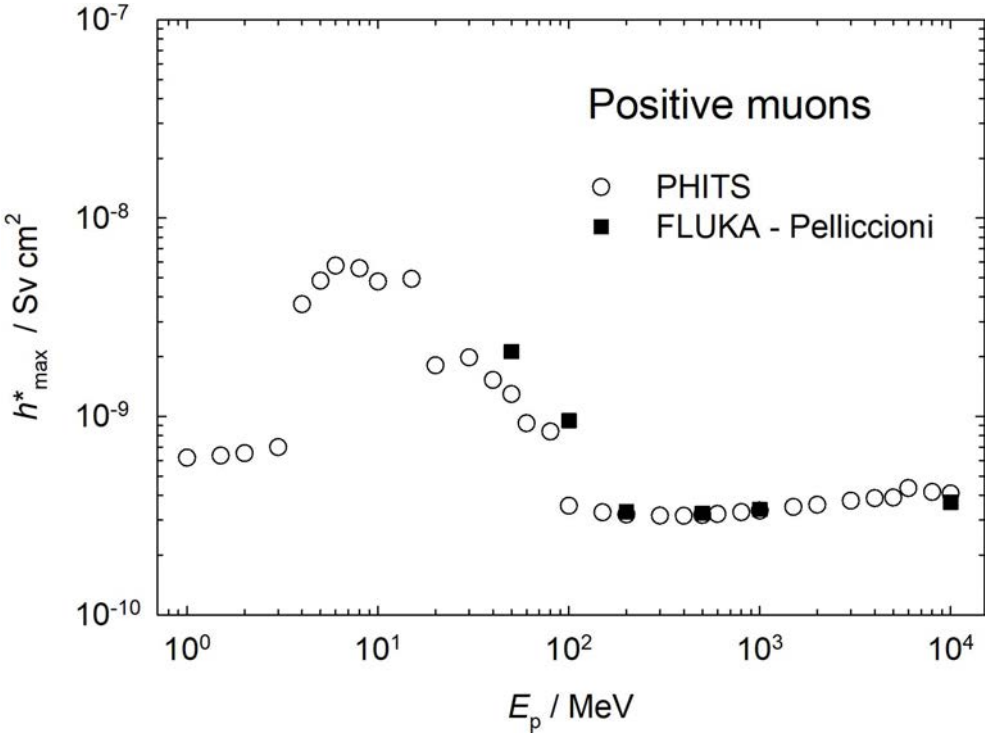

Figure 20 Comparison of h^*_{max} for positive muons.

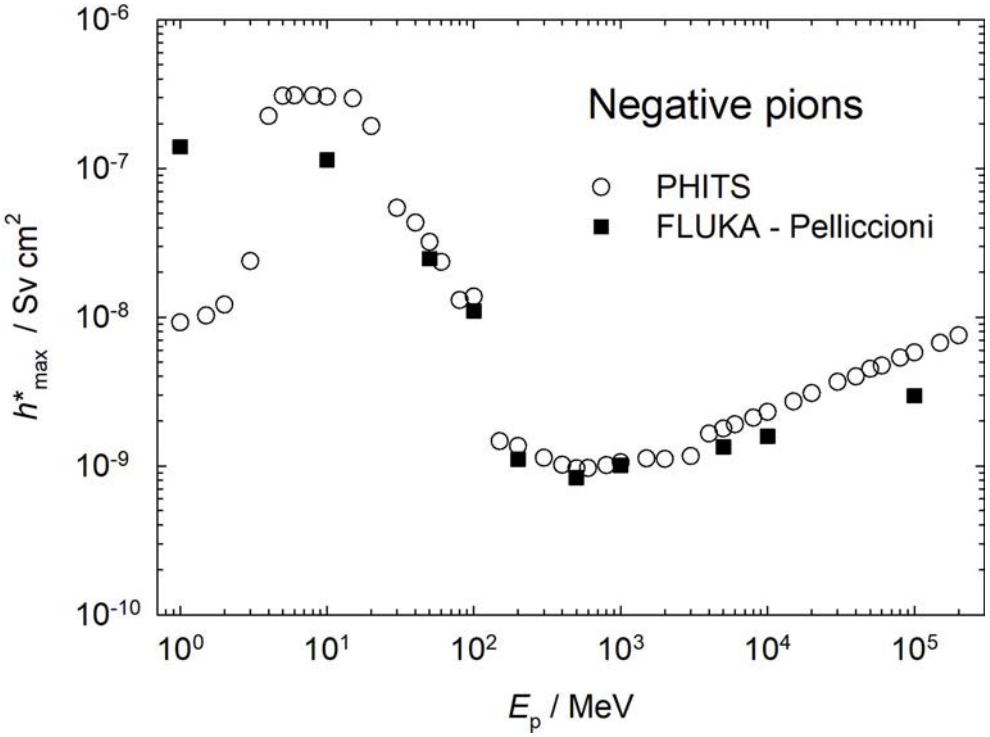

Figure 21 Comparison of h^*_{max} for negative pions.

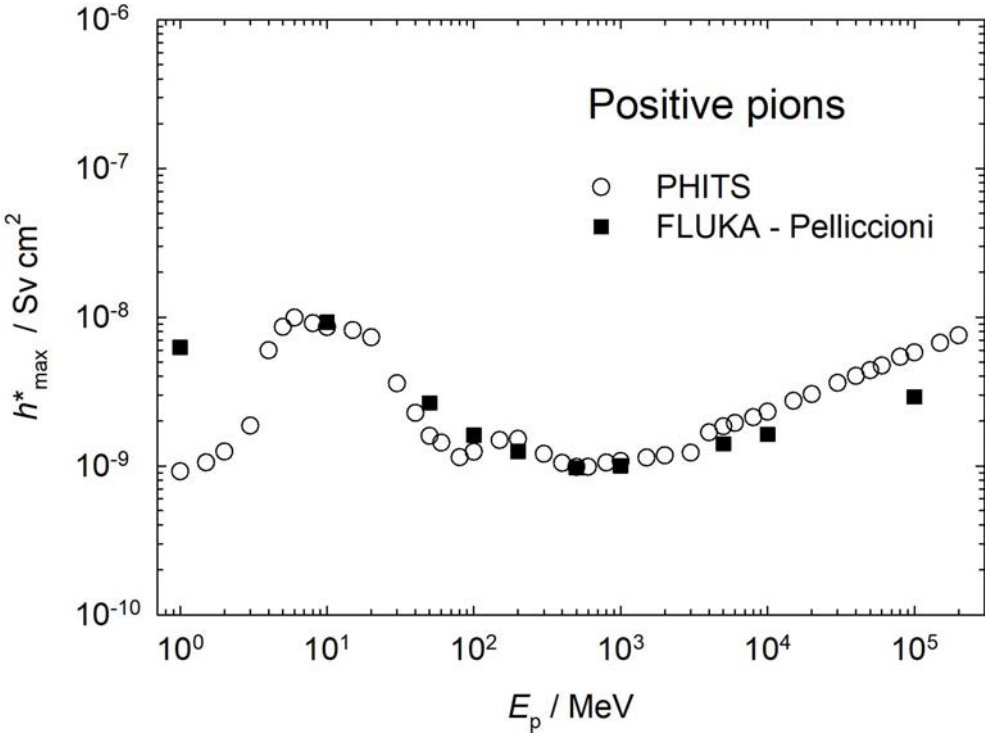

Figure 22 Comparison of h^*_{max} for positive pions.

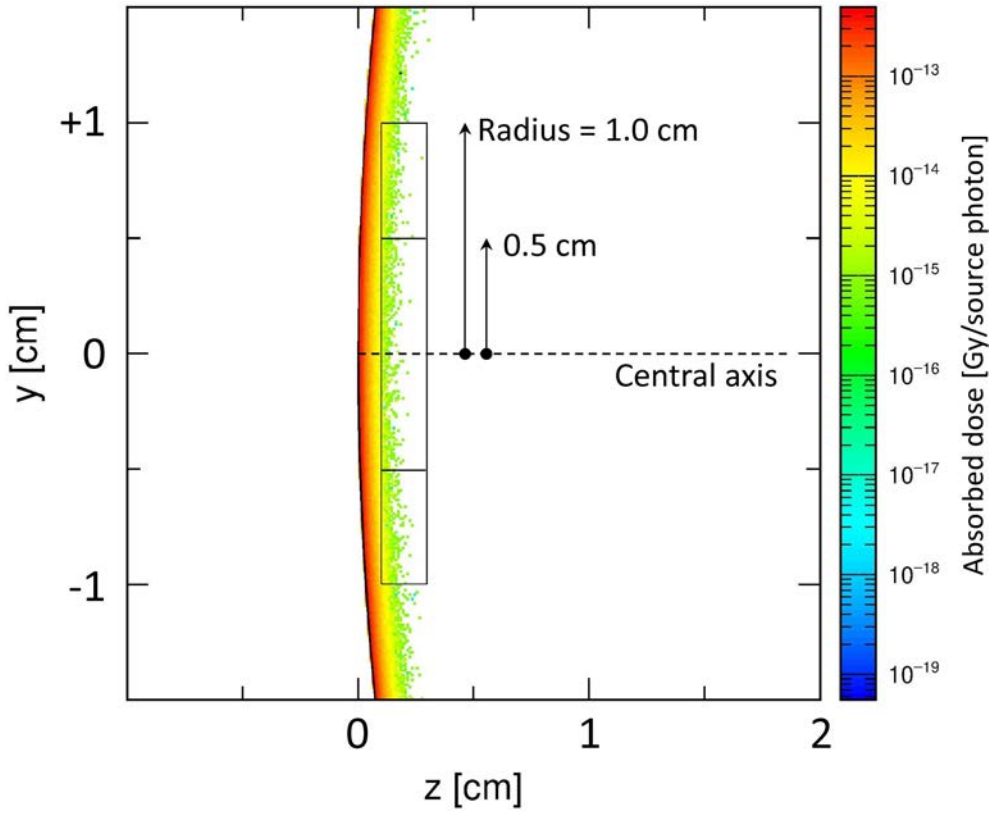

Figure 23 Absorbed dose distribution in the frontal region of the ICRU sphere.

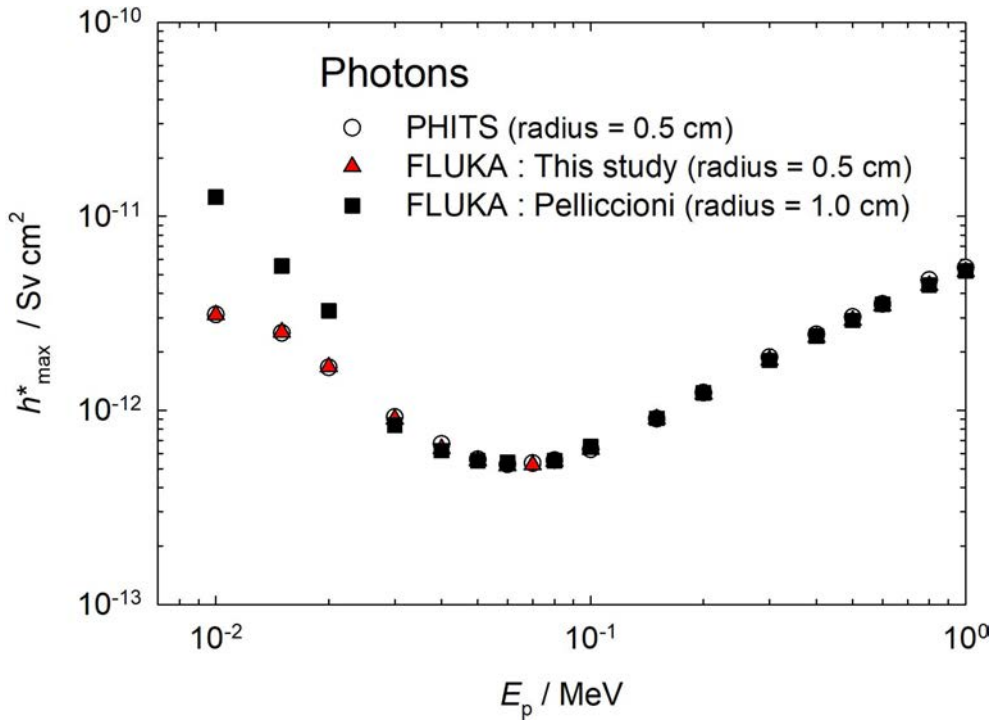

Figure 24 Effect of radius of the scoring region on h^*_{max}.

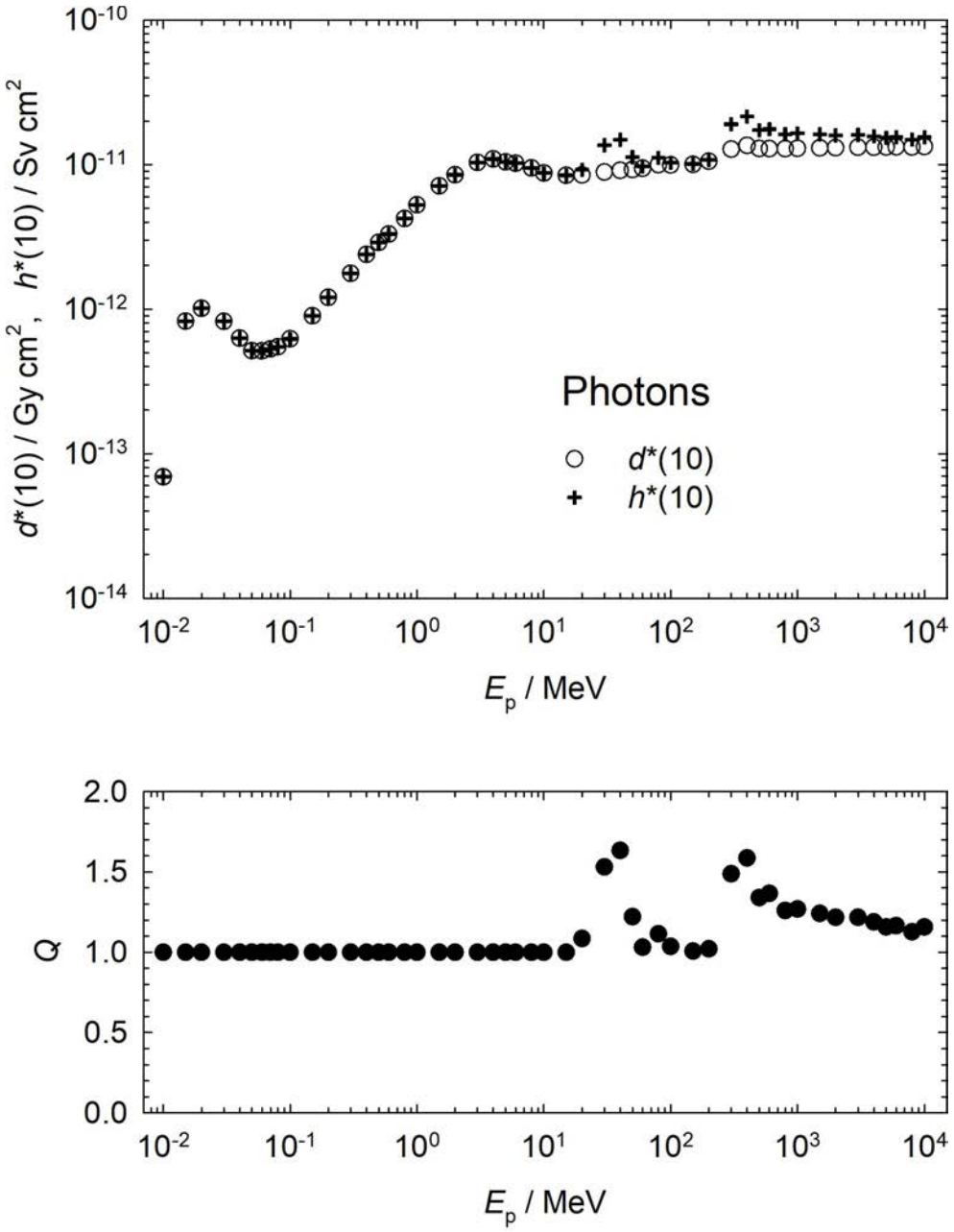

Figure 25 Photons: $d^*(10)$, $h^*(10)$, and Q.

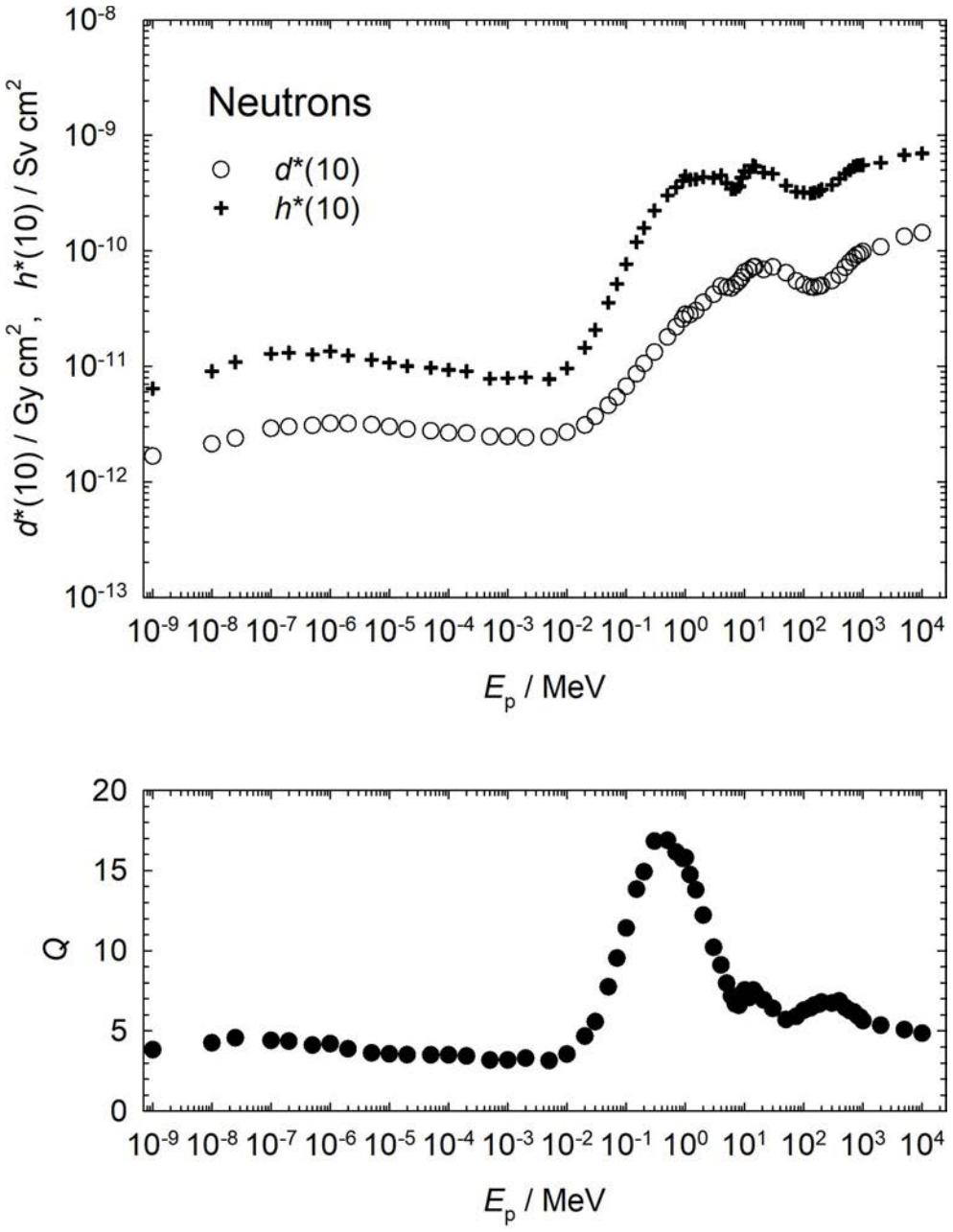

Figure 26 Neutrons: $d^*(10)$, $h^*(10)$, and Q.

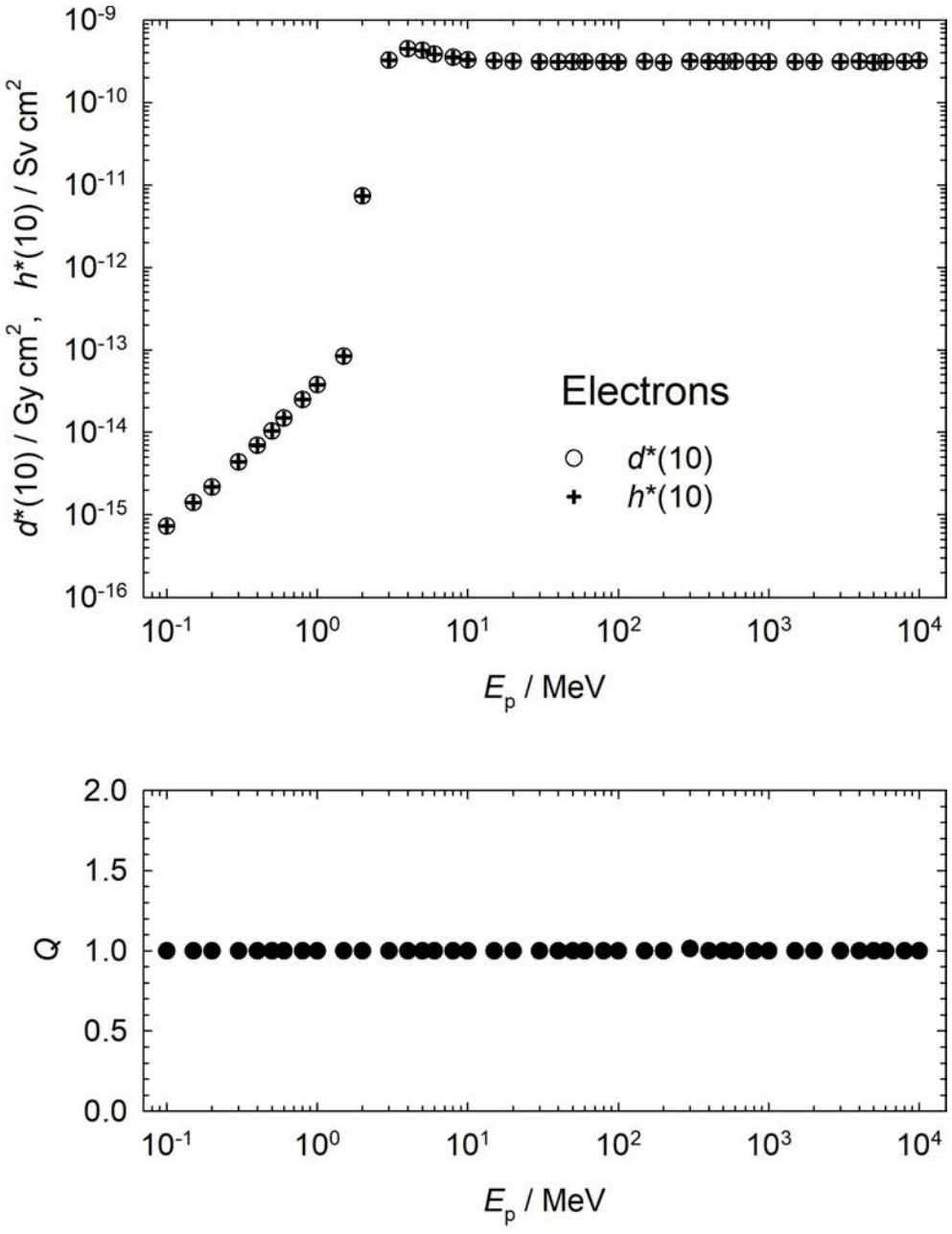

Figure 27 Electrons: $d^*(10)$, $h^*(10)$, and Q.

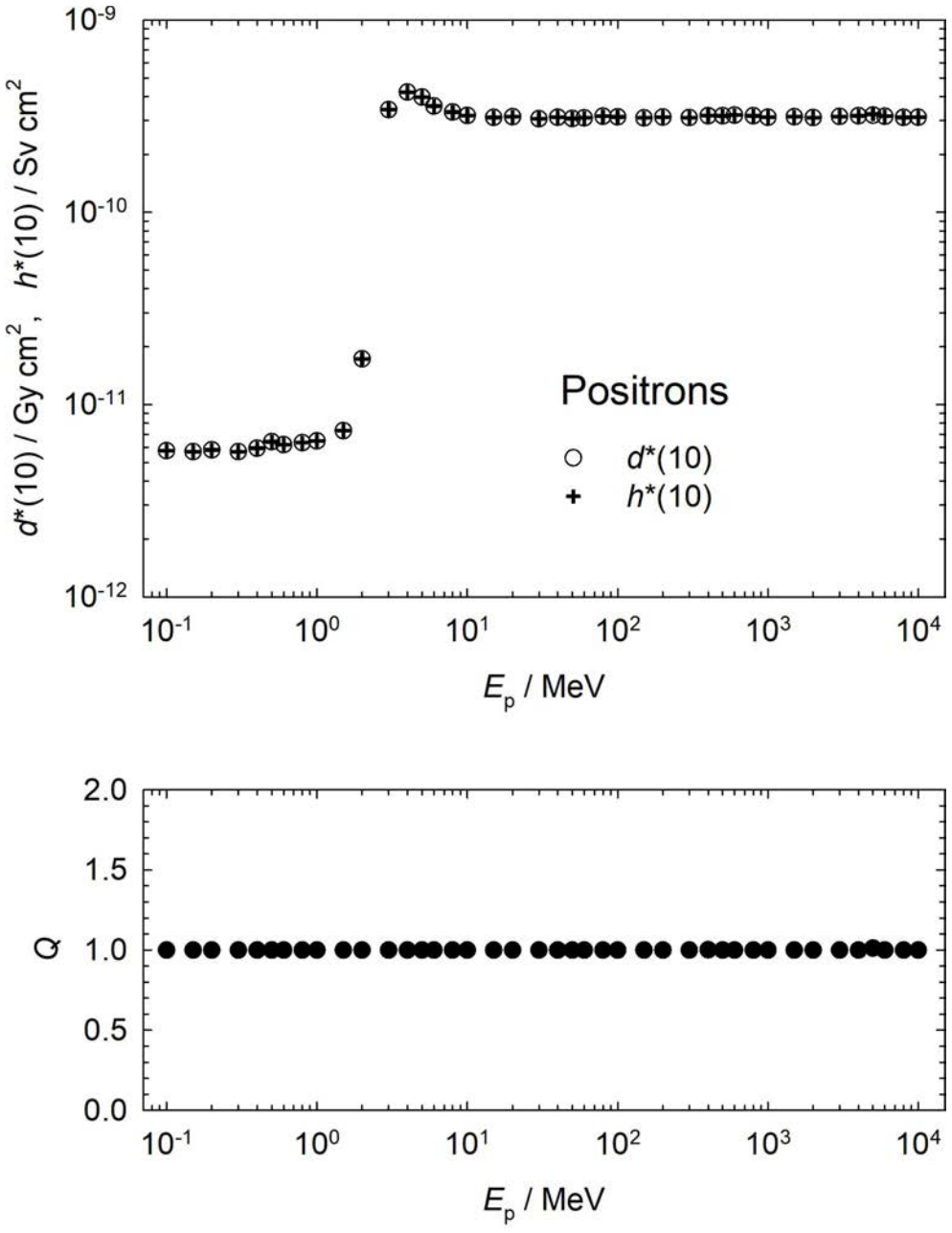

Figure 28 Positrons: $d^*(10)$, $h^*(10)$, and Q.

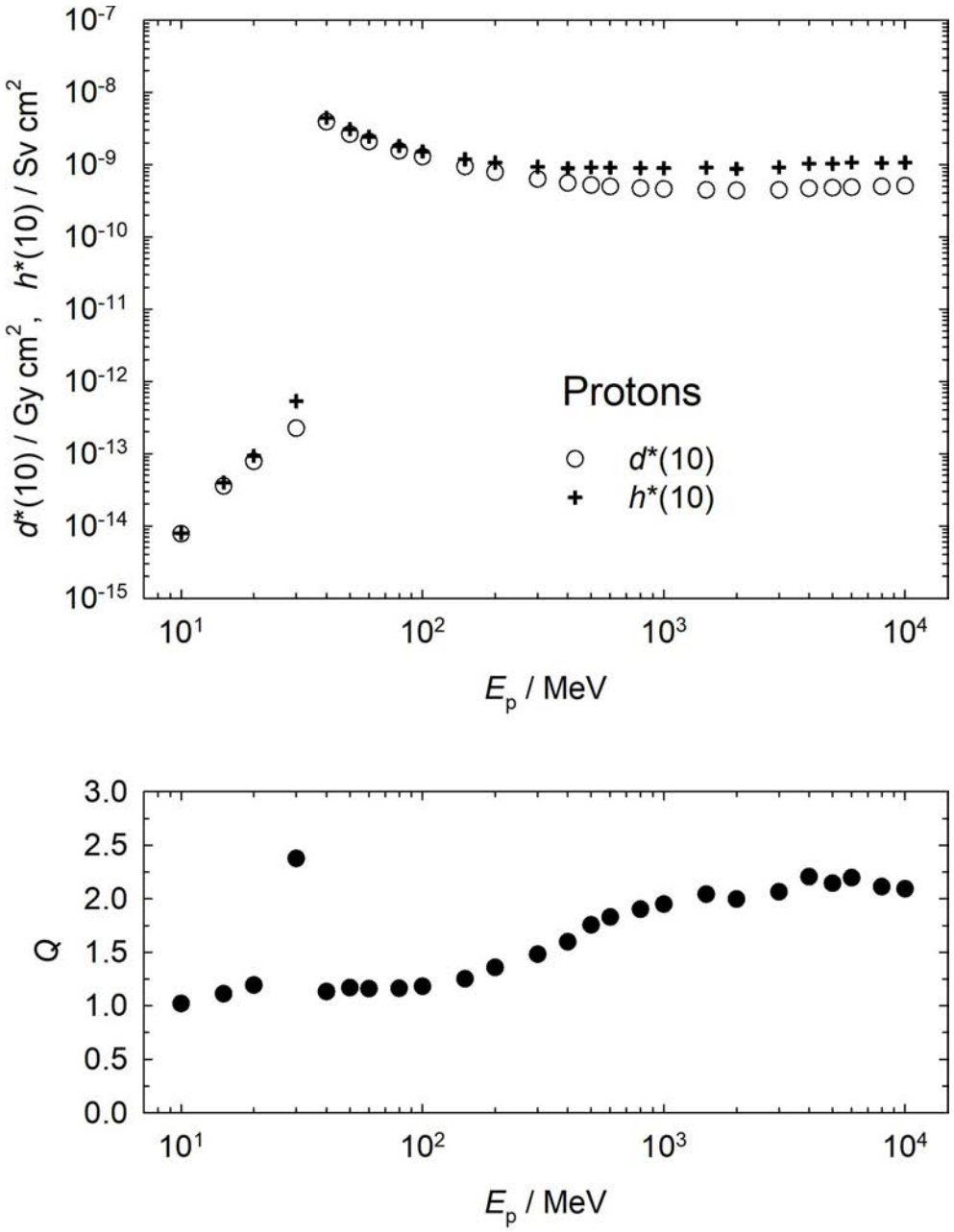

Figure 29 Protons: $d^*(10)$, $h^*(10)$, and Q.

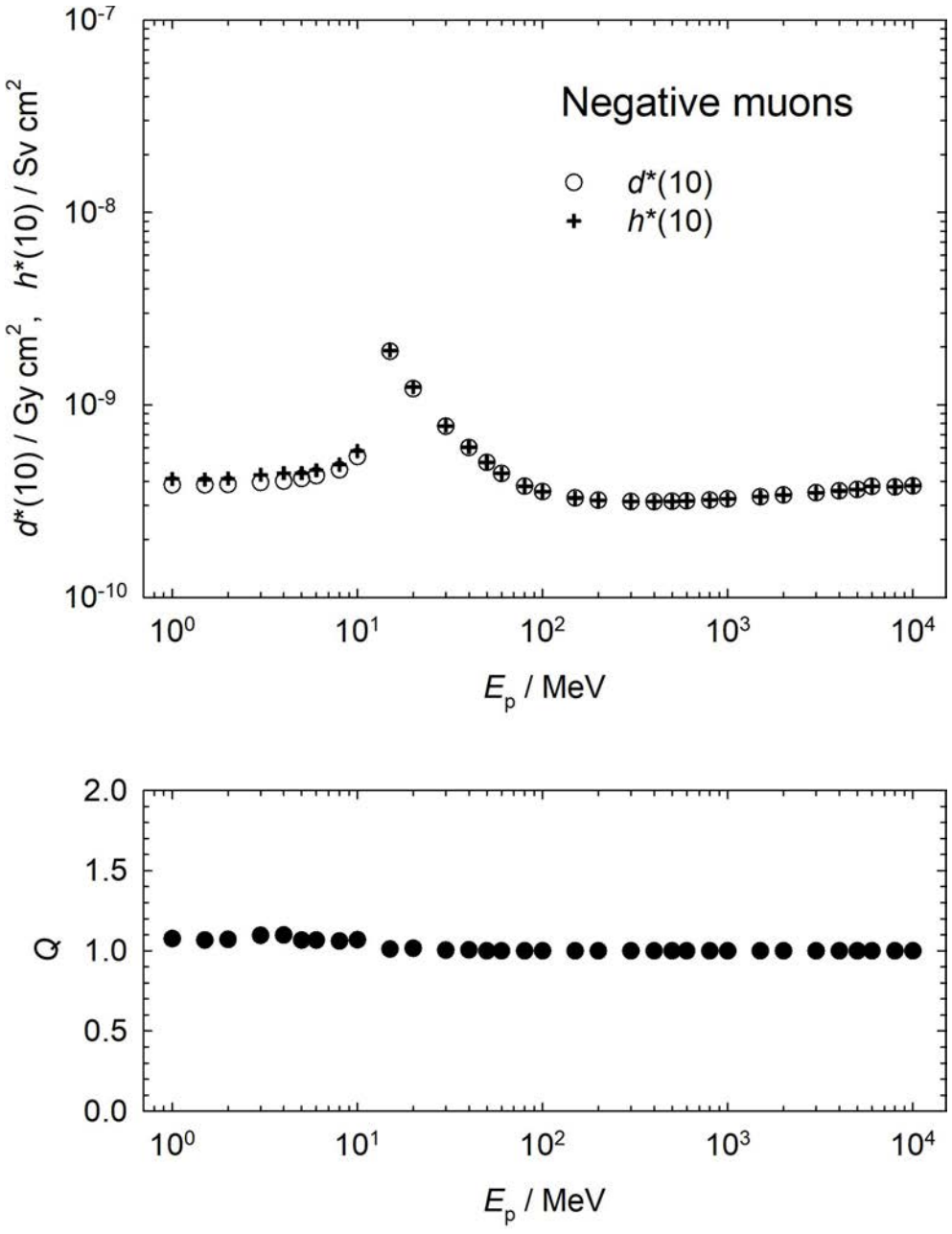

Figure 30 Negative muons: $d^*(10)$, $h^*(10)$, and Q.

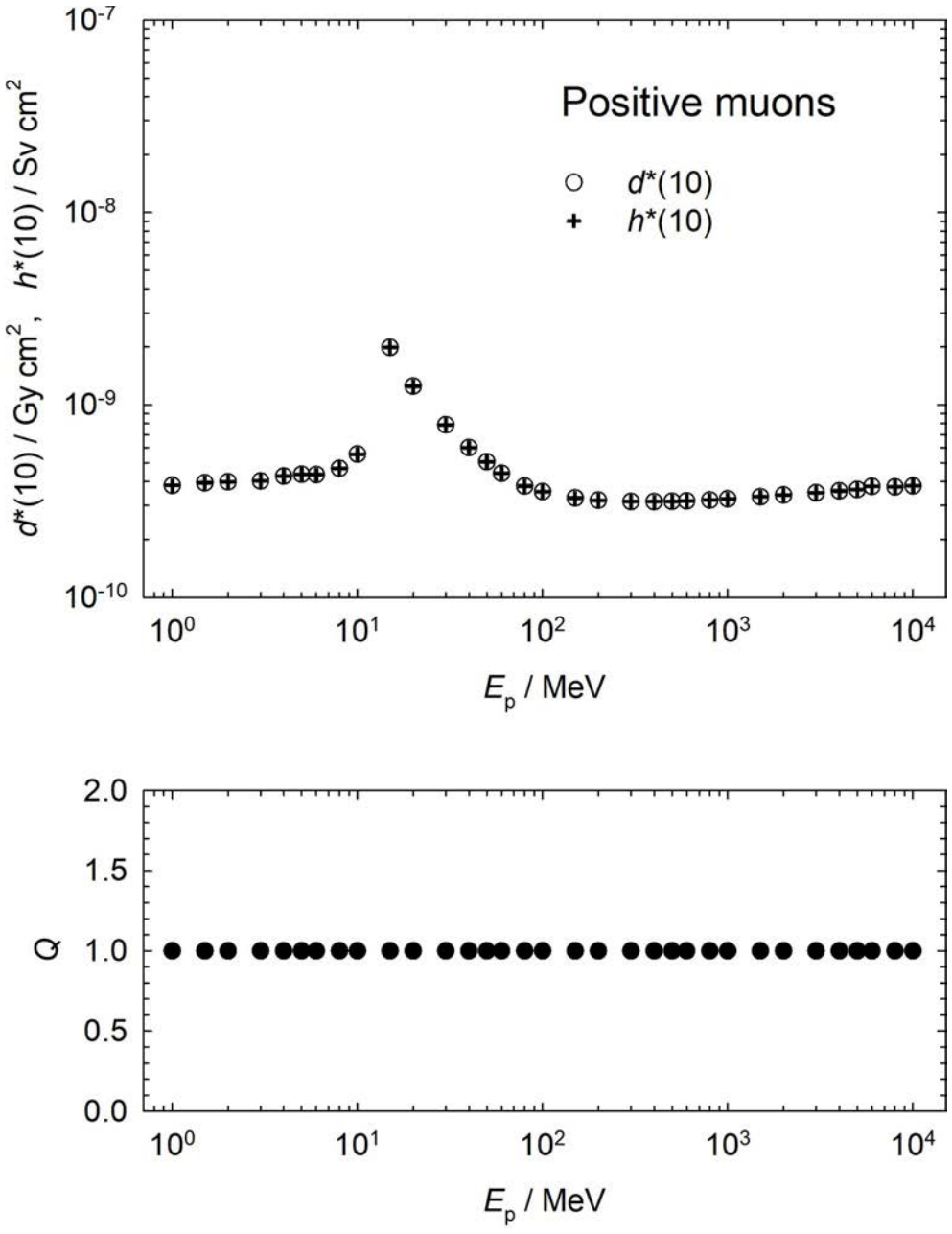

Figure 31 Positive muons: $d^*(10)$, $h^*(10)$, and Q.

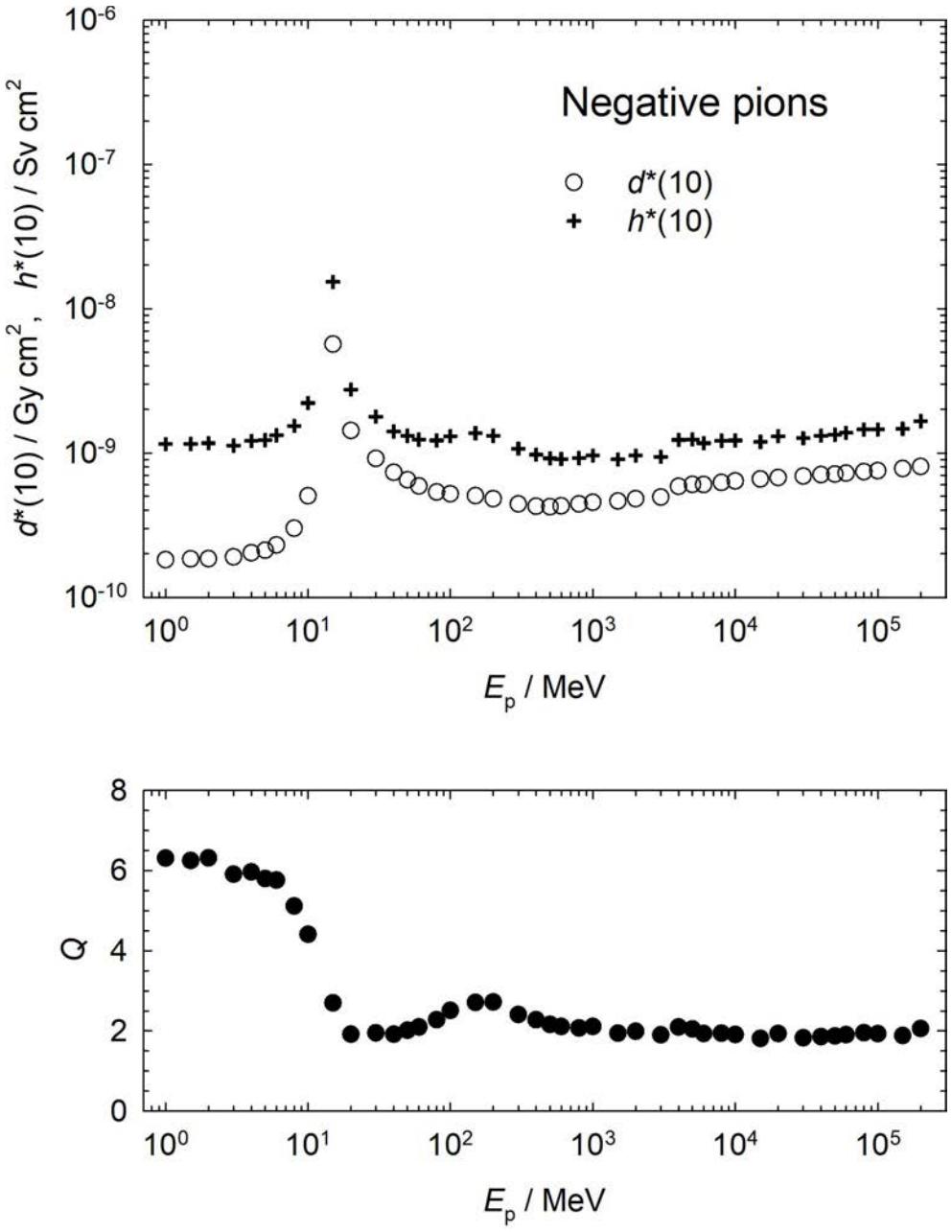

Figure 32 Negative pions: $d^*(10)$, $h^*(10)$, and Q.

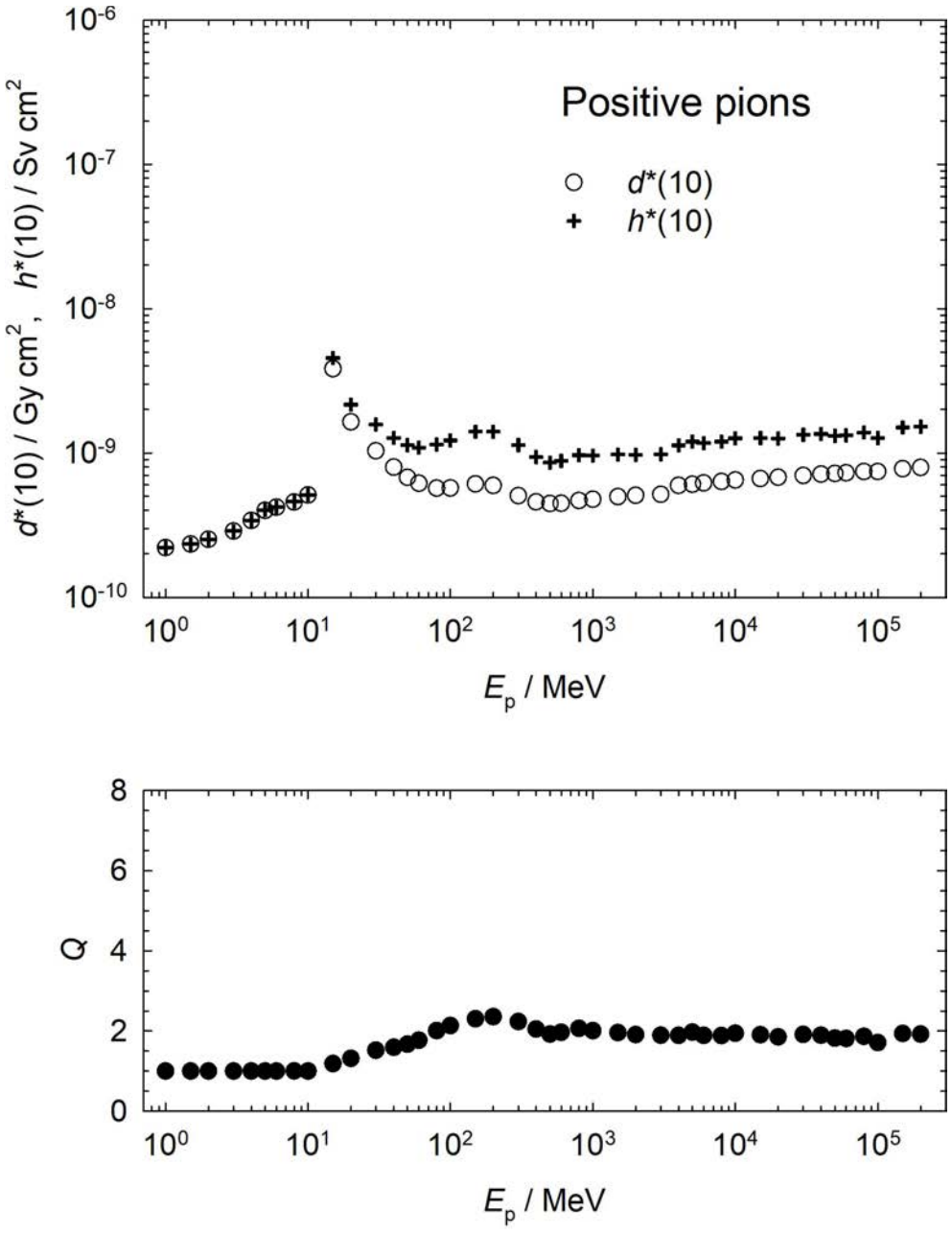

Figure 33 Positive pions: $d^*(10)$, $h^*(10)$, and Q.

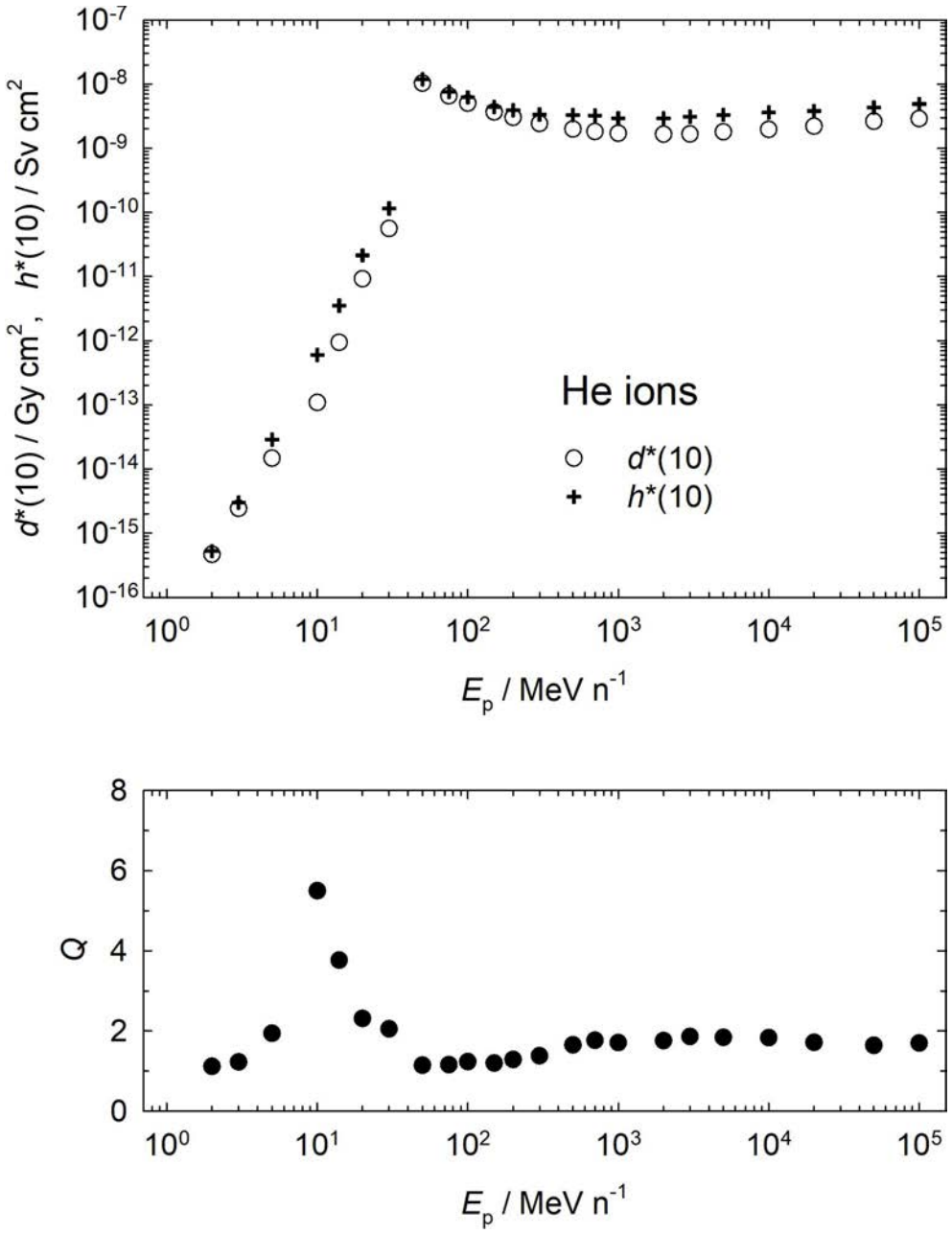

Figure 34 Helium ions: $d^*(10)$, $h^*(10)$, and Q.

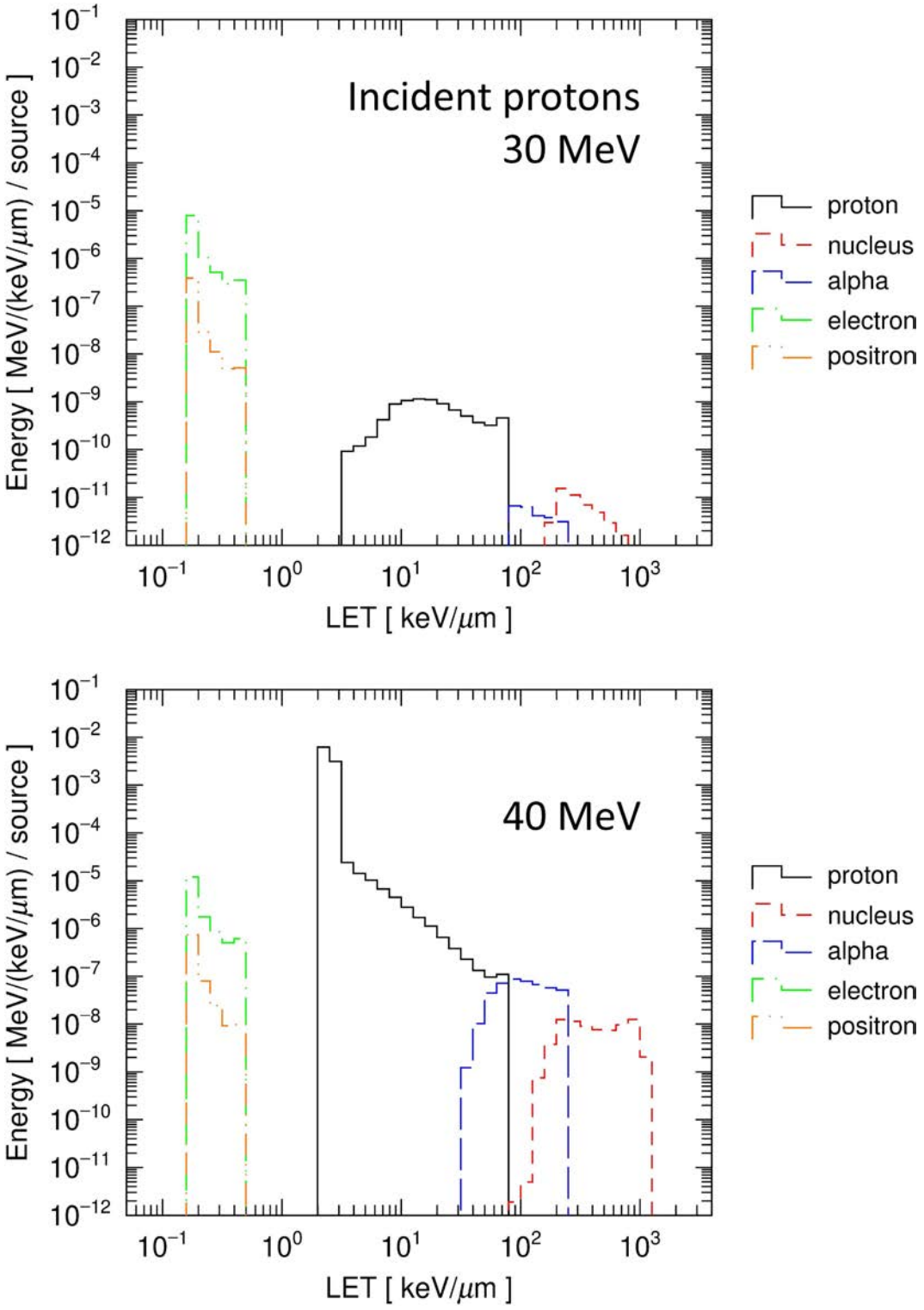

Figure 35 LET distributions of charged particles in the ICRU sphere irradiated by protons.

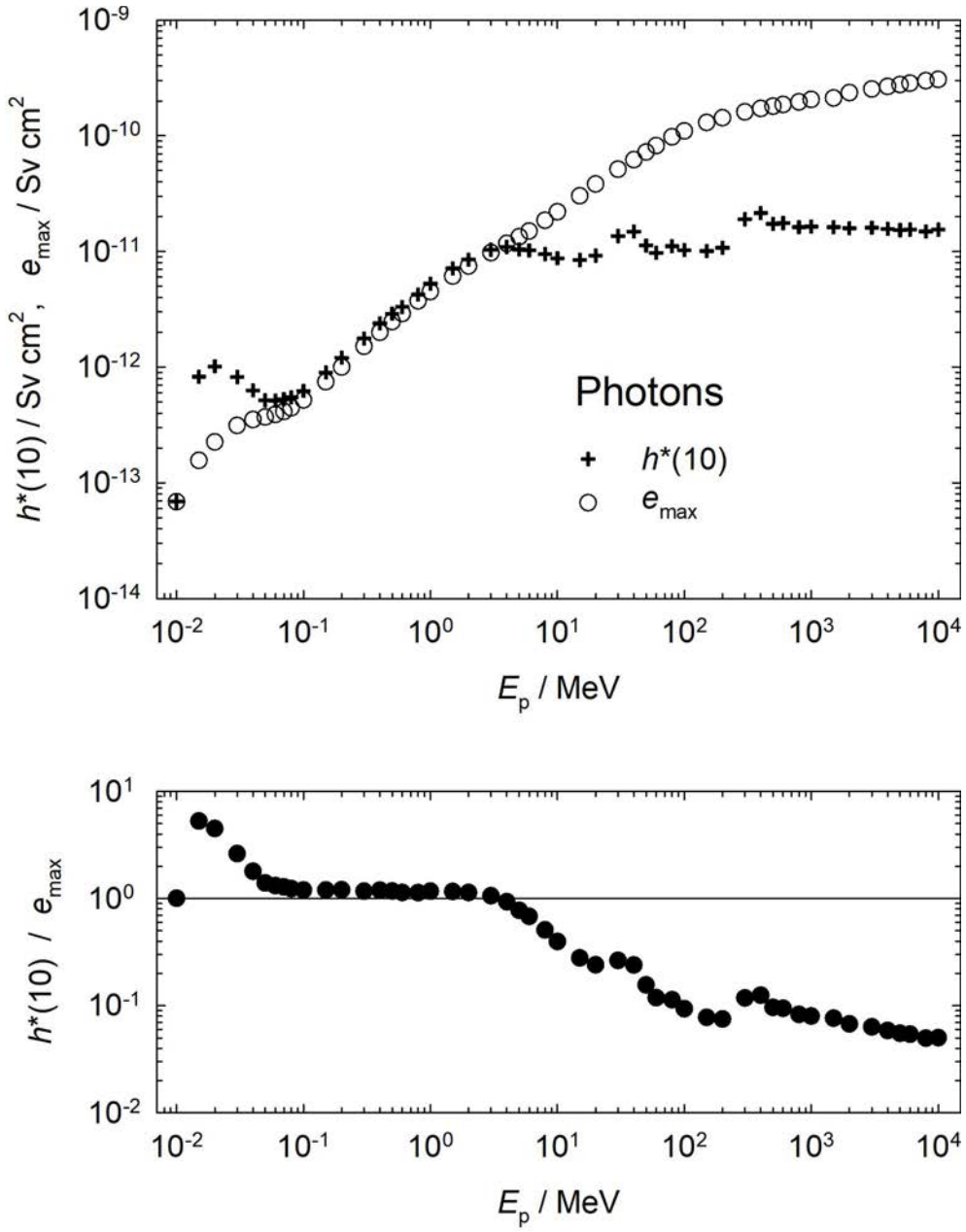

Figure 36 Photons: $h^*(10)$, e_{max}, and $h^*(10)/e_{max}$.

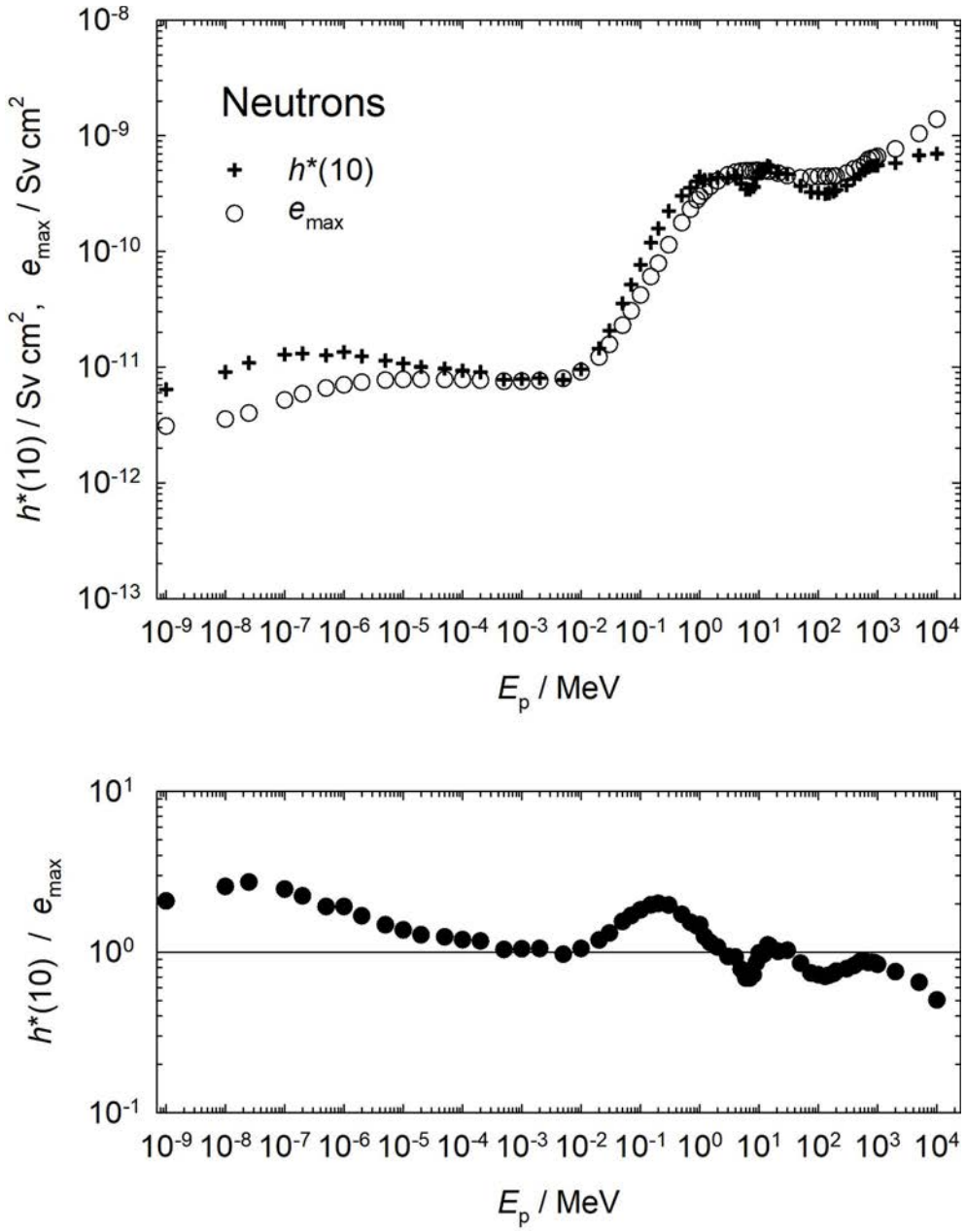

Figure 37 Neutrons: $h^*(10)$, $e_{\max}$, and $h^*(10)/e_{\max}$.

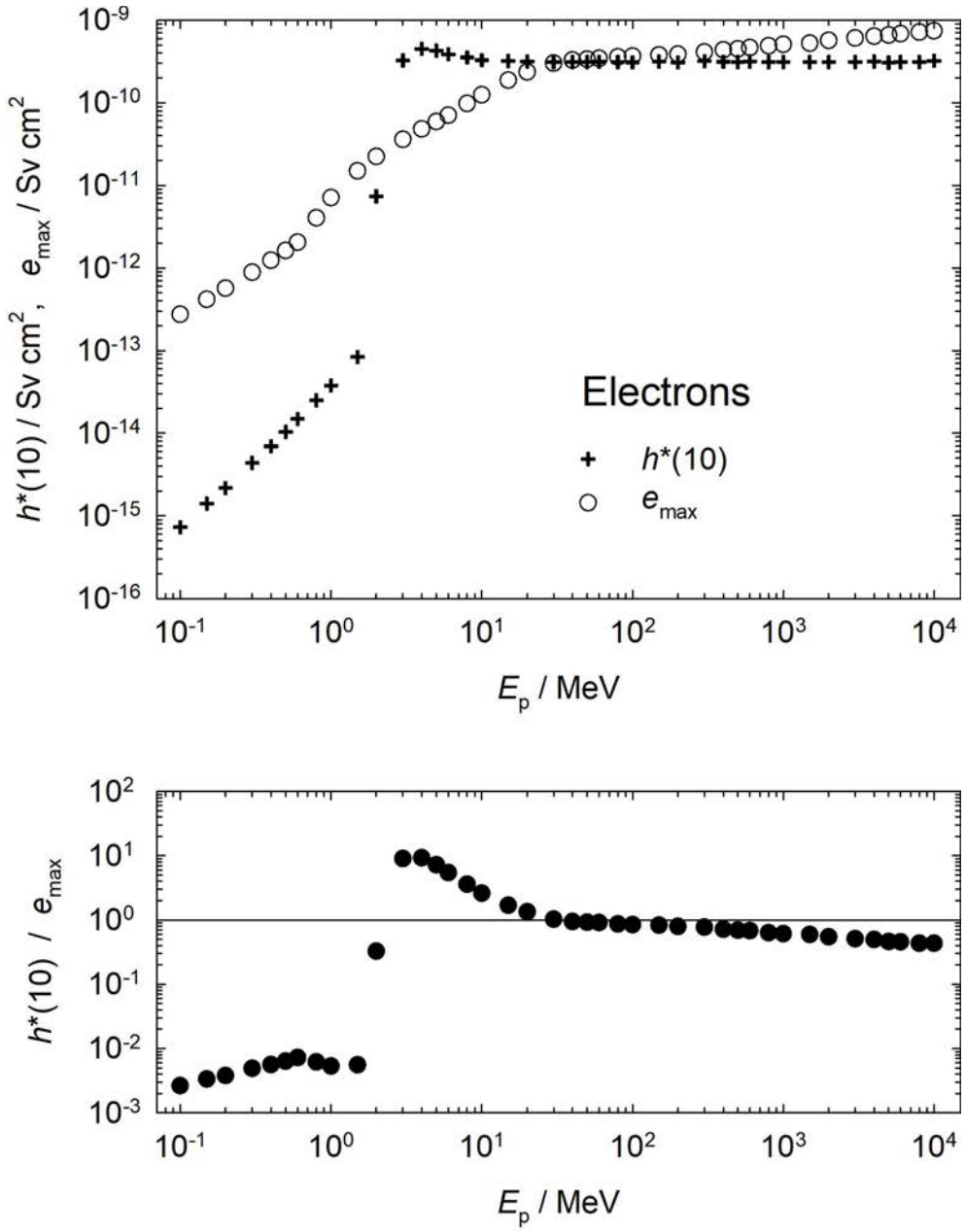

Figure 38 Electrons: $h^*(10)$, e_{max}, and $h^*(10)/e_{max}$.

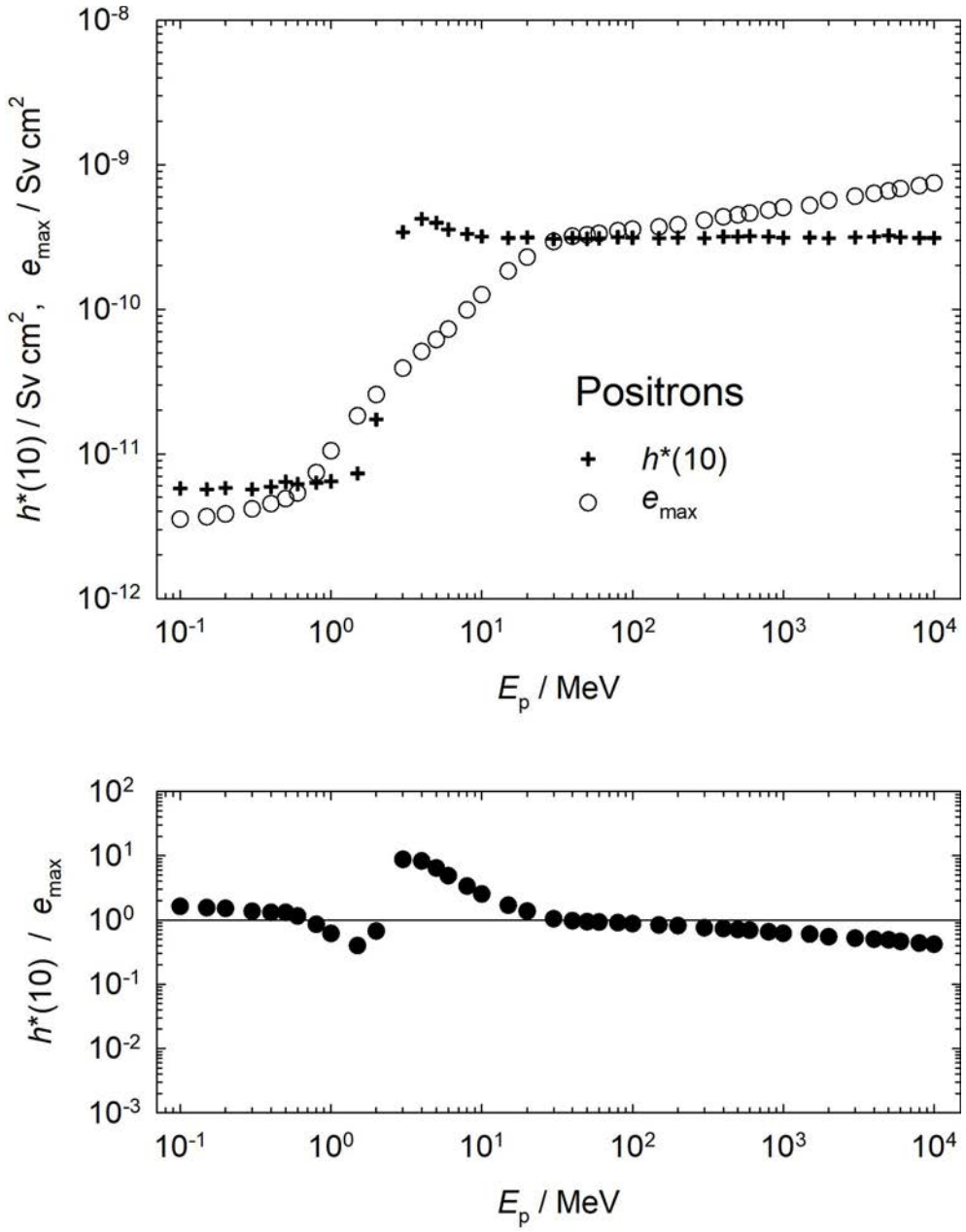

Figure 39 Positrons: $h^*(10)$, $e_{\max}$, and $h^*(10)/e_{\max}$.

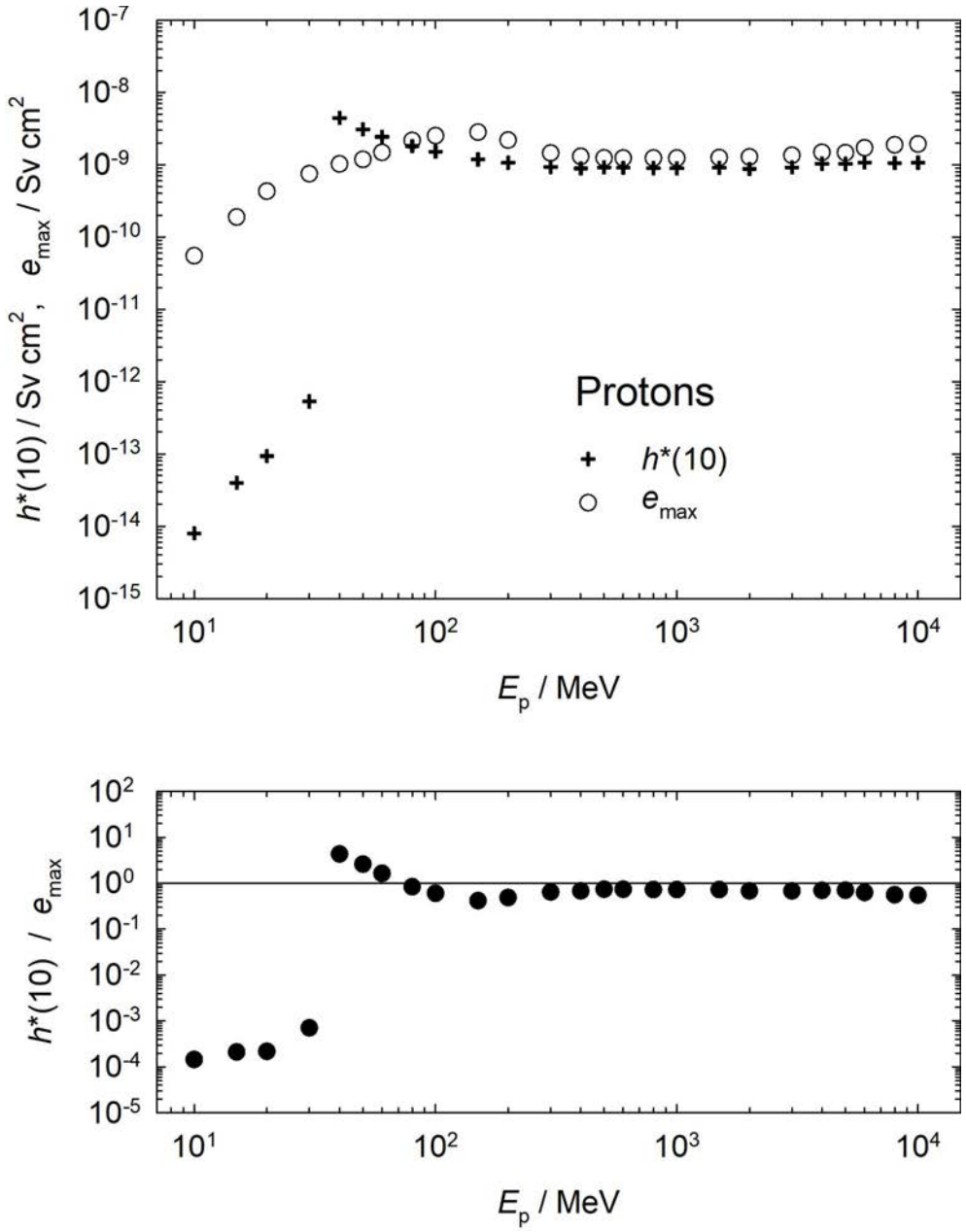

Figure 40 Protons: $h^*(10)$, e_{max}, and $h^*(10)/e_{max}$.

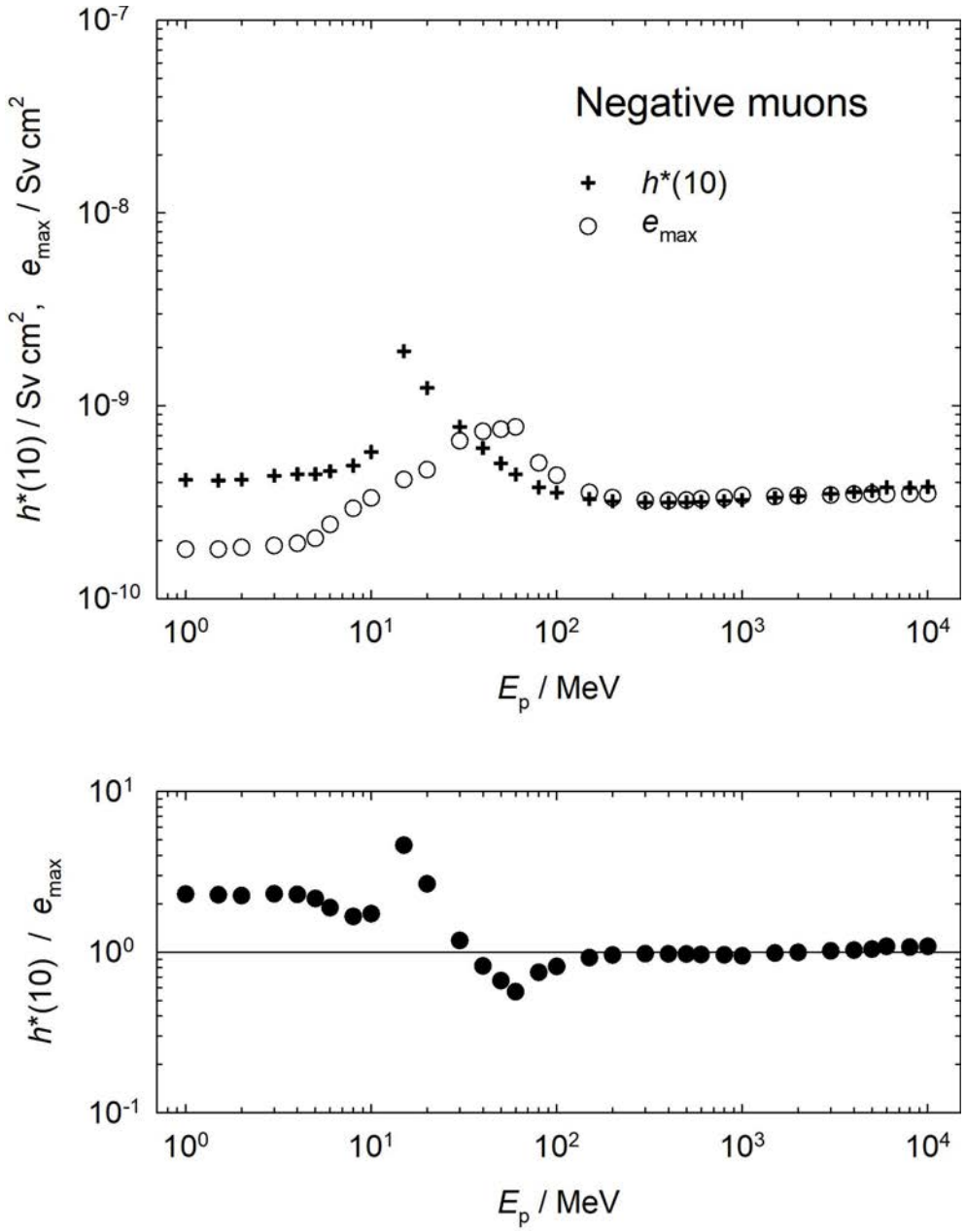

Figure 41 Negative muons: $h^*(10)$, $e_{\max}$, and $h^*(10)/e_{\max}$.

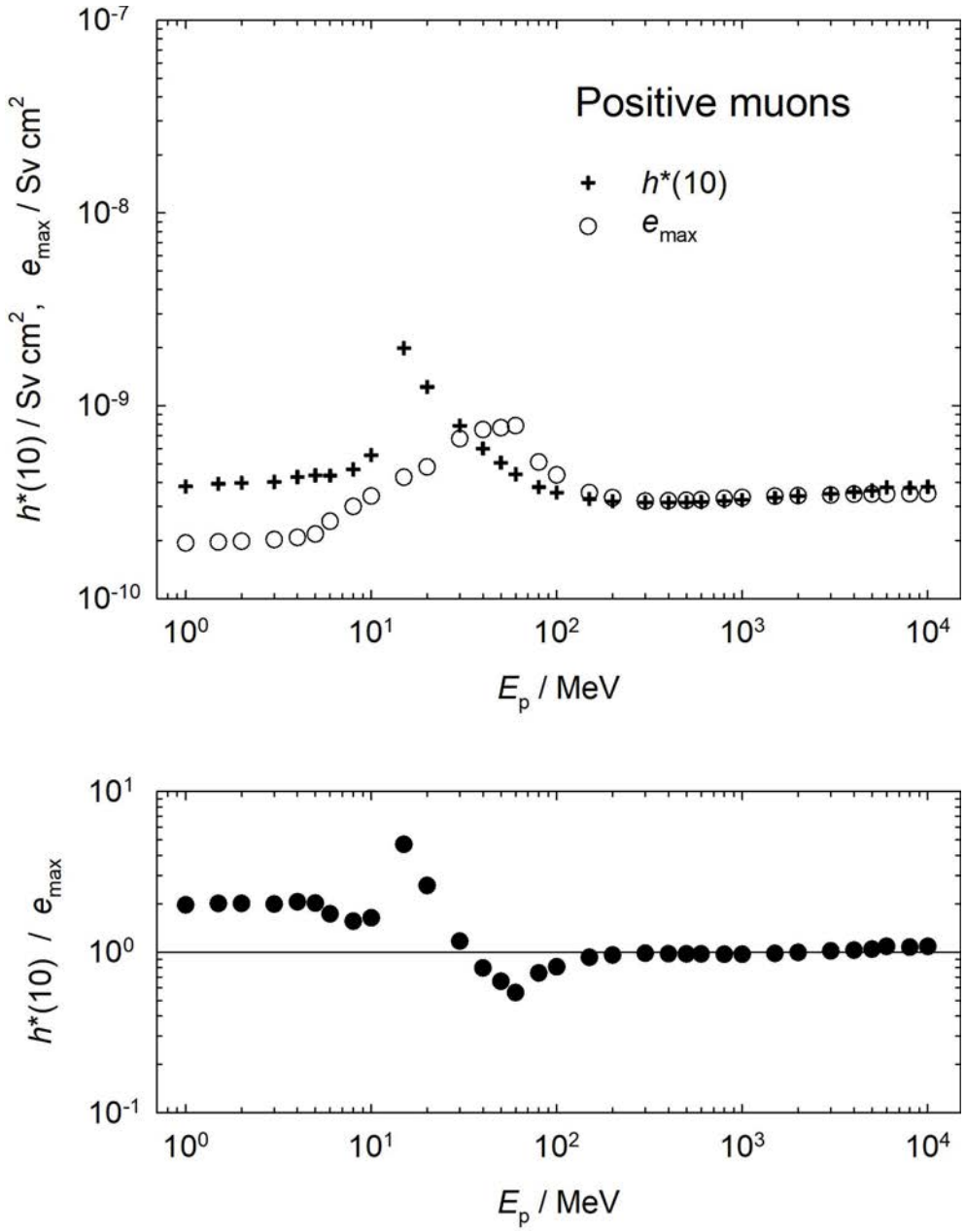

Figure 42 Positive muons: $h^*(10)$, e_{max}, and $h^*(10)/e_{max}$.

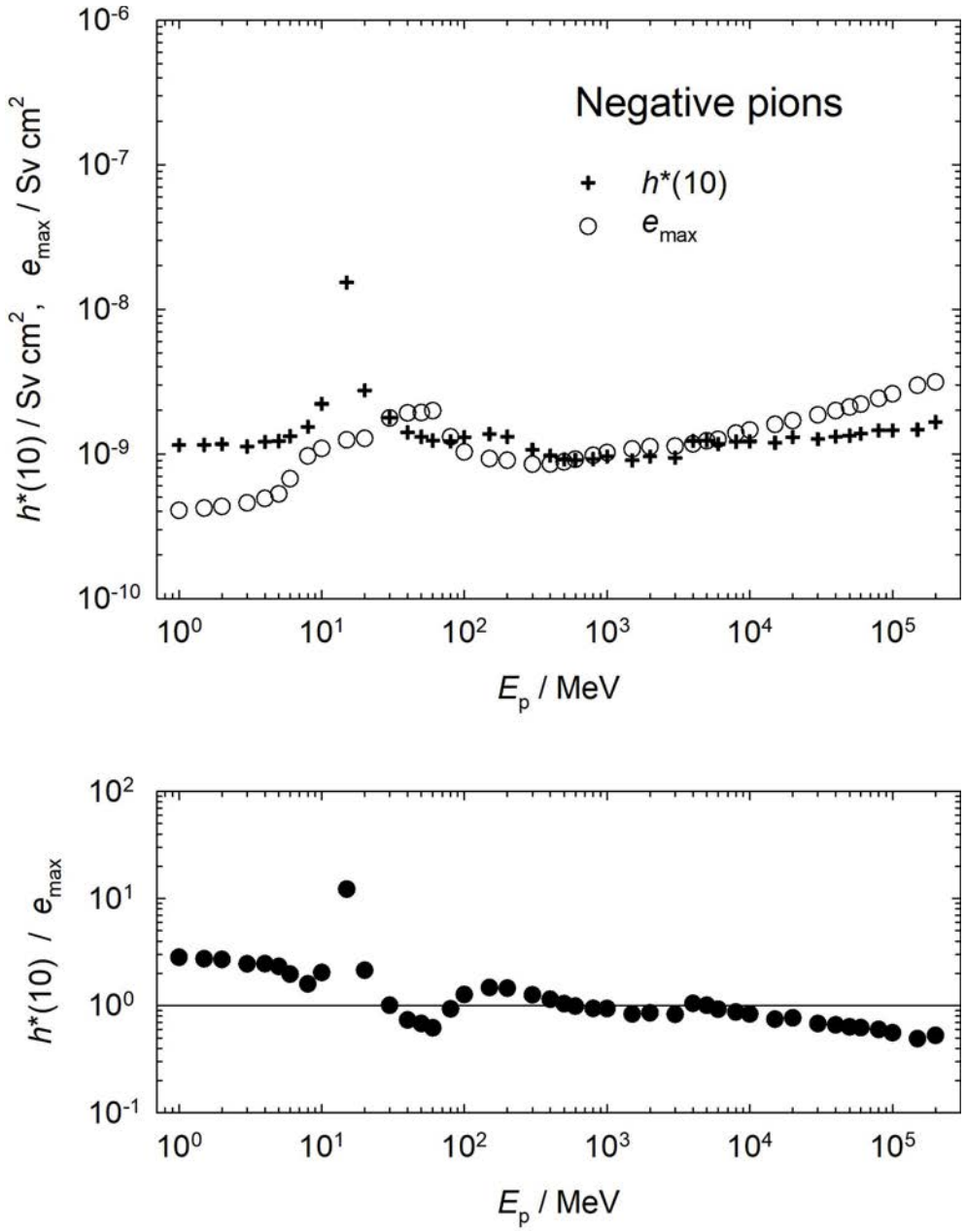

Figure 43 Negative pions: $h^*(10)$, e_{max}, and $h^*(10)/e_{max}$.

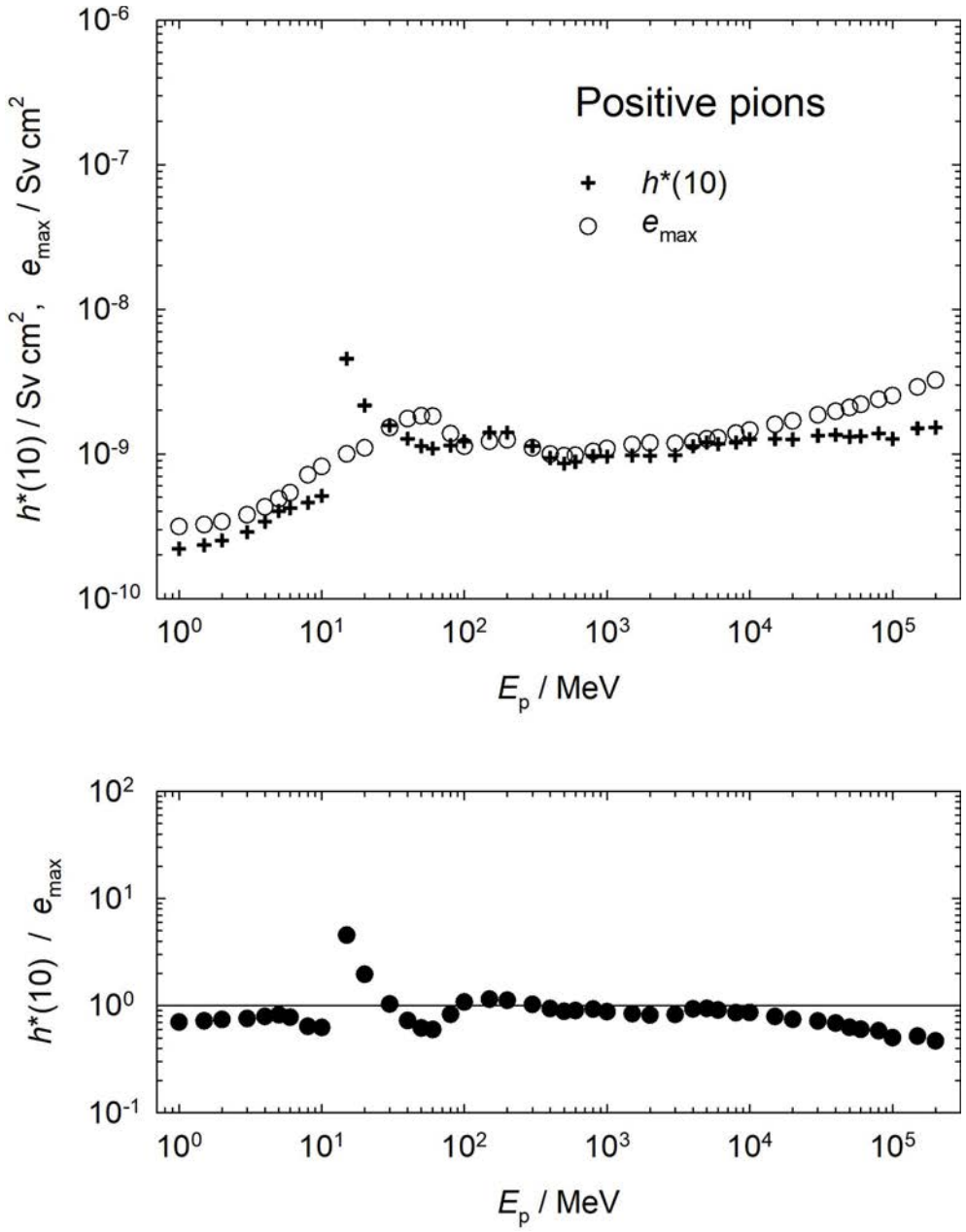

Figure 44 Positive pions: $h^*(10)$, $e_{\max}$, and $h^*(10)/e_{\max}$.

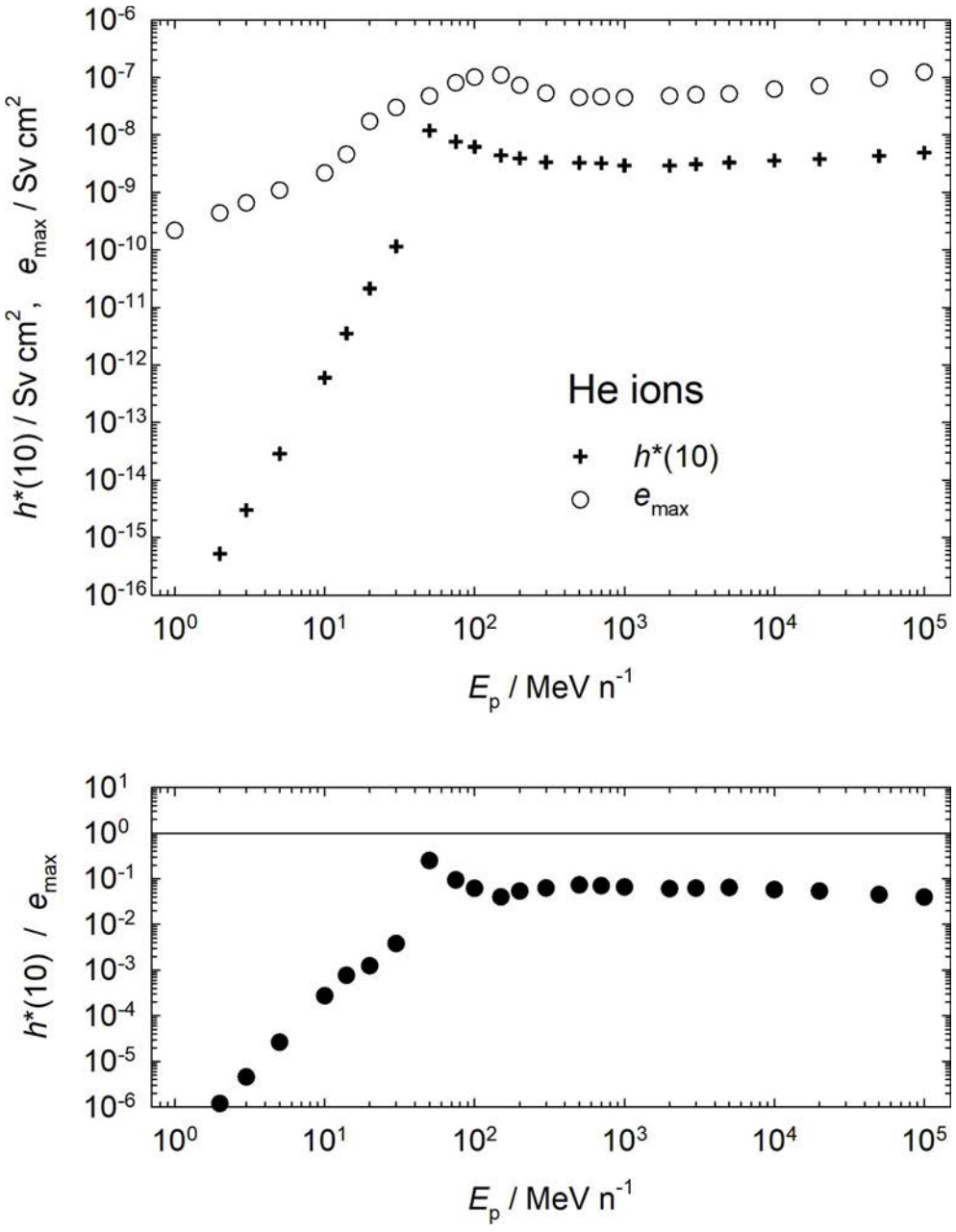

Figure 45 Helium ions: $h^*(10)$, e_{max}, and $h^*(10)/e_{max}$.

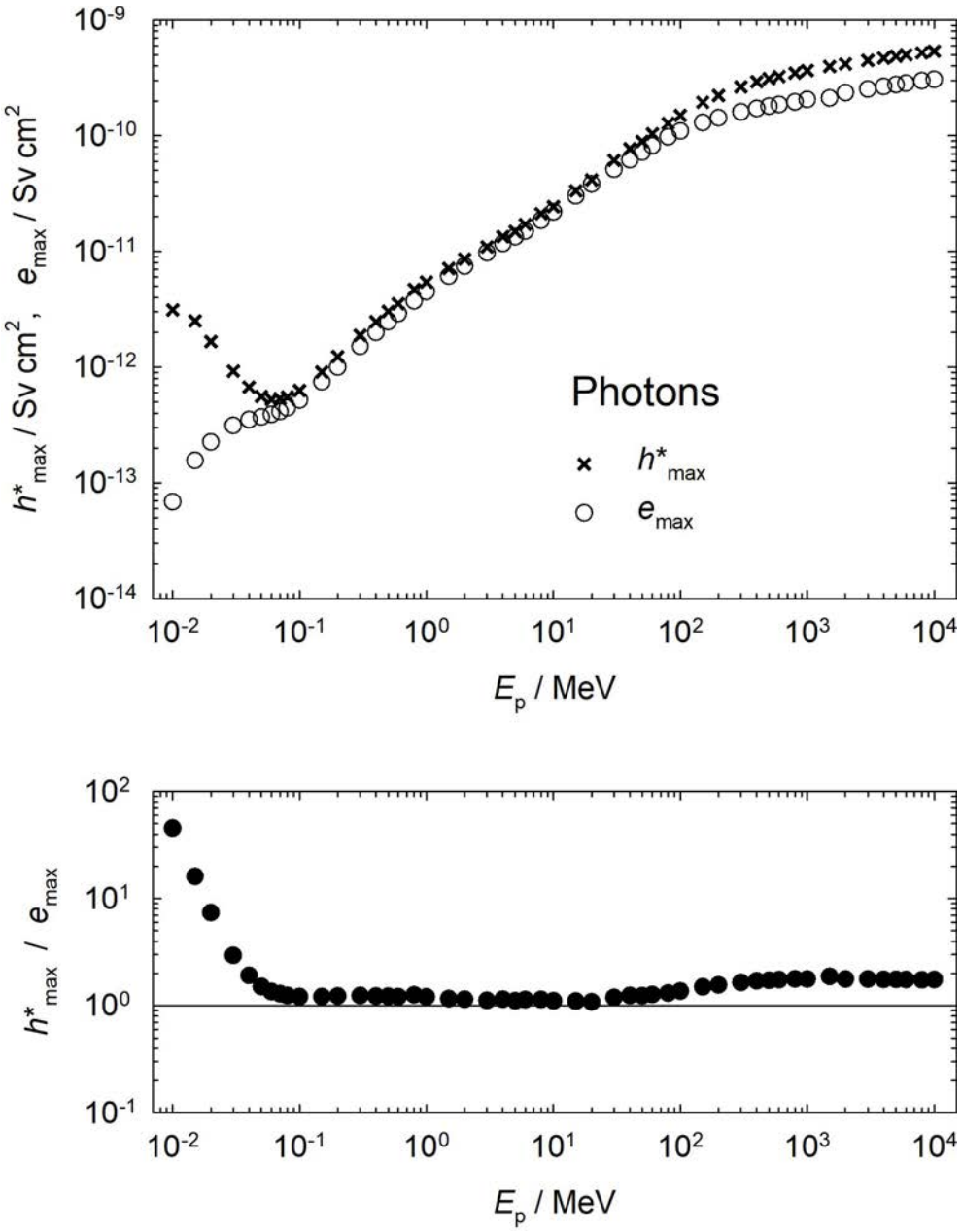

Figure 46 Photons: h^*_{max}, e_{max}, and h^*_{max}/e_{max}.

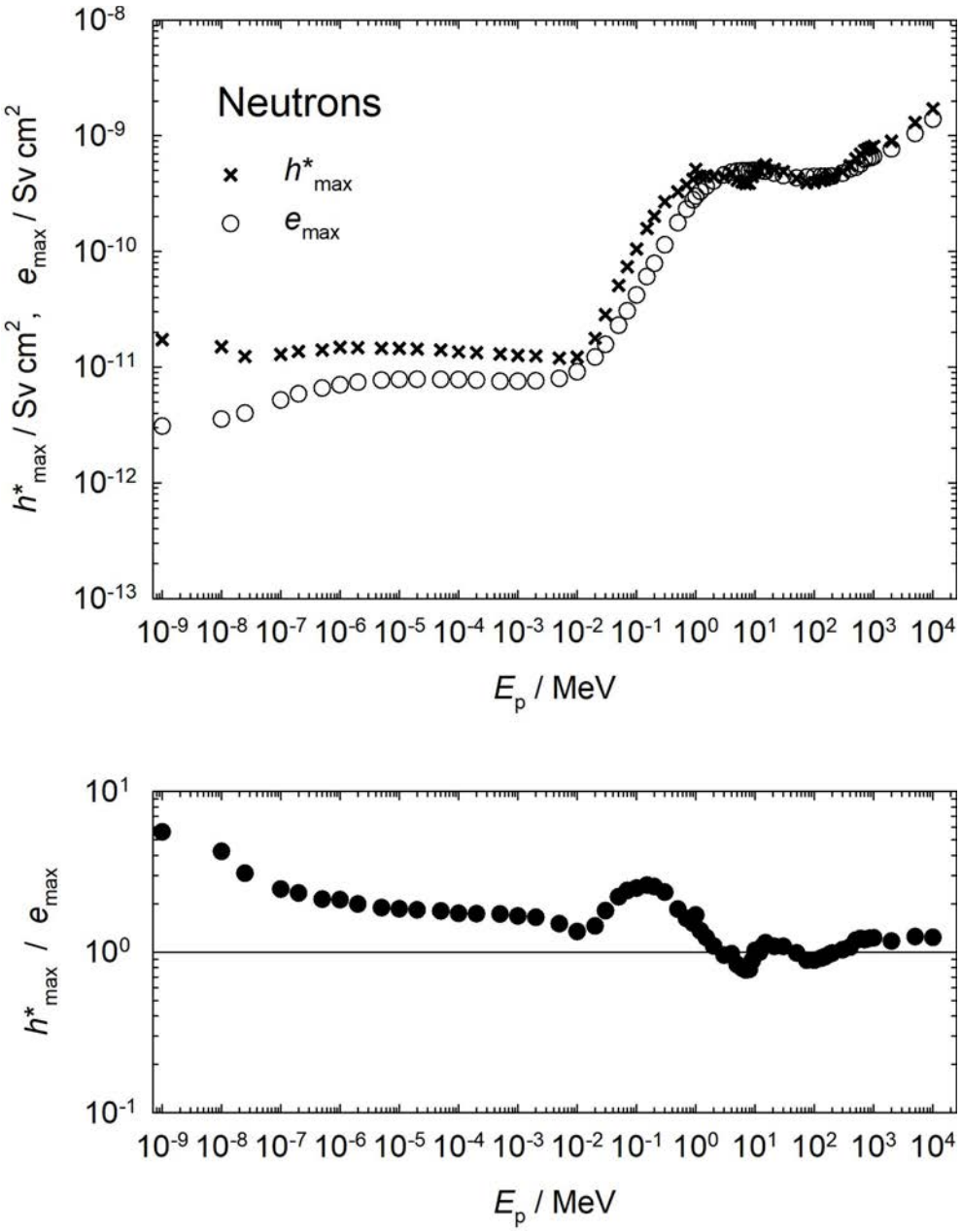

Figure 47 Neutrons: h^*_{max}, e_{max}, and h^*_{max}/e_{max}.

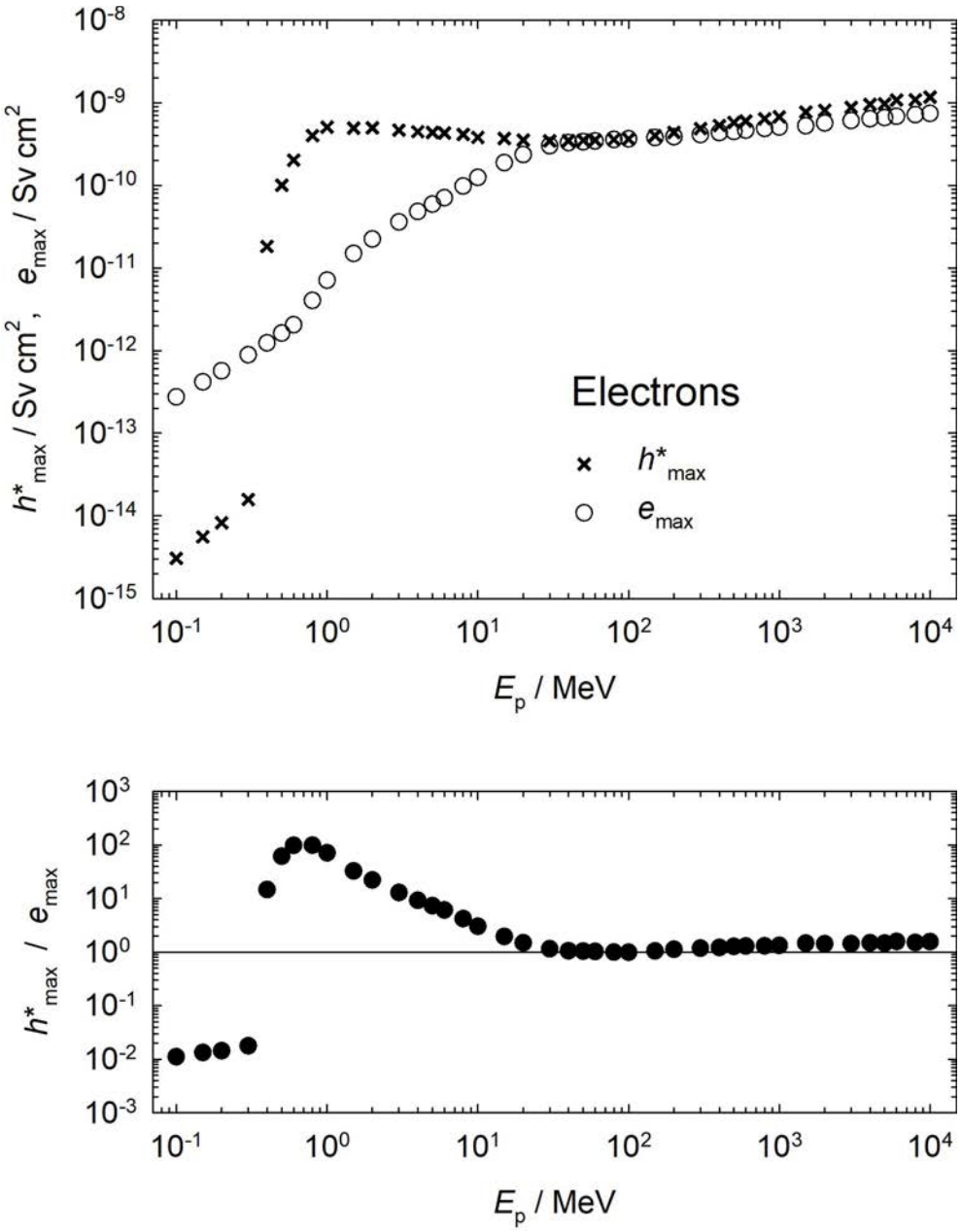

Figure 48 Electrons: h^*_{max}, e_{max}, and h^*_{max}/e_{max}.

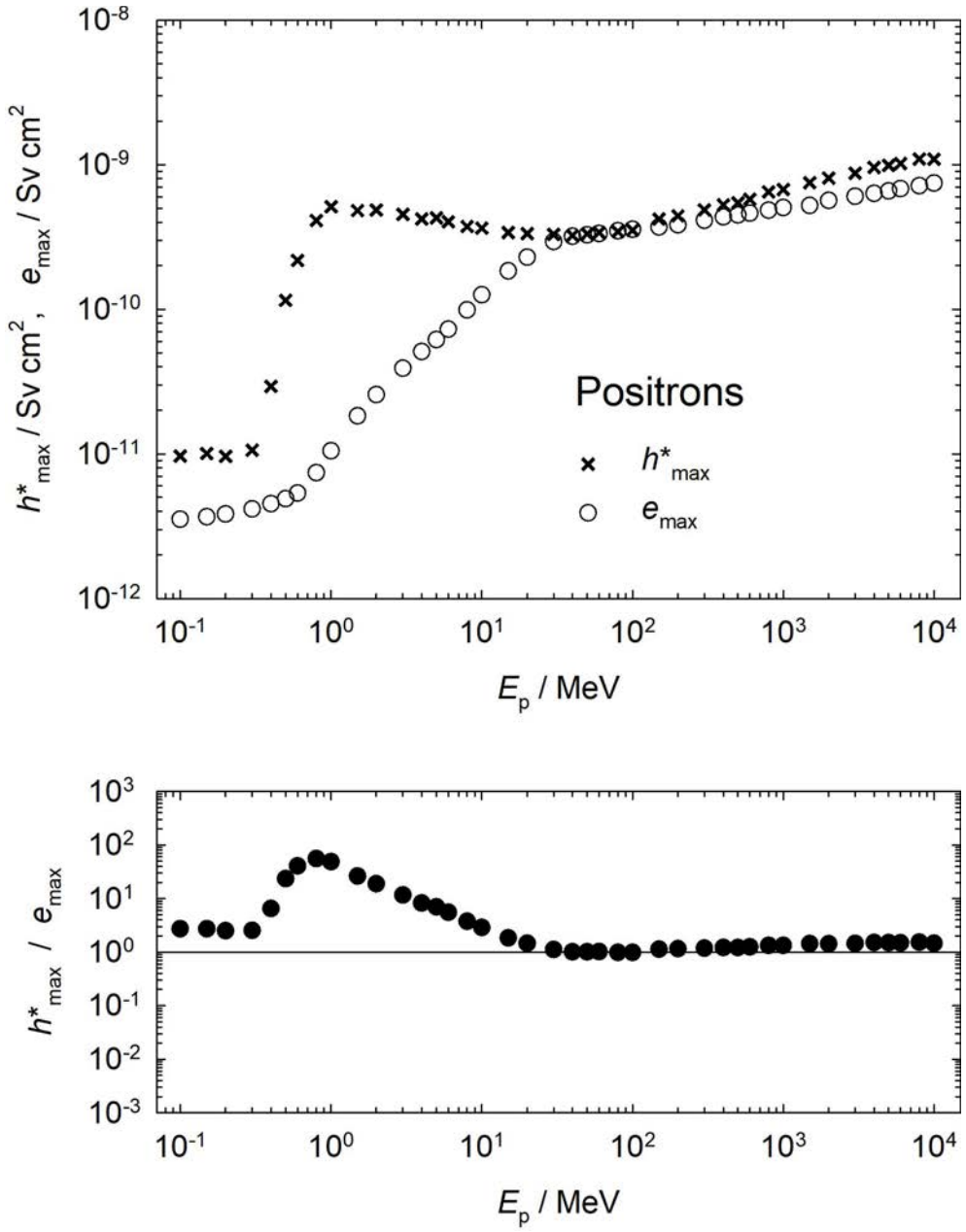

Figure 49 Positrons: h^*_{max}, e_{max}, and h^*_{max}/e_{max}.

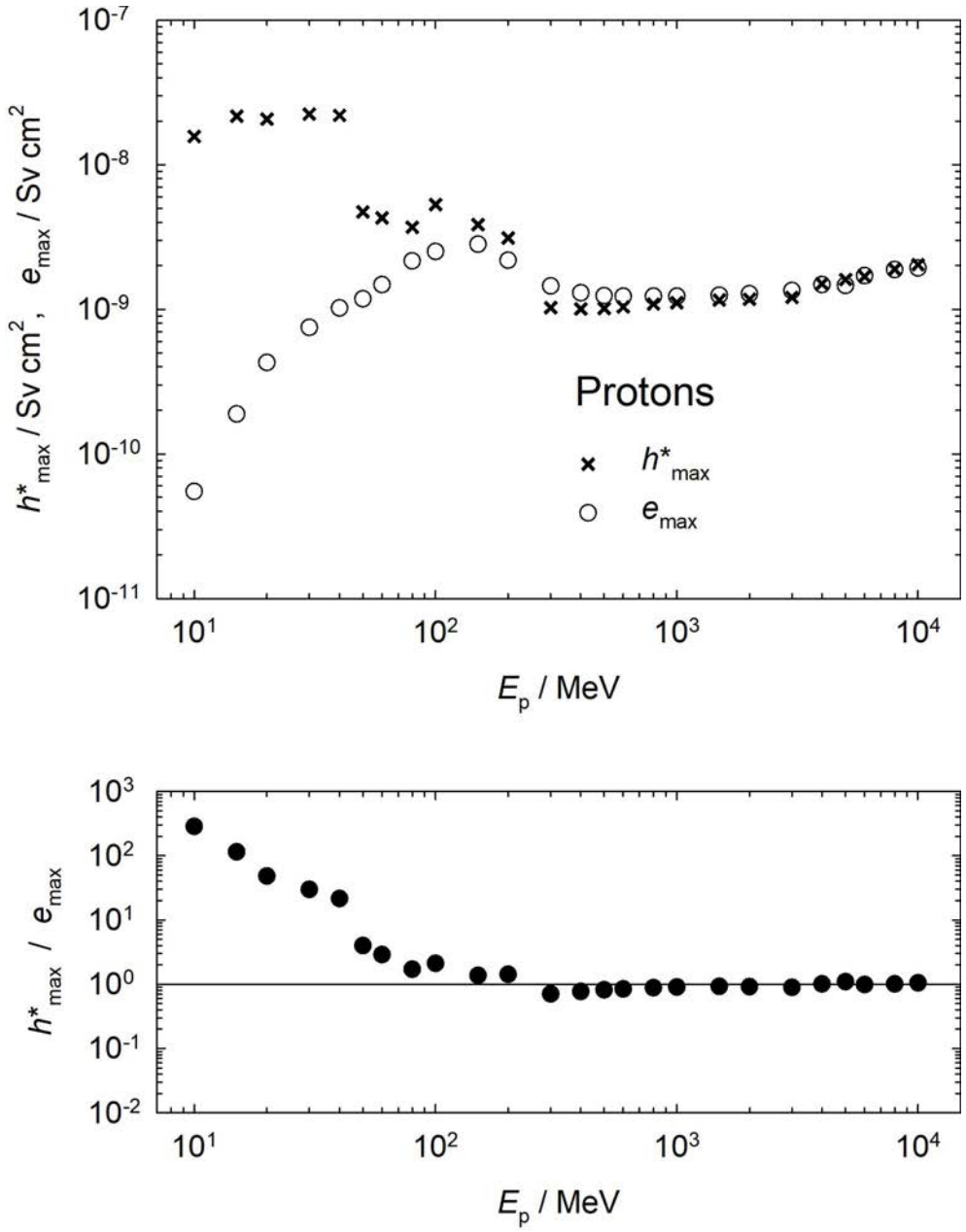

Figure 50 Protons: h^*_{max}, e_{max}, and h^*_{max}/e_{max}.

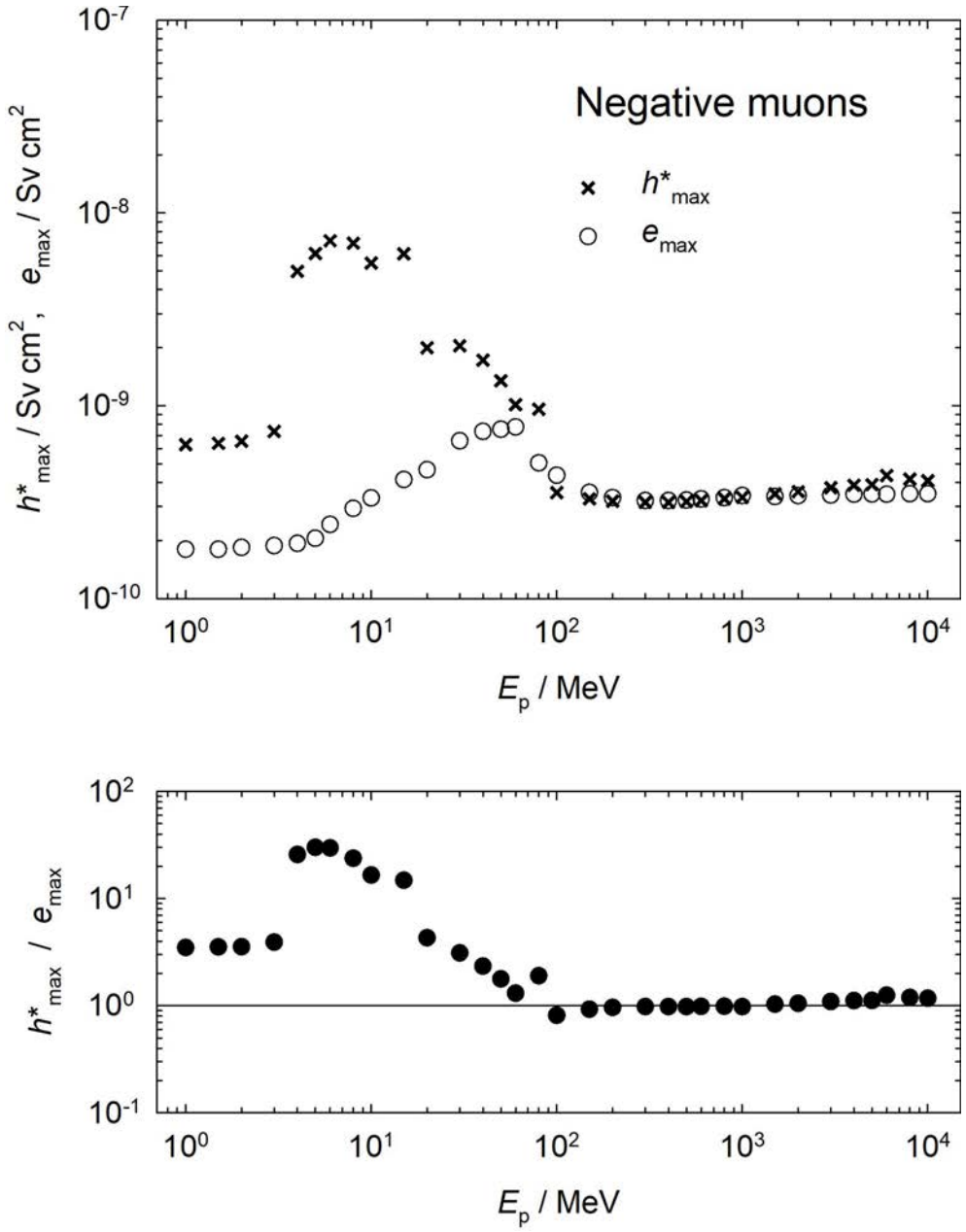

Figure 51 Negative muons: h^*_{max}, e_{max}, and h^*_{max}/e_{max}.

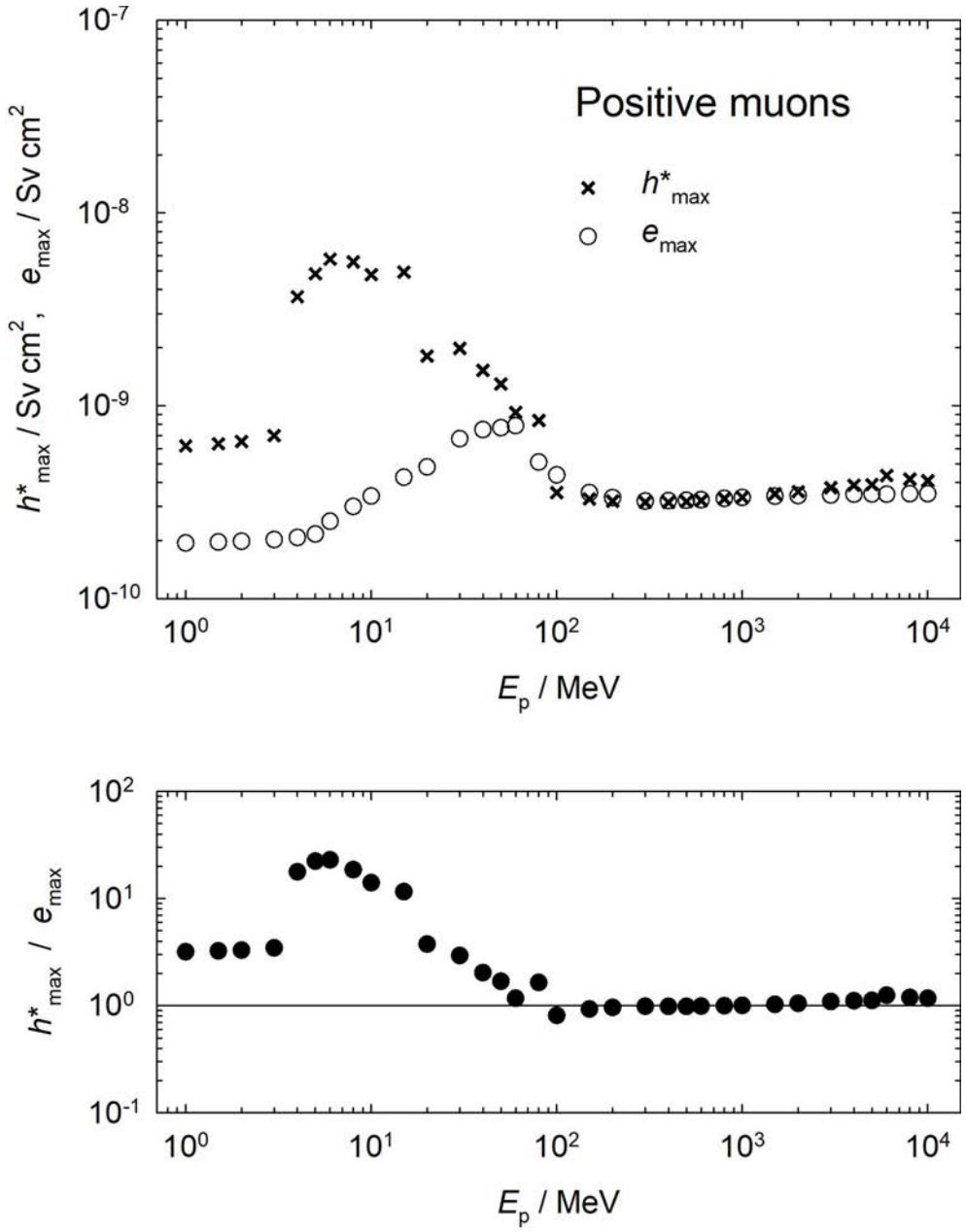

Figure 52 Positive muons: h^*_{max}, e_{max}, and h^*_{max}/e_{max}.

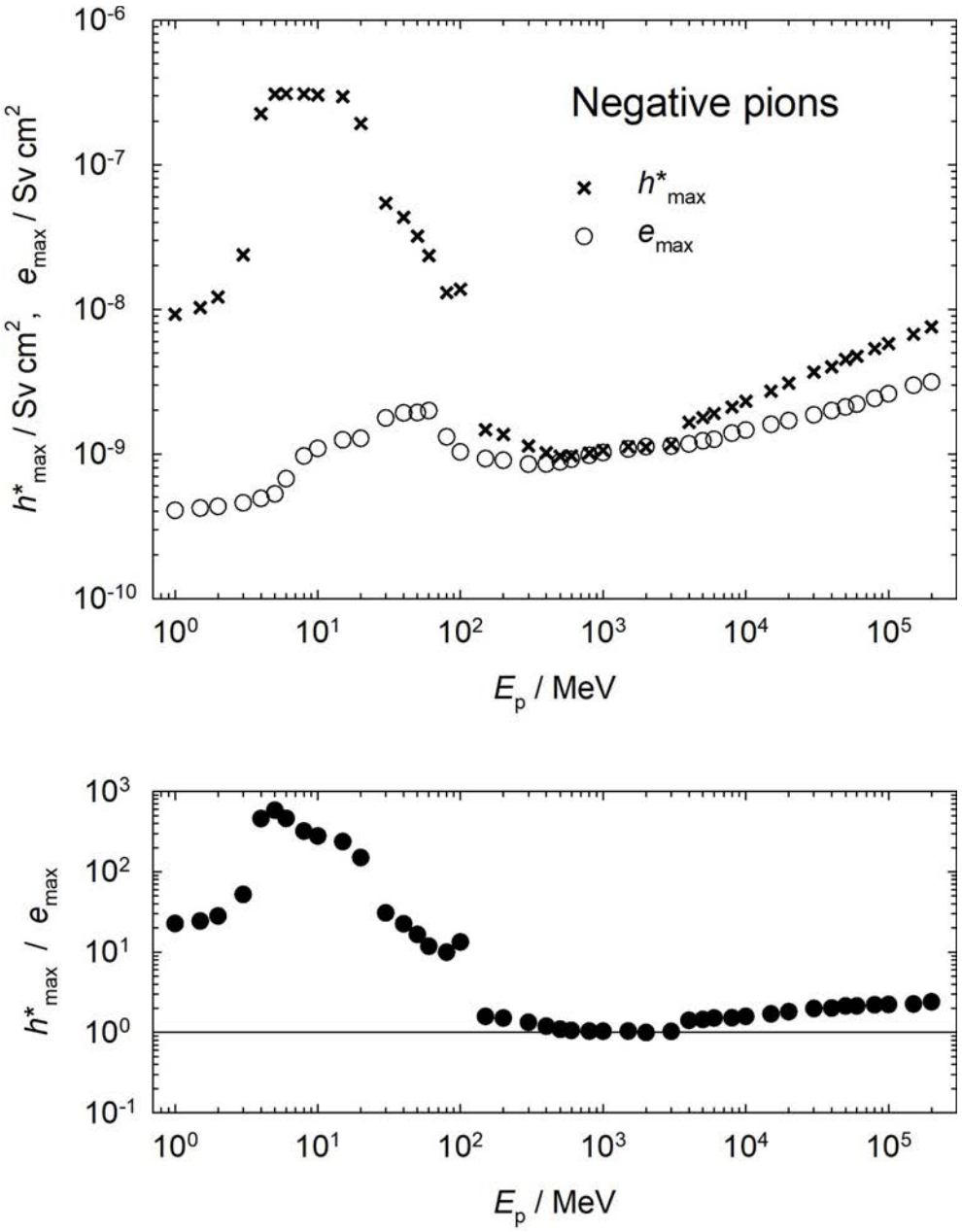

Figure 53 Negative pions: h^*_{max}, e_{max}, and h^*_{max}/e_{max}.

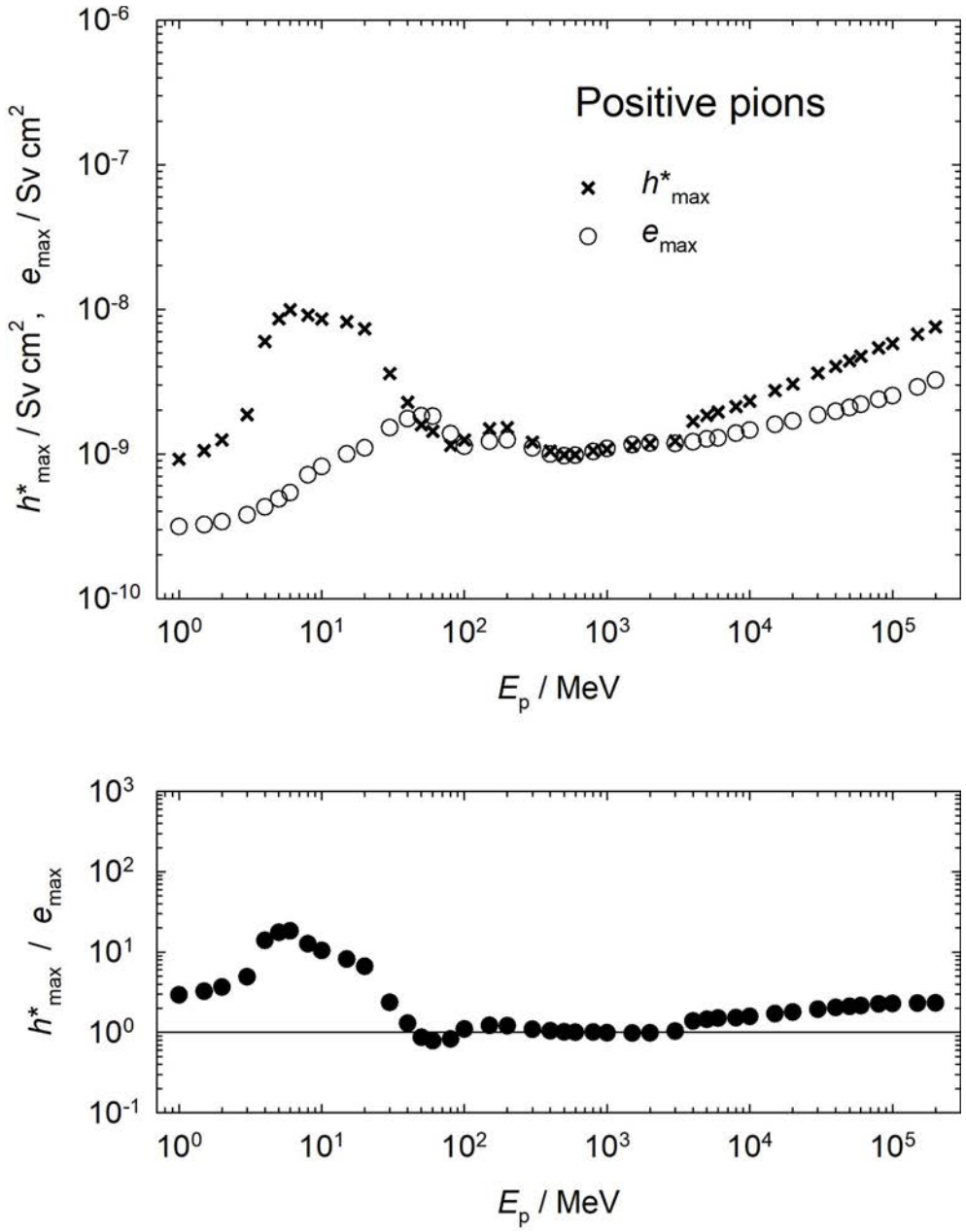

Figure 54 Positive pions: h^*_{max}, e_{max}, and h^*_{max}/e_{max}.

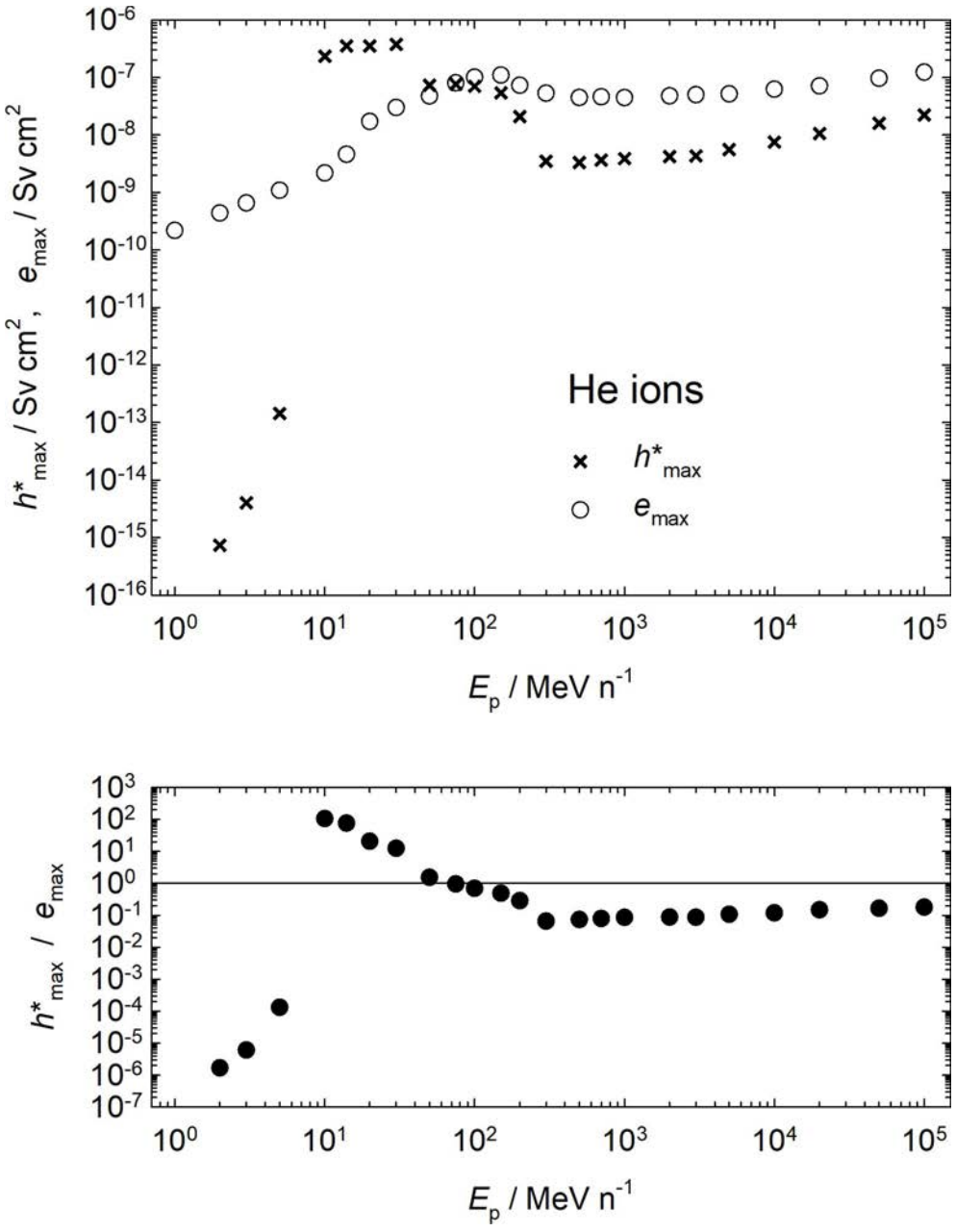

Figure 55 Helium ions: h^*_{max}, e_{max}, and h^*_{max}/e_{max}.

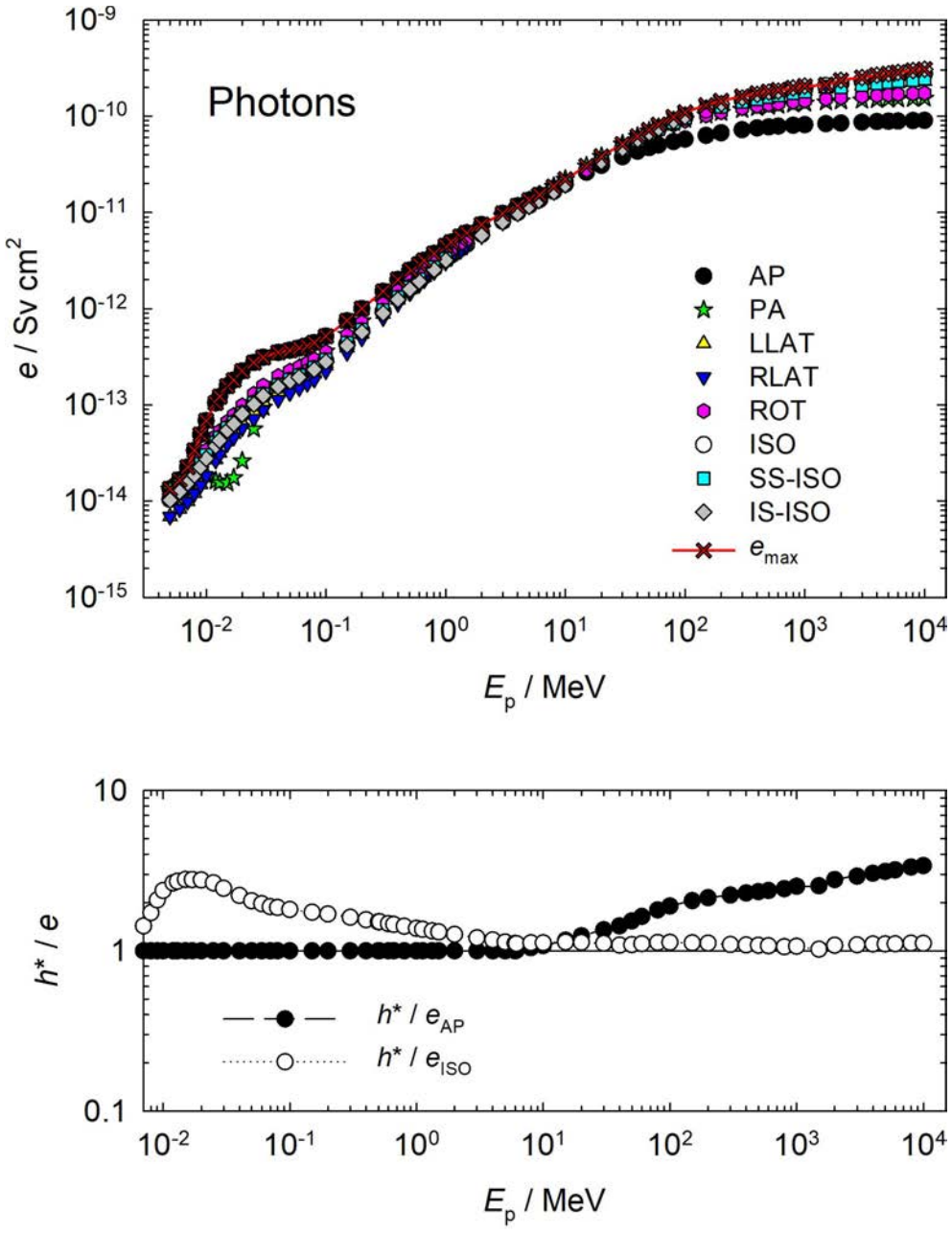

Figure 56 Photons: e and h^*/e.

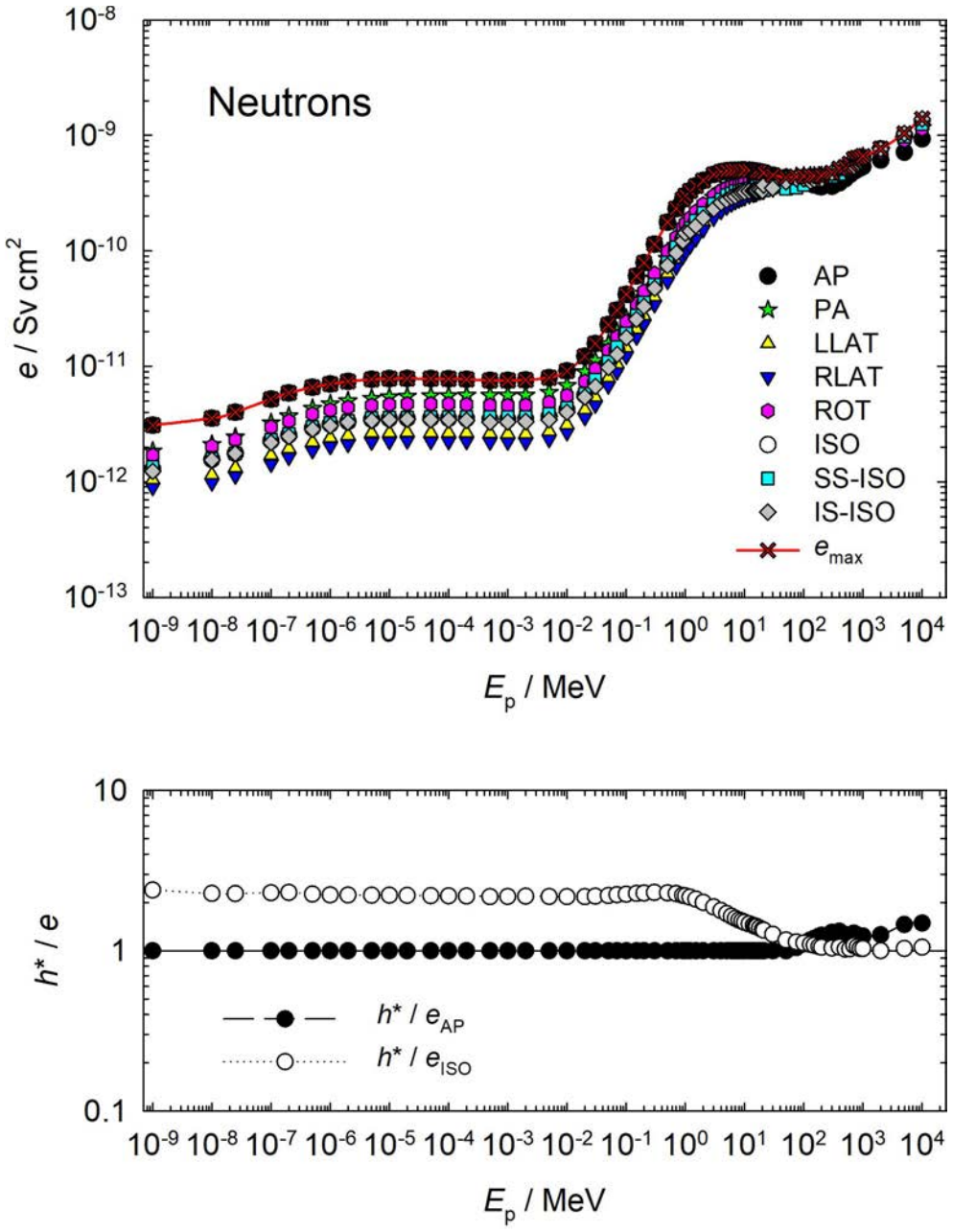

Figure 57 Neutrons: e and h^*/e.

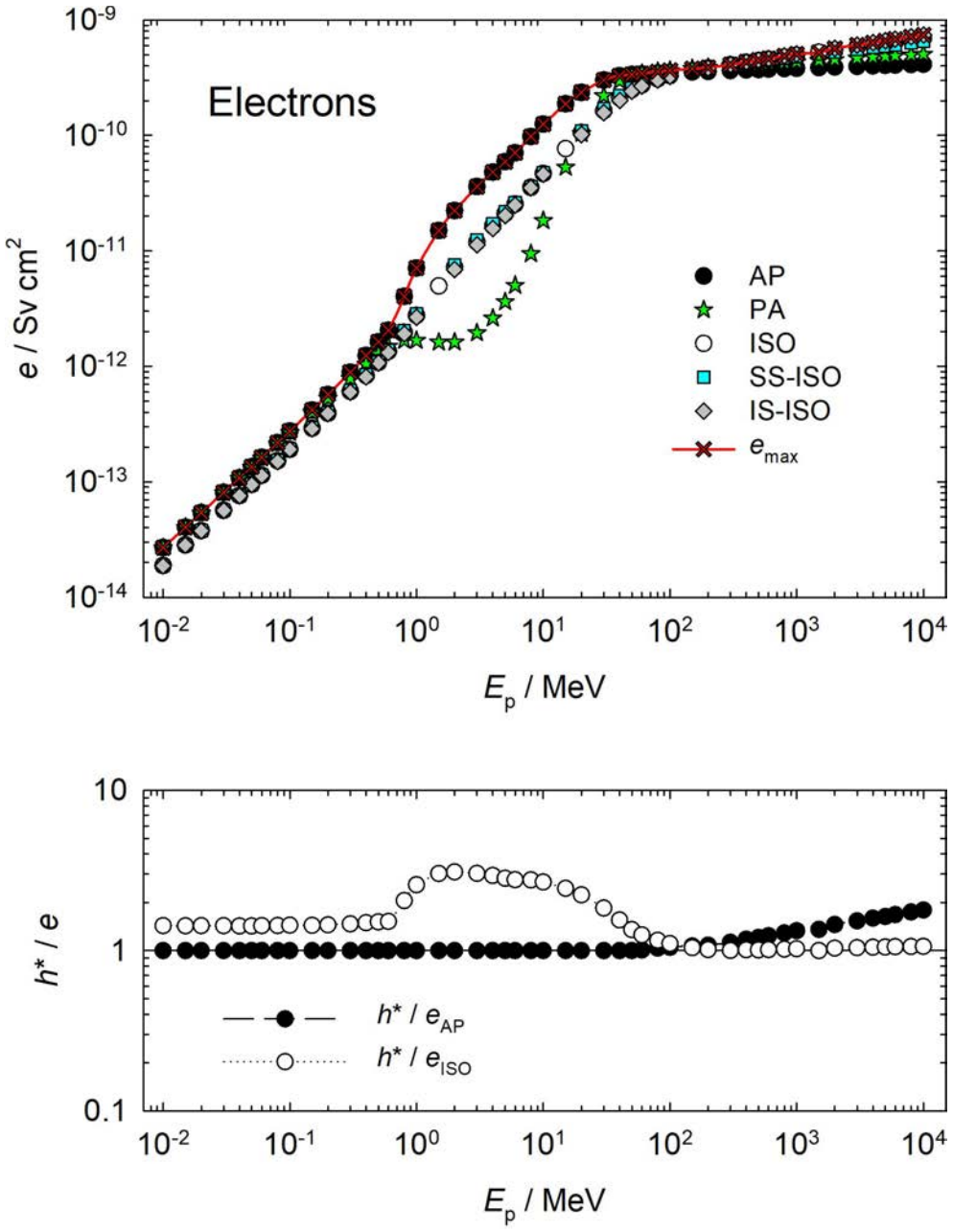

Figure 58 Electrons: e and h^*/e.

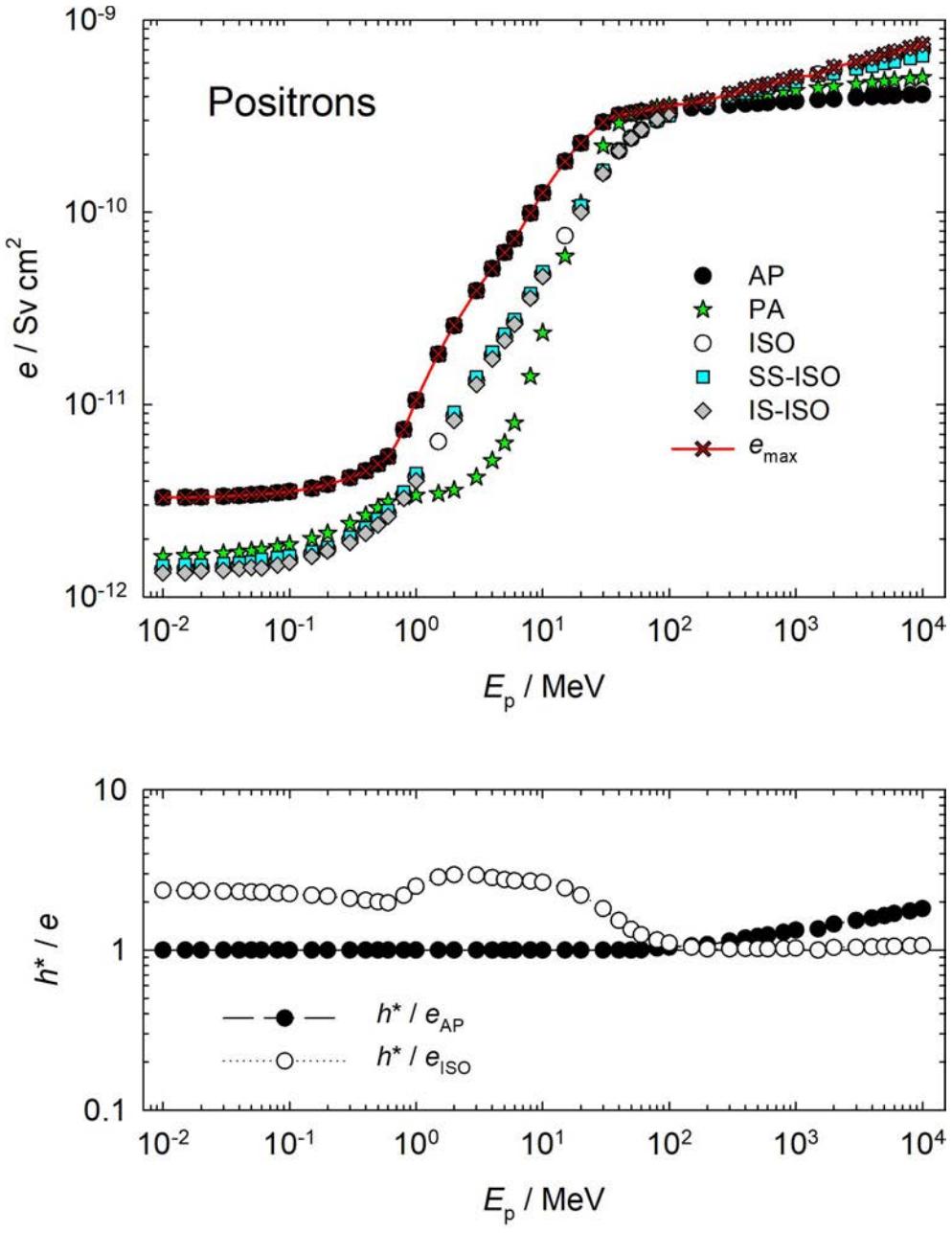

Figure 59 Positrons: e and h^*/e.

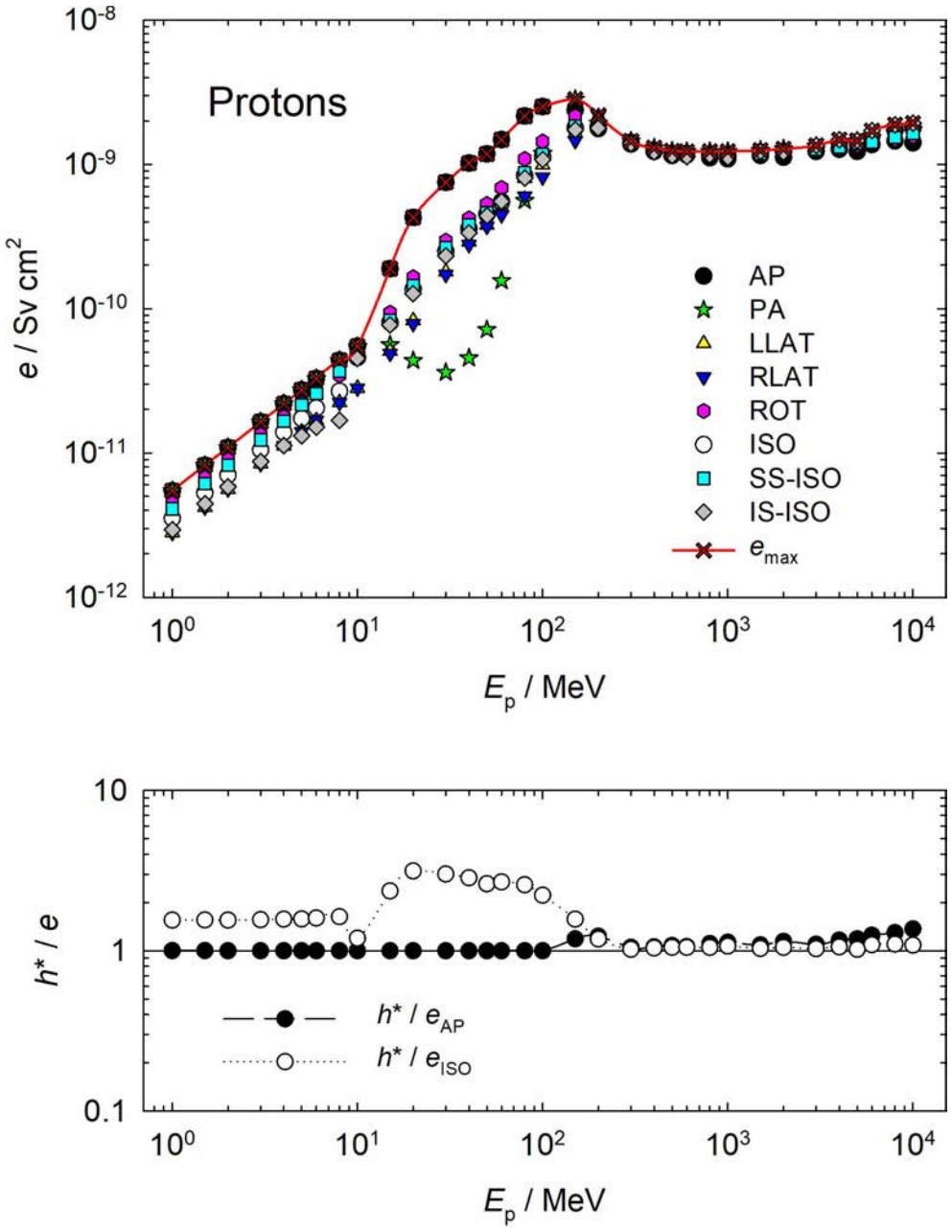

Figure 60 Protons: e and h^*/e.

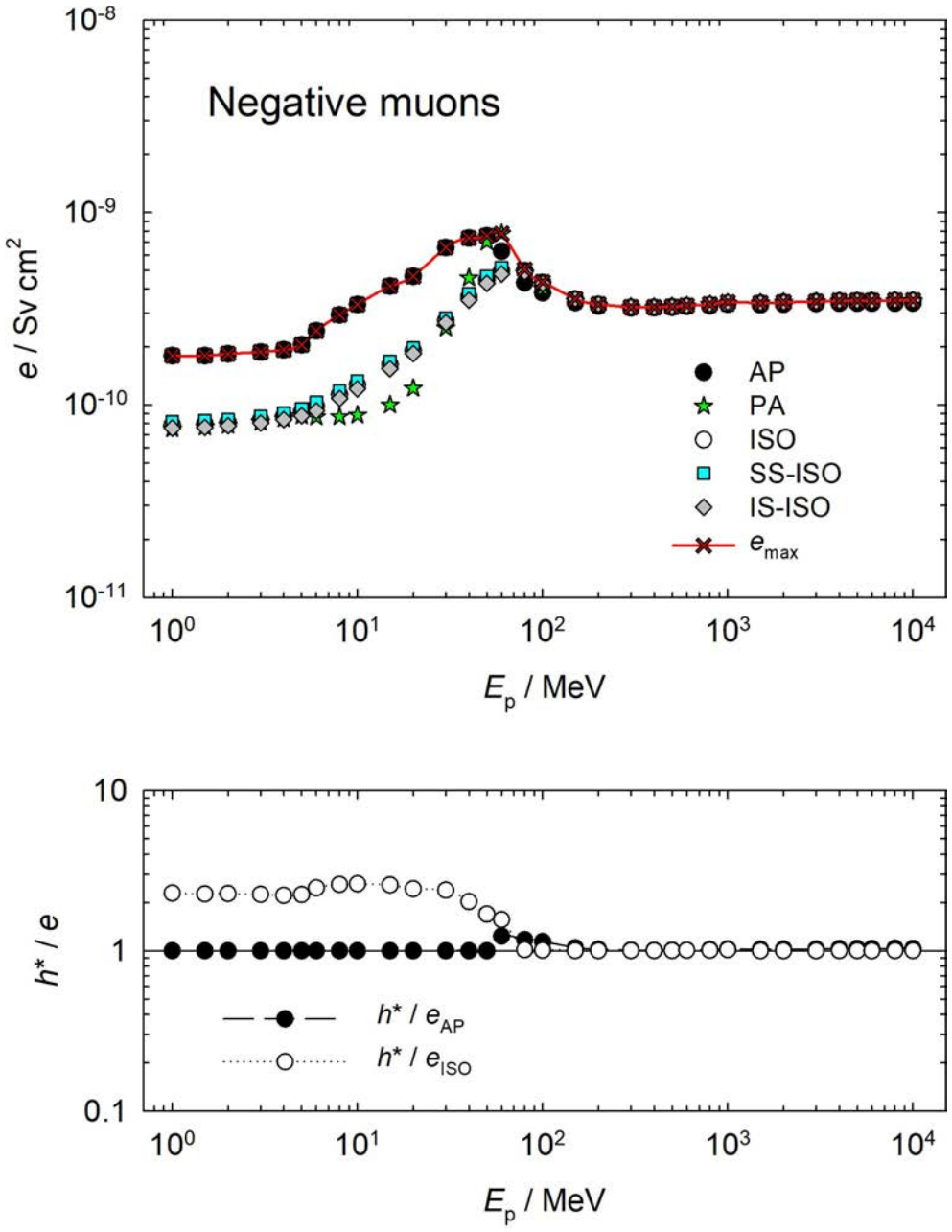

Figure 61 Negative muons: e and h^*/e.

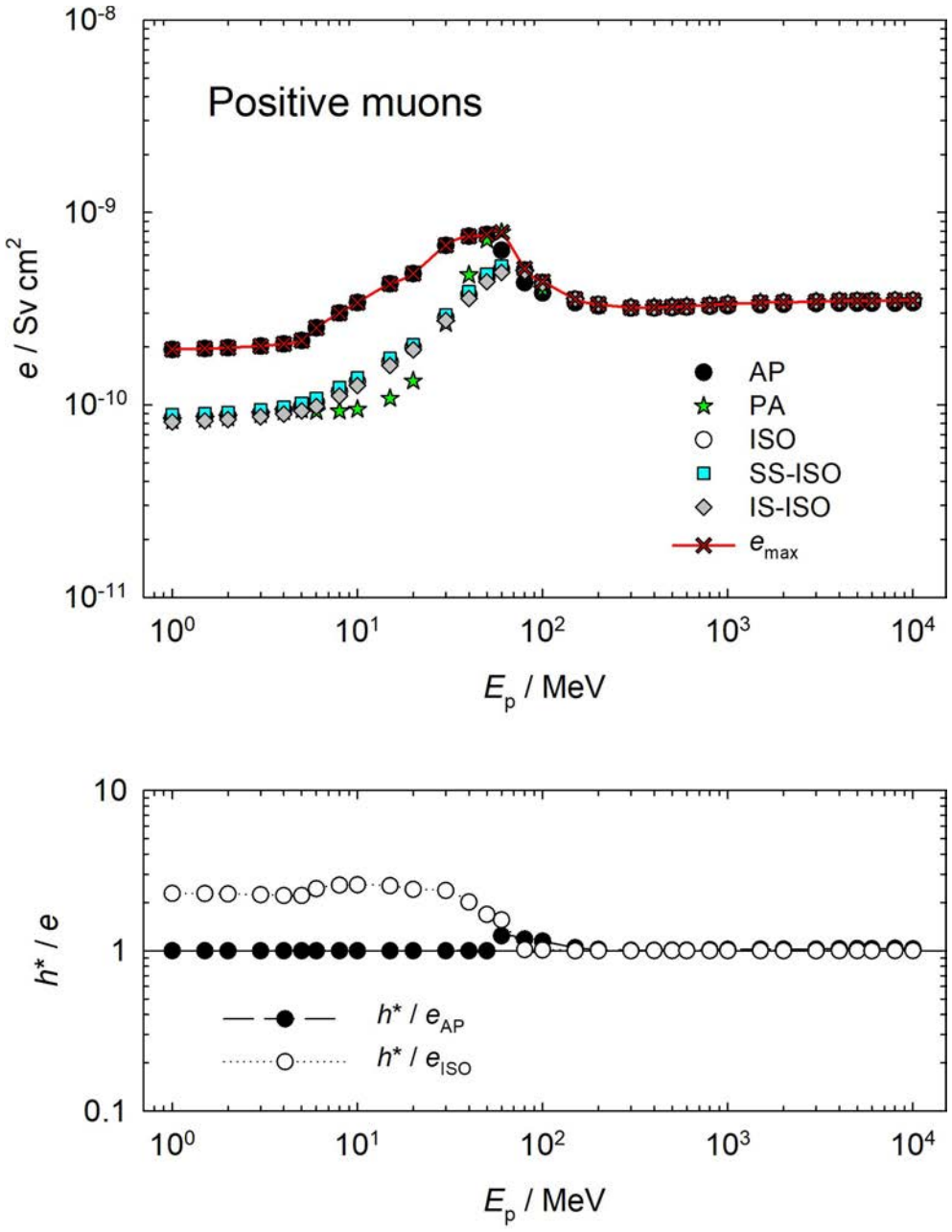

Figure 62 Positive muons: e and h^*/e.

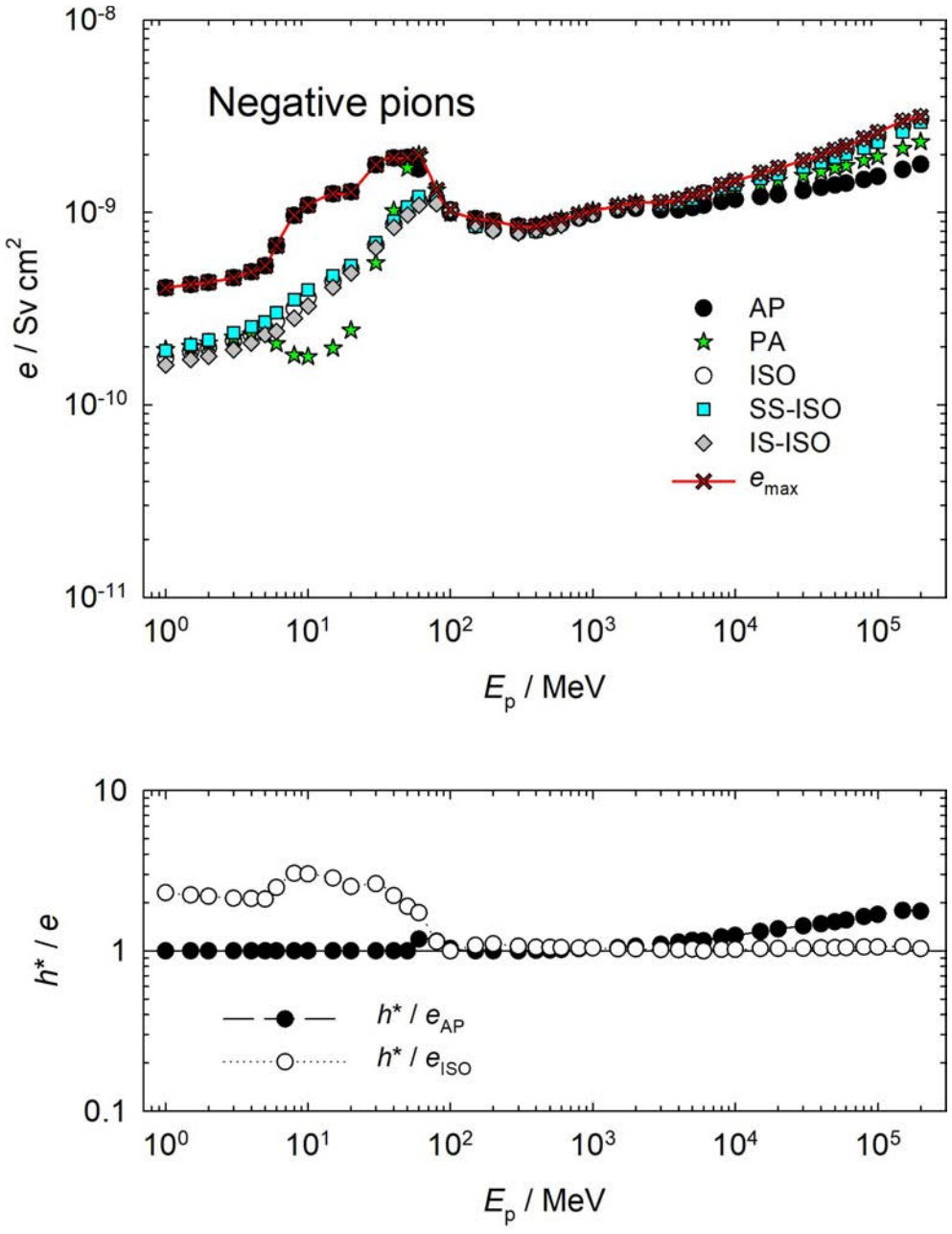

Figure 63 Negative pions: e and h^*/e.

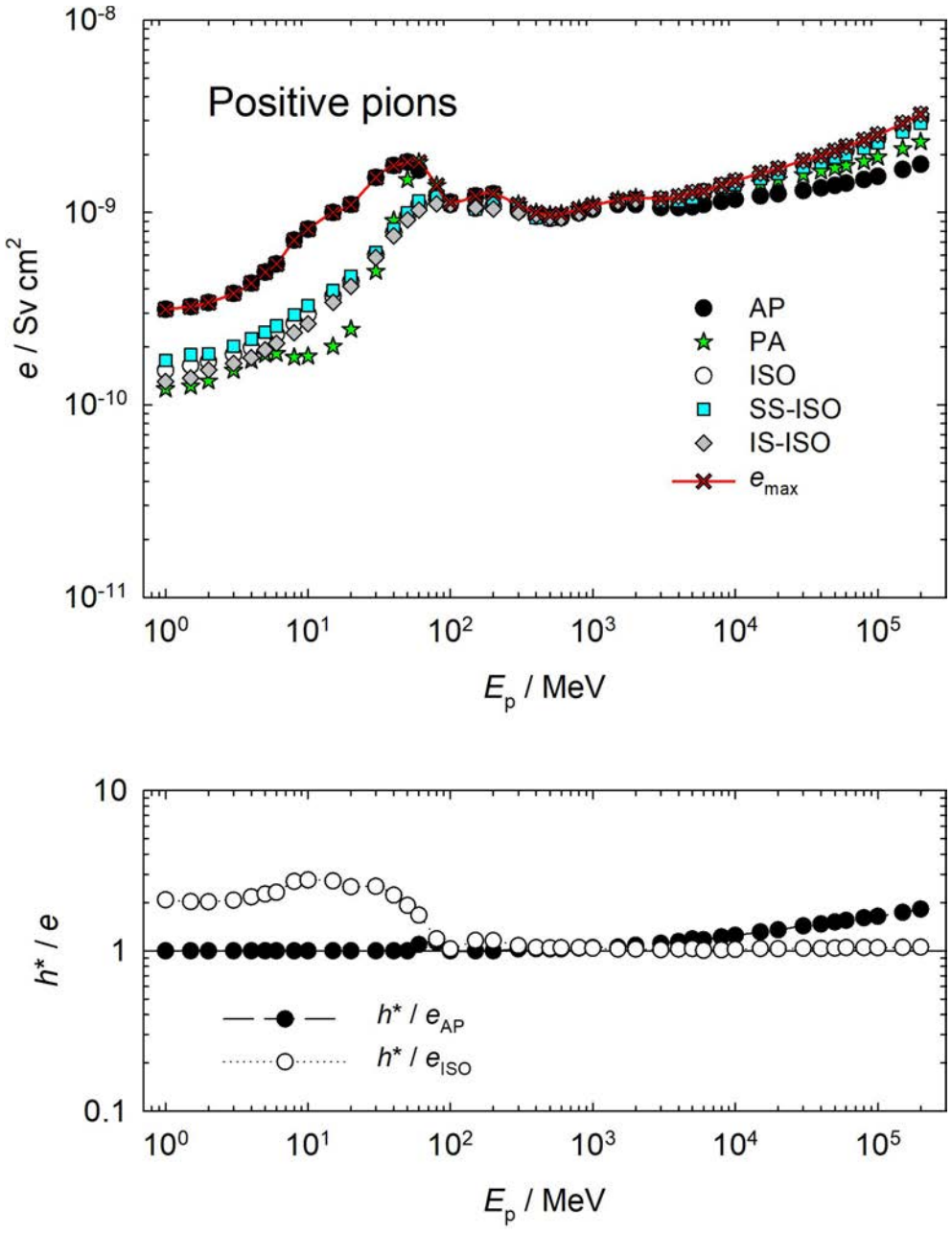

Figure 64 Positive pions: e and h^*/e.

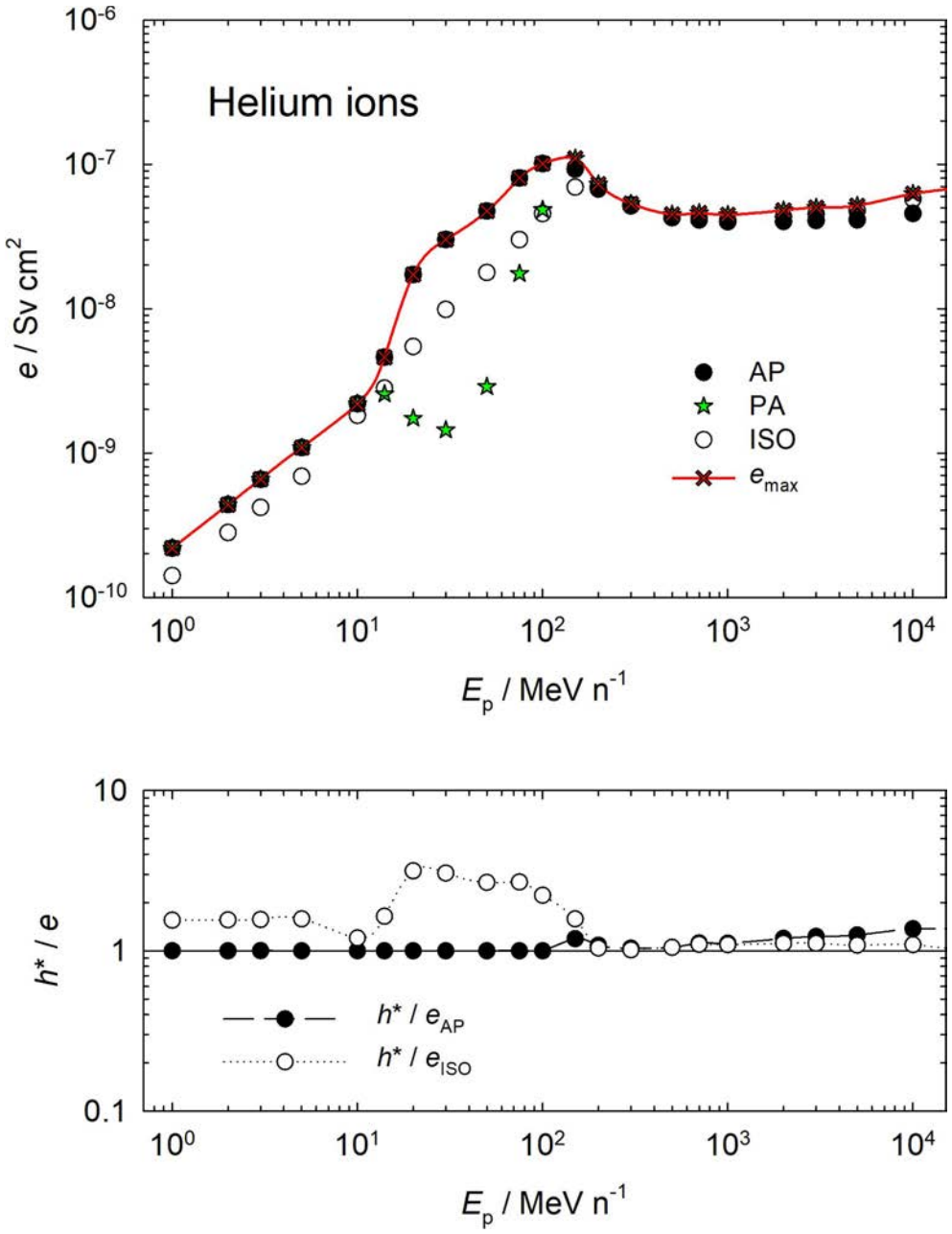

Figure 65 Helium ions: e and h^*/e.